

MULTIRESOLUTION PROCESSING OF SATELLITE IMAGES AND  
GEOGRAPHIC INFORMATION SYSTEMS TECHNIQUES FOR  
LAND-USE CLASSIFICATION

By

YURONG TAN

A DISSERTATION PRESENTED TO THE GRADUATE SCHOOL  
OF THE UNIVERSITY OF FLORIDA IN PARTIAL FULFILLMENT  
OF THE REQUIREMENTS FOR THE DEGREE OF  
DOCTOR OF PHILOSOPHY

UNIVERSITY OF FLORIDA

1994

Copyright 1994

by

Yurong Tan

## ACKNOWLEDGEMENTS

This research was performed using the facilities of the Remote Sensing Applications Laboratory (RSAL) of the Department of Agricultural Engineering at the University of Florida. The author is grateful for the assistance provided by the RSAL director, Dr. Sun F. Shih; RSAL manager, Orlando Lanni; and RSAL assistants, Jonathan D. Jordan, Chih-Hung Tan, and Bruce E. Myhre. The author is also grateful for the comments and review of this manuscript by Dr. Donald L. Myhre of the Soil and Water Science Department at the University of Florida.

The author extends his appreciation to each of the members of his advisory committee, Dr. Brian J. Boman, Dr. Edward P. Lincoln, Dr. Allen R. Overman, and Dr. Byron E. Ruth for their comments and advice rendered during this research, particularly to the committee chairman, Dr. Sun F. Shih of the Department of Agricultural Engineering at the University of Florida, for the guidance and support provided throughout the course of his graduate study at the University of Florida.

The greatest gratitude of the author goes to his wife, Siru, who always shared the joy as well as frustrations and provided unconditional support in every aspect during this seemingly endless process. The author is in debt to his son, Guolong, for the patience he undertook while this research was being actively pursued.

Lastly, the author acknowledges that this research would not have been completed without the continuous support and encouragement from his loving parents.



## TABLE OF CONTENTS

ACKNOWLEDGEMENTS .....	iii
LIST OF TABLES .....	vii
LIST OF FIGURES .....	ix
ABSTRACT .....	xii
CHAPTERS	
1 INTRODUCTION .....	1
Overview .....	1
Statement of Research Problem .....	3
Concept of Multiresolution Processing .....	8
2 OBJECTIVES OF RESEARCH .....	13
3 REVIEW OF LITERATURE .....	14
Conventional Image Enhancement .....	14
Multiresolution Enhancement .....	20
Color Composite Generation .....	20
Radiometric Enhancement .....	27
Other Enhancement Methods .....	36
Summary: Assessment of Problems .....	40
4 PRINCIPLE OF MERGING IMAGES .....	46
Principle of Merging Images .....	46
Assumptions .....	47
Arithmetic of Random Variables .....	48
Confining Method .....	53
Preserving Method .....	63
Differencing Method .....	69
Summary: Principle of Merging Images .....	73
5 DEMONSTRATION OF MERGING METHODS .....	76
Satellite Image Data .....	76
Variance of Merged LAC Images .....	81
Comparison of Merged LAC Images .....	91
Ratioing of Satellite Images .....	106
Multiresolution Enhancement .....	113
Summary: Appraisal of Merging Methods .....	116
6 MATERIALS AND METHODOLOGY FOR MULTIRESOLUTION LAND-USE CLASSIFICATION .....	119
Data Source and Equipment .....	119

	SPOT Image Data and Study Area .....	119
	ACIR Photography .....	122
	Image Processing Systems .....	122
	Photogrammetric Stereo Plotter .....	123
	Procedures for Merging SPOT Dataset .....	124
	Pre-merging Processing .....	124
	Generating Merged Dataset .....	126
	Evaluation of Merged Data .....	129
	Image Response and Citrus Canopy Cover .....	132
	Photogrammetric Measurement .....	132
	Canopy Cover Estimation .....	134
	Land-use Classification .....	136
	Précis and Concept .....	137
	Extracting Signature Patterns .....	139
	GIS-base Discrete Classification .....	141
7	DISCUSSIONS AND ANALYSES OF MULTIRESOLUTION LAND-USE CLASSIFICATION .....	148
	Evaluation of Merged Image .....	148
	Radiometric Quality .....	148
	Spatial Improvement and Spectral Integrity .....	151
	Image Response and Citrus Canopy Cover .....	157
	Estimation of Citrus Canopy Cover .....	157
	Relation of Image response to Canopy Cover .....	159
	Differentiation of Canopy Cover .....	166
	Effect of Multiresolution Merging .....	177
	Land-use Classification .....	183
	Potential for Signature Extraction .....	184
	GIS Discrete Classification .....	189
8	CONCLUSIONS AND RECOMMENDATIONS .....	195
	Research Conclusions .....	195
	Recommendations .....	199
APPENDICES		
A	RGB COLOR DISPLAY .....	202
B	IHS TRANSFORM FOR IMAGE DISPLAY .....	203
C	PROGRAM CODES TO UNPACK AVHRR LAC DATA .....	206
D	CLASSIFICATION DECISION RULES .....	209
REFERENCES .....		213
GLOSSARY .....		220
BIOGRAPHICAL SKETCH .....		224

## LIST OF TABLES

<u>Table</u>	<u>Page</u>
1-1 Available sources of Landsat and SPOT resource satellite data and system characteristics .....	5
4-1 Summary of the characteristics of different merging approaches .....	75
5-1 Wavelength characteristics of NOAA-11 AVHRR LAC images .....	77
5-2 standard deviation ( $\sigma$ ), normalized variance ( $\sigma^2$ ), mean ( $\mu$ ), maximum and minimum values of NOAA-11 AVHRR LAC images .....	80
5-3 Offset constant (C) used in the differencing method for merging LAC images .....	82
6-1 Standard deviation ( $\sigma$ ), mean ( $\mu$ ), and maximum and minimum values, and correlation coefficients (r) of SPOT multiresolution dataset .....	127
6-2 Multiresolution datasets and corresponding merging equations .....	130
6-3 Parameters used in ERDAS STATCL and ELAS TMTR modules for signature extraction .....	142
7-1 Standard deviation ( $\sigma$ ) and mean brightness values ( $\mu$ ) for multiresolution merged SPOT images .....	149
7-2 Summary for correlations between a merged image and its original multispectral counterpart .....	153
7-3 Between-waveband correlations (r) within multiresolution merged datasets .....	154
7-4 Summary for corelations between citrus canopy size and image response for multiresolution merged images .....	178
7-5 Variation of image data correlation (r) between panchromatic and original multispectral wavebands among selected groves ...	179

7-6	Standard deviations ( $\sigma$ ) of merged image data for selected citrus groves .....	180
7-7	Summary of spectral signatures unveiled by ERDAS STATCL module .....	185
7-8	Summary of spectral signatures unveiled by ELAS TMTR module .....	188
7-9	Canopy cover for spectral classes by GIS- based discrete classification technique .....	190

## LIST OF FIGURES

<u>Figure</u>	<u>Page</u>
1-1     Schematics of merging multiresolution satellite images .....	9
3-1     Schematics of principal component analysis for multispectral datasets .....	18
4-1     Relation of radiometric variance to merging coefficient ( $\beta$ ) and correlation coefficient ( $r$ ) for the confining method .....	57
4-2     Effect of variance difference on the radiometric quality of merged images for the confining method .....	61
4-3     Relation of radiometric variance to merging coefficient ( $\beta$ ) and correlation coefficient ( $r$ ) for the preserving method .....	66
4-4     Effect of variance difference on the radiometric quality of merged images for the preserving method .....	68
5-1     Location of clipped NOAA-11 AVHRR LAC images ....	79
5-2     Comparison between actual and estimated radiometric variance for merged LAC images (case I) .....	83
5-3     Comparison between actual and estimated radiometric variance for merged LAC images (case II) .....	84
5-4     Comparison between actual and estimated mean digital count for merged LAC images (case I) ....	85
5-5     Comparison between actual and estimated mean digital count for merged LAC images (case II) ...	86
5-6     Original clipped NOAA-11 LAC images of red and NIR wavebands .....	93
5-7     Merged LAC images by the preserving method (case I) .....	94

5-8	Merged LAC images by the preserving method (case II) .....	96
5-9	Merged LAC images by the confining method (case I) .....	97
5-10	Merged LAC images by the confining method (case II) .....	98
5-11	Merged LAC images by the differencing method (case I) .....	100
5-12	Merged LAC images by the differencing method (case II) .....	101
5-13	Summary (mosaic) of merged LAC images for three methods (case I) .....	104
5-14	Summary (mosaic) of merged LAC images for three methods (case II) .....	105
6-1	Location of clipped SPOT multiresolution dataset and study area .....	121
7-1	Comparison of SPOT 20-m NDVI and 10-m NDVI <sub>p</sub> images .....	156
7-2	Effect of citrus canopy cover on SPOT green waveband response .....	160
7-3	Effect of citrus canopy cover on SPOT red waveband response .....	161
7-4	Effect of citrus canopy cover on SPOT panchromatic waveband response .....	163
7-5	Effect of citrus canopy cover on SPOT NIR waveband response .....	164
7-6	Coincident plot of SPOT green waveband response for select citrus groves .....	168
7-7	Coincident plot of SPOT red waveband response for select citrus groves .....	169
7-8	Coincident plot of SPOT NIR waveband response for select citrus groves .....	170
7-9	Effect of tree crown variations on SPOT green waveband response variability for partial canopy groves .....	172



7-10	Effect of tree crown variations on SPOT red waveband response variability for partial canopy groves .....	173
7-11	Effect of tree crown variations on SPOT NIR waveband response variability for partial canopy groves .....	174
7-12	Relation of citrus tree variations to canopy cover difference .....	176

Abstract of Dissertation Presented to the Graduate School  
of the University of Florida in Partial Fulfillment of the  
Requirements for the Degree of Doctor of Philosophy

MULTIRESOLUTION PROCESSING OF SATELLITE IMAGES AND  
GEOGRAPHIC INFORMATION SYSTEMS TECHNIQUES FOR  
LAND-USE CLASSIFICATION

By

Yurong Tan

December, 1994

Chairman: Dr. Sun Fu Shih

Major Department: Agricultural Engineering

Combining multiresolution images to improve land-use information assessment is an important subject in remote sensing applications. The problem in finding effective methods for multispatial processing must be resolved through the development of new procedures for merging satellite images. The effect of combining image data on the quality of merged datasets must also be assessed toward land-use classification applications and multispectral analyses.

In digitally merging satellite images, the statistical variation analyses for combining random variables can be used to understand the various forms of image data merging and assess the radiometric quality of pre-merged images. The selection of an effective merging approach must be made with consideration of both the correlation and radiometric variance difference between the combining images and the merging coefficients. Merging images is a radiometric transformation



among the various land-use types in a scene. This principle can be used to collaborate Landsat MSS, Landsat TM, SPOT, and other satellite data for broader applications.

To generate enhanced datasets, the preserving approach should be used for non-negatively correlated images, and the differencing approach for those with negative correlations. The commonly used, but ineffective confining method should be avoided. The efficacy of waveband ratioing is limited to the land-use elements with weak/negative correlations and larger values in the numerator image.

The preserving method with a  $\beta=0.5$  coefficient was effective in generating both spatially and radiometrically enhanced SPOT multiresolution merged datasets which consistently rendered significantly more spectral signatures from a satellite scene. This enhanced differentiation provides a greater amount of information for applications including land-use classification and image interpretation.

The photogrammetric estimation of citrus canopy cover is feasible and accurate. Except for the NIR waveband, citrus canopy cover is inversely related to SPOT image spectra of partial canopy groves, suggesting a strong influence of soil substrate on satellite image response. The canopy-size classification of citrus groves was improved through the combined use of merged SPOT dataset and GIS-based classification techniques. Citrus groves with a higher percentage of canopy cover had more uniform trees and less variable spectral responses.

## CHAPTER 1 INTRODUCTION

### Overview

Information about land use plays an increasingly important role in the management and preservation of natural resources. For instance, land-use data are used in the operations of water resources management which range from water-use permitting to the development and implementation of regional planning and management strategies. In environmental and water quality monitoring, land-use activities are often indicative of the source and type of pollutants (Novotny and Chesters, 1981; Fukushima and Muraoka, 1988), particularly from agricultural and urban lands (USEPA, 1984; Pionke and Urban, 1985). In many cases, it is the change of land use that creates immense environmental concerns. Agricultural land-use data are needed to forecast and monitor production as well as to assess damage caused by diseases and natural catastrophic events. Also, land-use data are used in many other ways including forest management (Coleman et al., 1990), urban development and planning (Colwell and Poulton, 1985), hydrological investigations, and applications of geographic information systems (Ehlers, 1989; Piwowar et al., 1990; Tan and Shih, 1991a). Therefore, the availability of quality and timely land-use information becomes an indispensable factor

which prescribes our efforts in better managing natural resources.

Traditionally, land-use data are collected through aerial photography, ground surveys, and existing maps. While these methods are reliable and accurate, they are expensive and time-consuming. In addition, the process of traditional methods is tedious, and therefore often provides land-use data that are years out of date, while data availability becomes a limiting factor in some cases. When a large coverage area is needed, the difficulties involved increase in magnitude as well as in complexity. Fortunately, the synoptic coverage and periodic availability of satellite remote sensing data provide an excellent opportunity for the acquisition of timely land-use data and the monitoring of extensive land-use activities. This significantly amplifies our ability to understand the effects of land use types and to manage the impacts and consequences resulting from the change of land use activities. With increasing environmental awareness, more careful planning and monitoring of land-use activities becomes an important consideration in all levels of resources management.

To derive land-use information from satellite data, a land-use classification procedure is used within an automated computer image processing system. Such procedures generate statistically similar spectral classes which are then related to different land-use types (Lillesand and Kiefer, 1979; Thomas et al., 1987) through a ground-truthing process. To

improve the acquisition of land-use information from space, continuous research efforts are underway in the development of both new sensing systems (Engel, 1986; Spotlight, 1991; EOSAT, 1992a, 1992b) and image processing techniques.

### Statement of Research Problem

Obtaining land-use data or land-use information by satellite remote sensing requires a significant improvement both in accuracy and in specificity in order to be used operationally in many applications (Lo et al., 1986; DeGloria et al., 1986). For instance, day-to-day operations in water resources management seldom use satellite-based land-use data, mainly because of the lack of desired specificity or details. One facet to the solution of this problem is to improve the quality of raw data through advanced sensing technology and sensor system design. This has been initiated by the development of new sensing systems which will be onboard Landsat-7 (EOSAT, 1992a, 1992b) and the French *Système Probatoire de l'Observation de la Terre* (SPOT) resources satellite four referred to as SPOT-4 (Spotlight, 1991). Equally important is the development of data processing techniques to analyze and classify the remotely sensed data so that improved land-use information becomes feasible in practical applications.

Combining multispectral satellite data that have different spatial resolutions to extract more subtle land-use information has become an important component in image

processing techniques. In the process, the spectral and spatial advantages rendered by different sensing systems (Table 1-1) are combined complementarily into a merged dataset. This provides an unparalleled opportunity that expands our ability beyond using any of the original individual datasets to acquire land-use information. Because of the challenge of future sensor systems which will provide multiresolution sensing as well as onboard registration capabilities (Spotlight, 1991; EOSAT, 1992a, 1992b) and the tremendous amount of image data already captured by satellite sensors operating over a wide range of spatial resolutions and spectral wavebands (Shih, 1984; Moore, 1989; Ehlers, 1989), merging multiresolution satellite images creates an immense opportunity to make contributions to the improvement of current land-use data acquisition from space. As a result, multiresolution processing is anticipated to be a very powerful image processing technique in future remote sensing applications.

To date, much research work remains to be done in order to effectively use multiresolution satellite imagery for resources management. For instance, finding effective methods to digitally merge multiresolution datasets continues to be the central problem in multiresolution processing. A good merger will be able to take full advantage of the spectral and spatial benefits of multiresolution images so that resultant merged datasets will have incomparable radiometric quality



Table 1-1. Available sources of Landsat and SPOT resource satellite data and system characteristics.

Type of Sensor	Spectral characteristics			Spatial resolution (m)
	Band#	Wavelength( $\mu$ )	Color	
----- Landsat-1 and Landsat-2 -----				
RBV <sup>a</sup>	1	0.475-0.575	Blue-green	76
	2	0.580-0.680	Yellow-red	76
	3	0.690-0.830	Red-infrared	76
MSS <sup>b</sup>	4	0.50 -0.60	Green	76
	5	0.60 -0.70	Red	76
	6	0.70 -0.80	Near infrared	76
	7	0.80 -1.10	Near infrared	76
----- Landsat-3 -----				
RBV <sup>a</sup>	Camera	0.505-0.750	Panchromatic	40
MSS <sup>b</sup>	4	0.5 - 0.6	Green	76
	5	0.6 - 0.7	Red	76
	6	0.7 - 0.8	Near infrared	76
	7	0.8 - 1.1	Near infrared	76
	8	10.4 -12.6	Thermal infrared	234
----- Landsat-4, Landsat-5 -----				
TM <sup>c</sup>	1	0.45 - 0.52	Blue	30
	2	0.53 - 0.61	Green	30
	3	0.62 - 0.69	Red	30

Table 1-1 -- continued.

Type of Sensor	Spectral characteristics			Spatial resolution (m)
	Band#	Wavelength( $\mu$ )	Color	
MSS <sup>b</sup>	4	0.78 - 0.91	Near infrared	30
	5	1.57 - 1.78	Intermediate infrared	30
	6	10.42 - 11.66	Thermal infrared	120
	7	2.08 - 2.35	Intermediate infrared	30
MSS <sup>b</sup>	1	0.50 - 0.60	Green	76
	2	0.60 - 0.70	Red	76
	3	0.70 - 0.80	Near infrared	76
	4	0.80 - 1.10	Near infrared	76
----- Landsat-6 <sup>c</sup> and Landsat-7 -----				
TM <sup>d</sup>	1	0.50 - 0.90	Panchromatic	15
	2	0.45 - 0.52	Blue	30
	3	0.53 - 0.61	Green	30
	4	0.62 - 0.69	Red	30
	5	0.78 - 0.91	Near infrared	30
	6	1.57 - 1.78	Intermediate infrared	30
	7	10.42 - 11.66	Thermal infrared	120
HRV <sup>f</sup>		2.08 - 2.35	Intermediate infrared	30
	-----SPOT <sup>e</sup> -1, SPOT-2, and SPOT-3 -----			
	1	0.51 - 0.73	Panchromatic	10
	2	0.50 - 0.59	Green	20
	3	0.61 - 0.68	Red	20
		0.79 - 0.89	Near infrared	20

Table 1-1 -- continued.

Type of Sensor	Spectral characteristics		Spatial resolution (m)	
	Band#	Wavelength( $\mu$ )      Color		
----- SPOT <sup>e</sup> -4 -----				
HRV <sup>f</sup>		0.61 - 0.68	Panchromatic	10
	1	0.50 - 0.59	Green	20
	2	0.61 - 0.68	Red	20
	3	0.79 - 0.89	Near infrared	20
	4	1.58 - 1.75	Intermediate infrared	20

Source: modified from Shih, 1984; Spotlight, 1991; and EOSAT, 1992a; 1992b.

<sup>a</sup> Return beam vidicon camera.

<sup>b</sup> Multispectral scanner.

<sup>c</sup> To be replaced by Landsat-7 because of failure to reach orbit.

<sup>d</sup> Thematic mapper.

<sup>e</sup> (French) *Système Probatoire de l'Observation de la Terre* (SPOT).

<sup>f</sup> High resolution visible.

Note: Operation of Landsat 1: 7/23/1972 - 1/06/1978  
 Landsat 2: 1/22/1975 - 2/25/1982  
 Landsat 3: 3/05/1978 - 3/31/1983  
 Landsat 4: 7/16/1982 - present.  
 Landsat 5: 3/01/1984 - present.  
 Landsat 6: launched in 1993, but failed to reach orbit.  
 Landsat 7: identical to Landsat 6 and to be launched in 1997.  
 SPOT 1 : 2/22/1986 - 12/30/1990  
 SPOT 2 : 1/22/1990 - present.  
 SPOT 3 : ?/?/1992 - present.  
 SPOT 4 : To be launched in 1995.



and enhanced spatial information. These quality factors of image data are vital not only to the utility of the merged datasets for potential applications, but also to any remote sensing efforts that attempt to improve our capability in monitoring land-use resources. Therefore, this research was focused on the techniques for combining multiresolution satellite images as well as on the utility of multiresolution processing for land-use classification and image interpretation.

### Concept of Multiresolution Processing

Multiresolution processing is an image processing technique used to combine or merge multispectral images that have different spatial resolutions. One of the images to be combined will have a high spatial resolution or a smaller size of picture element (pixel), and a panchromatic waveband, while the others will be multispectral (or multi-waveband), but with a relatively lower spatial resolution, or a larger pixel. These images of different spatial resolutions are digitally merged to reconstruct a new set of images that can inherit the spectral and spatial characteristics of both the multispectral and panchromatic images. The process is schematically illustrated in Figure 1-1.

The purpose of multiresolution processing is to generate a new set of images with enhanced spectral and spatial qualities by taking the spectral and spatial advantages of the

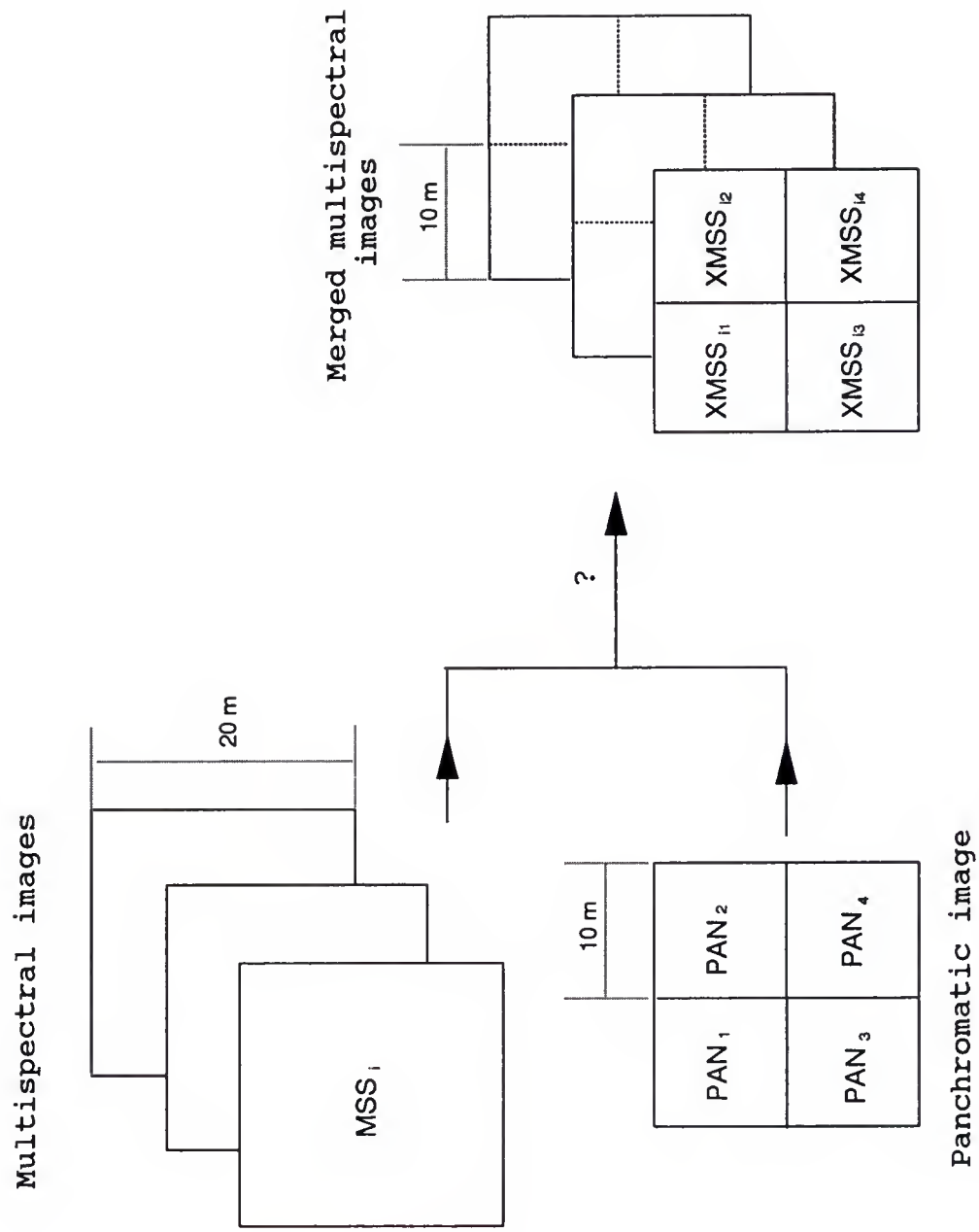


Figure 1-1. Schematics of merging multiresolution satellite images.

images to be combined. The spatial and spectral virtues of the original multiresolution image data are utilized complementarily. As a result, the merged dataset becomes spectrally as well as spatially more powerful for remote sensing applications.

One example of multiresolution processing is to merge the SPOT high resolution visible (HRV) panchromatic and multispectral images that have respective 10-m and 20-m spatial resolutions (Cliche et al., 1985; Carper et al., 1990). The panchromatic image with a 10-m resolution can reveal subtle spatial details of scene objects, but its usage for multispectral analyses (land-use classification) is hampered by its very broad spectral waveband. The 20-m multispectral data with three spectral wavebands are more useful for land-use classification, however a high spatial resolution multispectral dataset is more desirable for extracting subtle information from the scene. When such multiresolution images are merged, the spectral and spatial advantages are combined into a new set of images which are multispectral and with a 10-m spatial resolution. As a result, the new merged dataset will have a greater potential for remote sensing applications.

There are two major steps involved in the process of multiresolution processing. The first deals with the co-registration of the multiresolution images. This can be done with two different approaches. The first one is to simply

project all images to a mutual geographic reference system which can be either the latitude-longitude system, or the universal transverse mercator (UTM) system, or the state plane coordinate (SPC) system. The second approach is to treat one of the images as a master and the rest as slaves. After selecting a number of tie points that are mutual to all images including the master one, the slave images are rectified to the master image. In the second approach, no actual geographical coordinate system (e.g. UTM) is utilized and the slave images are referenced relative to the master image. Usually, this relative approach produces a smaller error of co-registration because transitional reference (e.g. maps) and digitizing operations for map data entry are not involved. To register multiresolution images, it is also necessary to invoke an image resampling procedure before or during the registration process. Virtually all image processing software packages provide the facilities for image resampling and registration operations.

The second step involves the use of mathematical manipulations to digitally combine, pixel by pixel, the numerical image data. This is a very critical step because the spectral, radiometric, and spatial qualities of the merged dataset depend on the selection of a good combining algorithm. At the end, a new set of multispectral images are generated which are radiometrically, spatially, and spectrally enhanced. While the combining algorithms reported in the literature vary

considerably, their introduction is the results of speculations and arbitrary elaborations because the basic principle of digitally merging satellite images is not well understood. Therefore, it has become essential to explore and to understand the principle of image data manipulations so that the techniques of multiresolution processing can be developed to effectively enhance satellite remote sensing applications including land-use classification.

## CHAPTER 2 OBJECTIVES OF RESEARCH

The main objective of this research was to study the principle of digitally merging satellite images and to develop techniques for combining multiresolution satellite datasets, as well as to evaluate the utility of multiresolution processing for satellite-based land-use classifications. The specific objectives included:

1. To formulate the principle of digitally combining multispectral satellite images including those with different spatial resolutions.
2. To develop techniques and methods for digitally merging multiresolution satellite images.
3. To study the effects of multiresolution processing on the spectral, spatial, and radiometric qualities of merged multispectral datasets.
4. To study the effects of canopy sizes of citrus trees on the spectral responses of SPOT satellite data as well as to investigate the feasibility of a canopy-size differentiation of citrus crops on satellite images.
5. To investigate the utility and benefits of combining multiresolution satellite images for land-use classifications, particularly for citrus crops.



### CHAPTER 3 REVIEW OF LITERATURE

Because of the multispectral capabilities of contemporary satellite sensing systems, a geographic area can be imaged simultaneously with a number of spectral wavebands, resulting in a multi-image scene or dataset. In the discussions throughout this dissertation, a scene includes all the images acquired for one geographic area at one time, while an image is meant to represent the numerical data of only one spectral waveband.

#### Conventional Image Enhancement

Over the years that remote sensing data have become widely used, many techniques for image enhancement have been well developed and standardized in image processing software systems. Therefore, an in-depth discussion for each of these techniques seems inappropriate. However, a brief review of those techniques which were involved or used in many previous research efforts to combine multiresolution satellite images would be useful to the understanding of continued discussions. Those techniques included the contrast stretching, spatial filtering, and principal component analysis.

A contrast-stretching procedure is an image processing procedure used to arbitrarily rescale a set of image gray

shades to a larger range or to a full range (0-255) for increasing image contrast. The gray shades of an original satellite image of Landsat, SPOT, and other satellites usually spread over a portion of the available 0-255 dynamic range (or sometimes called data depth). As a result, such images with cramped gray shades do not have conspicuous tonal gradations. After a contrast-stretching process, the image values (often called image digital counts) of relatively dark pixels are scaled back further, while those of bright pixels are scaled up. As a result, original dark pixels will become darker while the bright ones become brighter in a contrast-stretched image (Gonzalez and Wintz, 1987). Very often, this simple procedure can produce satisfactory results for image interpretation. Note that the increase in image tonal contrast by a contrast-stretching procedure gives a false sense that the procedure can improve the image radiometric quality.

The contrast-stretching procedure can be applied to a portion of the existing image gray shades (Thomas et al., 1987) or to a subimage area (Gonzalez and Wintz, 1987) for a selective enhancement. Also, there are linear and nonlinear contrast stretching methods (Lillesand and Kiefer, 1979; Thomas et al., 1987) and the procedure is performed for each image or waveband independently.

A spatial filtering procedure includes both the high-pass and low-pass filters which are often used to remove or to



emphasize certain visual effects of a digital image. For instance, a low-pass filter is used for image smoothing and noise elimination while a high-pass filter is for edge enhancement (Lillesand and Kiefer, 1979). The simplest form of a low-pass filter is to replace the value of a pixel by the average computed from its neighborhood (e.g. 3 x 3 pixel array). By replacing a pixel's value with its neighborhood average, the large values (such as noises) will be compressed while the small values are inflated or exaggerated (Lillesand and Kiefer, 1979). As a result, a low-pass filtered image will appear smoother and have less contrast. In the case of a high-pass filter, the value of a pixel will be added to or subtracted from by its deviation from the average of its neighborhood (e.g. 3 x 3 array), depending on its relative magnitude with respect to the defined neighborhood average. Therefore, boundary pixels which usually have the largest deviations will become either much darker or brighter. Often, the deviations are doubled or even tripled in order to make edges or linear features more conspicuous (Lillesand and Kiefer, 1979). The operation of a spatial filtering procedure (high-pass or a low-pass) is performed independently for each image or waveband. An important point in spatial filtering is that the resultant image data are radiometrically altered by such filtering procedures.

As compared to the methods of both contrast stretching and spatial filtering, principal component analysis (PCA) is

a procedure which involves a multi-dimensional transformation for a set of multispectral images. In the process, the multi-waveband data are transformed from the original coordinate system formed by the spectral wavebands into one defined by new synthesized wavebands. There are several usages for a PCA procedure. First, it can be used to reduce the dimensionality of multi-waveband datasets (Thomas et al., 1987). For instance, when a PCA transform is applied, the image data of a two-waveband dataset can be effectively represented by the first principal component (PC1) as shown in Figure 2-1, thus reducing the dataset to essentially one dimension (or one synthesized waveband). The second usage is to increase the image contrast as well as the separability for land-use elements (Lillesand and Kiefer, 1979). For instance, the image data variance encompassed by the PC1 component (Figure 2-1) is greater than either of those for the two original wavebands. Therefore, the image of the PC1 component will have more contrast as well as greater separation among the different land-use elements in the image. The third usage of a PCA procedure is for the decorrelation of multispectral images (Gillespie et al., 1986). In such a case, a PCA transform is followed by a contrast-stretching procedure applied to the PC components, particularly the PC2 component as shown in Figure 2-1. Then, the first (PC1) and second (PC2) components are together retransformed back to their original multispectral space. In a decorrelated dataset, the

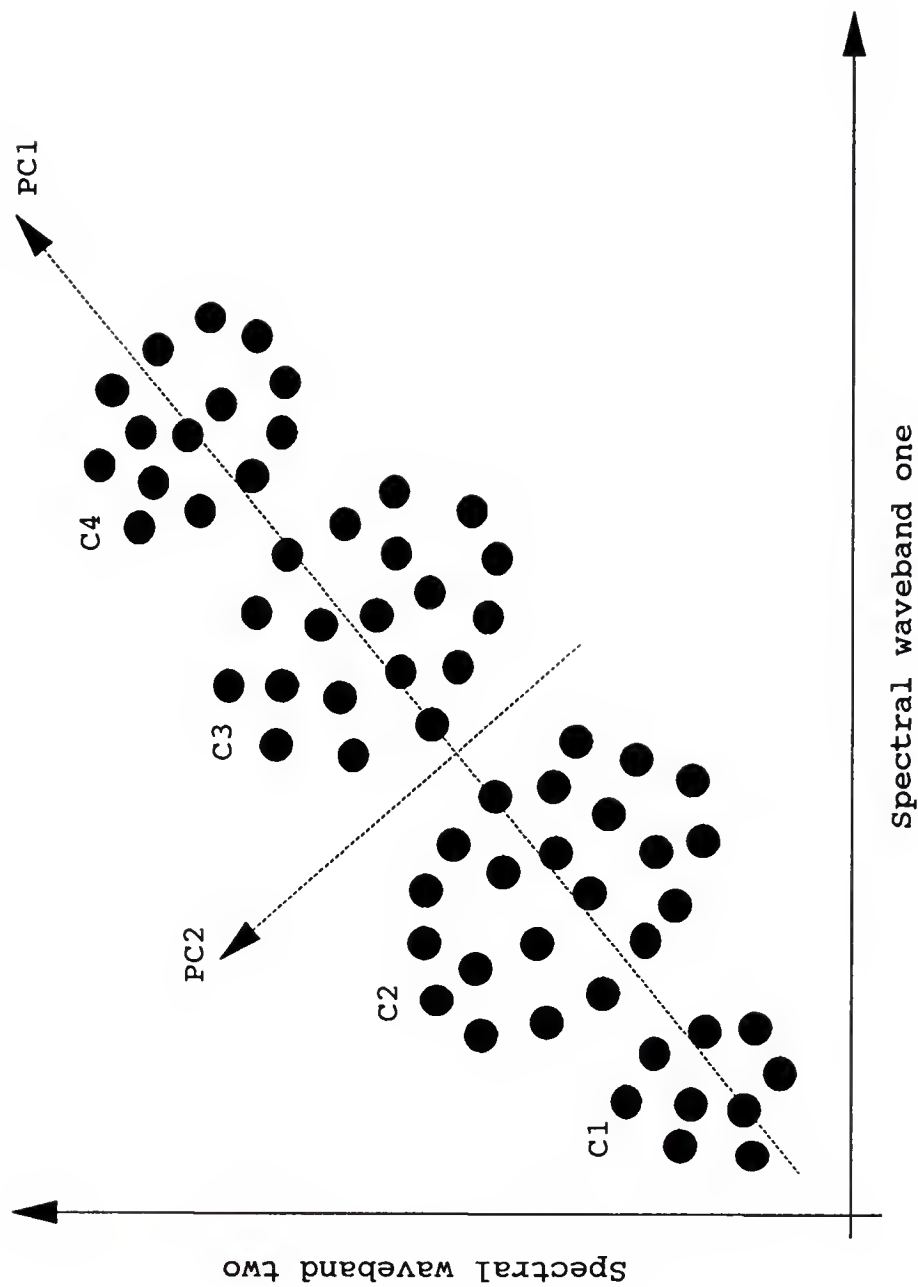


Figure 2-1. Schematics of principal component analysis for multispectral datasets.

identities for the various types of spectral elements may be significantly different from those of the original images (Gillespie et al., 1986).

If the PCA procedure is applied to a multispectral image dataset with  $n$  wavebands, the image data transformation will take place within a  $n$ -dimensional space. The results are that the amount of radiometric information represented by the first, the second, ... and the  $n$ th component will be in a decreasing order. Also, the transformed components can each be contrast-stretched (Lillesand and Kiefer, 1979) to further enhance the tonal gradations of transformed images. The PCA transform is usually carried out before initiating land-use classification procedures to reduce data dimensionality as well as to enhance the radiometric separability of spectral classes. Thomas et al. (1987) presents in-depth discussions about PCA transforms which are exemplified by using a Landsat multispectral scanner (MSS) dataset.

Finally, it is worthwhile to point out that the procedures of contrast stretching, spatial filtering, and principal component analysis will not enhance or improve the spatial resolution of the original images. In addition, a contrast-stretching procedure will not increase the actual number of gray shades in an image, even though the radiometric variance of stretched image data is increased.

### Multiresolution Enhancement

Combining the spatial and multispectral advantages of multiresolution satellite images for various resource management applications has inspired great interests in the remote sensing community. To merge satellite images with different spatial resolutions, both image co-registration and arithmetical data manipulations are required. If the images are already co-registered, the primary methods to manipulate the image data can be summarized into two broad approaches which include the generation of color composites and the enhancement of radiometric quality of merged images. Note that to generate a color composite usually requires three images for the blue, green, and red primary colors of a display device.

#### Color Composite Generation

The most commonly used methods for generating color renditions from image datasets are the well-known RGB (red, green, and blue) color display system (Appendix A) and the intensity-hue-saturation (IHS) color transform (Appendix B). For multiresolution datasets, the RGB system is simple and easy to use, but the resultant color composites often have a blocky appearance, particularly when the spatial resolution difference is large. Recently, the IHS transform has gained popularity mainly because of its effectiveness to produce more balanced color products for a wide range of datasets. To



generate a color composite from a multiresolution dataset, the IHS method first takes a forward transformation from the low spatial resolution images of three wavebands into the intensity (I), hue (H), and saturation (S) components (Appendix B). Then, a reverse transformation is carried out to convert the I, H, and S components to the RGB values in order to generate color composites through a RGB color display device. The high spatial resolution image is merged in the process by replacing the I component during the reverse transformation (Haydn et al., 1982; Carper et al., 1990). Note that a color composite by either the RGB system or the IHS transform uses a maximum of only three spectral channels and successful results often depend on a tedious trial-and-error process.

Daily et al. (1979) were among the first to recognize the importance of multiresolution processing of satellite data for remote sensing applications. An airborne radar image with a 10-m spatial resolution was co-registered with Landsat 80-m MSS images in an effort to improve geological interpretation for a desert environment. The superior textural variations of the radar image along with a 10-m spatial resolution were utilized to complement the low contrast as well as the low spatial resolution of Landsat MSS data which, in turn, compensated for the drawbacks of radar shadows. Through a direct RGB color display method, color composites generated from the co-registered dataset were able to delineate subtle

geologic units through a visual image interpretation. Using a similar approach, Wong and Orth (1980) also generated useful color composites from Seasat synthetic aperture radar (SAR) and Landsat MSS images which have 40-m and 80-m spatial resolutions, respectively. These two early studies underlined the benefits in the unified use of satellite data acquired by completely different sensing systems (multispectral vs. radar) for improving the interpretability of remote sensing images.

When the RGB color display system is used, satellite images do not readily define or fit into the red, green, and blue primary colors (Harris et al., 1990). In other words, the images can not simply substitute the red, green, and blue primaries in the RGB display system because of the spectral incompatibility which could lead to serious color distortions and poor-quality composites (Haydn et al., 1982; Harris et al., 1990; and Carper et al., 1990). As a result, the IHS color perception system has become the widely adopted approach to resolve the color distortion problems encountered in the RGB display of multispectral images. The entire process of an IHS transform for multiresolution processing takes four steps which include (i) co-registration of multiresolution images, (ii) a forward transformation from three multispectral images to the three IHS components, (iii) a reverse transformation from the IHS components to RGB values, usually with the replacement of the intensity component by the high spatial resolution image, and (iv) display the results through a RGB

color display system. For the IHS system, the intensity or brightness of a scene is a function of illumination (Boynton, 1979). Therefore, the intensity component should encompass a broader range of wavelength (Haydn et al, 1982) and is extensively associated with the spatial relations of scene objects (Judd and Wyszecki, 1975). For this reason, the intensity component is always assumed to be replaced by the high spatial resolution panchromatic image in the reverse IHS transformation.

Zobrist et al. (1979) were among the first to apply the IHS transform to satellite data for image enhancement. In the study, Landsat MSS 80-m and meteorological Seasat 25-m radar images were used. The intensity component transformed from the Landsat MSS data was simply replaced by the 25-m radar image. Then, an IHS reverse transformation was taken to create color composites.

Haydn et al. (1982) further demonstrated the utility of the IHS transform for image enhancement. Landsat MSS, Landsat return beam vidicon (RBV), and the Heat Capacity Mapping Mission (HCMM) thermal infrared (TIR) images with respective spatial resolutions of 80 m, 30 m, and 600 m were merged between the RBV and MSS and between the MSS and HCMM images. A direct replacement of the transformed intensity component by the corresponding high spatial resolution image was employed in the reverse transformation for each case. Also, ratioed data between spectral wavebands was demonstrated for the use



of the IHS transform. For example, while the intensity component was transformed from Landsat MSS wavebands four, five, and seven (denoted respectively as MSS4, MSS5, and MSS7), the H and S components were substituted, respectively, by the MSS5/MSS4 and MSS5/MSS6 ratioed data. Substantial enhancement in color composites was observed. The IHS color transform was adopted in the entire study because the direct RGB color model produced confusing and low quality image presentations. Using a similar methodology, Welch and Ehlers (1987) were able to produce enhanced color composites from Landsat (30 m) thematic mapper (TM) and SPOT HRV 10-m panchromatic images.

Very different approaches for using the IHS transform have also been reported. A color composite was created from a Seasat mono-band radar image (Daily, 1983). Both the strong and weak radar responses related to sloping targets and vegetation features were extracted, respectively, by high-pass and low-pass filters, and then used as the hue and saturation components while the original radar image was used directly as the intensity component for the IHS transform. The color composite was able to reveal major structural features invisible in the original black-and-white radar image. Harris et al. (1990) took a step further when combining Landsat 30-m TM and 10-m airborne radar images. In two instances, the high spatial resolution image was used directly as the intensity component, while the hue components were created from a

combination of Landsat TM wavebands two, four, and seven (denoted as TM2, TM4, and TM7) or of Landsat TM wavebands two, five, and seven (denoted as TM2, TM5, and TM7). However, the saturation component was held at a constant value (150). In another instance of the same study by Harris et al. (1990), the radar image was used as the intensity component and the geological units (numerical codes) in a digitized map as the hue component, while the saturation component was held at a constant (150). Based on a visual assessment, the study concluded that the color composites were able to define lithological and structural features that were absent from existing geological maps. These two studies by Daily (1983) and Harris et al. (1990) not only opened a new dimension in the use of the IHS transform for remote sensing applications, but also demonstrated the effectiveness and compatibility of the IHS transform for a broad range of data characteristics including satellite images and digital maps.

The use of the IHS transform can be extended to include the imagery digitized from an aerial color infrared (ACIR) photography (Grasso, 1993). In the study, a digitized ACIR high spatial resolution (10 m) image was merged with Landsat MSS and Landsat TM data to enhance geological interpretation. The intensity components transformed from either Landsat MSS or Landsat TM images were directly replaced by the ACIR image during the IHS reverse transformation. The color composites, which had a 8x linear spatial resolution factor, were still

useful for geological mapping. Also in the study, a different approach in utilizing the IHS transform was demonstrated in which the digitized ACIR image was used as the intensity component, the Landsat TM ratio data (TM5/TM7) as the saturation component while the hue component was held at a constant value (96). The results were very useful for delineating the high and low clay content areas. Note that the high and low TM5/TM7 ratios were essentially used to regulate the level of color saturation (S component) so that high clay content areas would show more vivid colors than its counterparts. However, results also showed that the colors of these composites could change very rapidly by just varying the hue component with a moderate magnitude. Though the concept of the latter example is somewhat different from the previous one by Harris et al. (1990) who emphasized the color diversity (H component) rather than the color purity (S component), good quality color composites can still be produced by the IHS transform. This indicates that the IHS color transform has tremendous flexibilities in adapting to a wide variety of geographic data.

In summary, when applying the RGB and IHS methods to generate color composites, it has been demonstrated that image interpretability can be significantly improved through a unified use of multiresolution datasets. This is particularly evident for the IHS transform which is capable of producing quality color composites under a broad range of circumstances.

Also, several studies have illustrated that the IHS transform seems to possess a virtually universal adaptability to geographic data. The multiresolution merged results in the form of color composites are indispensable for many remote sensing applications which involve image interpretation. However, to generate color composites is not the ultimate goal of multiresolution processing of satellite imagery data. The radiometric quality of merged images is far more important than a color display and vital to the potential of post-merging applications such as land-use classification. In addition, a severe disadvantage for color composites is that tremendous efforts are needed to extract quantitative land-use information from the color products while a maximum of only three spectral wavebands can be handled at one time.

### Radiometric Enhancement

In the radiometric enhancement approach, arithmetical algorithms are used to digitally combine the multiresolution image data in order to generate merged images which can achieve the purpose of multiresolution processing. Direct substitution of the high spatial resolution image for the RGB color display system often created color composites with blocky appearances because of the spatial resolution differences. To overcome such a weakness, digital manipulations of the image data have become necessary. In a study by Cliche et al. (1985), simulated SPOT HRV panchromatic



and multispectral images from an airborne dataset, which had 11 spectral wavebands, were digitally merged, pixel by pixel, using the following methods

$$\text{I.} \quad \text{MI}_i = A_i * (\text{PAN} * \text{HRV}_i)^{\frac{1}{2}} + B_i \quad [3-1]$$

$$\text{II.} \quad \text{MI}_i = A_i * (\text{PAN} * \text{HRV}_i) + B_i \quad [3-2]$$

$$\text{III.} \quad \text{MI}_1 = A_1 * (\text{PAN} * \text{HRV}_1)^{\frac{1}{2}} + B_1 \quad [3-3a]$$

$$\text{MI}_2 = A_2 * (\text{PAN} * \text{HRV}_2)^{\frac{1}{2}} + B_2 \quad [3-3b]$$

$$\text{MI}_3 = A_3 * (0.25\text{PAN} + 0.75\text{HRV}_3) + B_3 \quad [3-3c]$$

where  $\text{MI}_i$  is the merged multispectral images,  $i$  (in methods I and II and subscripts 1-3 in method III) is waveband index, PAN and HRV are, respectively, the simulated SPOT panchromatic and multispectral images, and  $A_i$  and  $B_i$  are coefficients or scaling factors to maintain the merged data within the 0-255 dynamic range.

From the color composites generated through the use of the RGB color display system, the study concluded that, while the improvement on spatial resolution was apparent for all three methods, method (III) produced the best color composite. The improvement by method (III) was attributed to the use of different merging algorithms which helped preserve the SPOT  $\text{HRV}_3$  near infrared information. For method (II), the pixel values were low and concentrated, resulting in dark and no-contrast merged images. Because of the high correlations in the merged images between the near infrared and visible

wavebands, method (I) produced wash-out images. Even though all these merging methods were based on arbitrary speculations and the results were displayed using the RGB system, the potential benefits of digitally merging image datasets were indicated with improved spatial information.

In digitally merging multiresolution images, speculations for a combining approach do not bring about consistent results. In an effort to find a general approach that does not depend on arbitrary elaborations, Price (1987) contended that the high correlations between the panchromatic and both the multispectral green and red wavebands within a SPOT multiresolution dataset could be utilized to estimate the corresponding high spatial resolution multispectral merged images. In the study, the original SPOT 10-m panchromatic and 20-m multispectral images were artificially degraded, by averaging, to 20-m panchromatic ( $P_{20}$ ) and 40-m multispectral ( $M_{40}$ ) images, respectively. Then, the whole approach took two steps. The 20-m multispectral merged images (MI) were first estimated from the degraded panchromatic  $P_{20}$  data by a regression equation

$$MI_i = A_i * P_{20} + B_i + D \quad [3-4]$$

where  $MI_i$  is the estimated multispectral image  $i$  based on the degraded (20-m) panchromatic image,  $A_i$  and  $B_i$  are regression coefficients determined from the degraded panchromatic  $P_{20}$  and the original 20-m spatial resolution multispectral image, and



D is a correction factor to balance the numerical sum of estimated subpixels with the recorded value of a low resolution pixel ( $M_{40}$ ). If the sum of the estimated digital counts of subpixels did not equal the recorded value of the low resolution pixel in question, a correction was applied. The estimated 20-m images from the degraded (40-m) panchromatic waveband were able to retain 99% of the variances of the original 20-m images of the green and red wavebands. However, a potentially serious problem could have existed with a high correlation between the two estimated images because they both depended on the same identical panchromatic data. In fact, the multispectral images were used only as complementary information through a correction procedure.

A different approach was undertaken to estimate the SPOT near-infrared (NIR) image which in general does not correlate well with the panchromatic waveband. The (estimated) merged 20-m NIR image ( $MI_3$ ) was first obtained from a lookup table created by both the degraded 20-m panchromatic ( $P_{20}$ ) and the original 20-m NIR images. Then correction was applied similar to those used for the green and red wavebands. Results indicated that only 75% of the radiometric variance of the original NIR image was retained during the merging process. Though the broad spectral bandwidth of the panchromatic image encompasses part or even the entire range of the multispectral

green and red wavebands, it is impossible that the portion of image digital count for a merged high spatial resolution image can be separated from a panchromatic pixel. The difficulty is analogous to isolating from a jar of oil the part that came from a particular peanut. In addition, the process of spatial degradation (by averaging pixels) could smooth out or compress the radiometric information in the original image data.

To explore the utility of digital manipulations for datasets acquired by multiple sensors, Landsat MSS and Shuttle imaging radar A-band (SIR-A) images were digitally merged in a lithological mapping study (Chavez et al., 1983). However, the high spatial resolution of the 40-m radar image was not utilized to its advantage for enhancing the spatial resolution of the Landsat 80-m MSS images. Instead, the spatial resolution of the radar image was artificially degraded for compatibility with that of the Landsat MSS data. From the results of various arithmetical manipulations including addition, subtraction, ratioing, and difference-ratioing of the co-registered SIR-A and Landsat MSS image data, it was concluded that the addition and ratioing methods were useful for discriminating some geologic units while the applicability of the subtraction method is limited only to negatively correlated images. The results by Chavez et al. (1983) have two important implications. First, digital manipulations of image data can be extended to include those images acquired by different sensing systems. Second, the arithmetical

manipulations of image data can be applied to images with different spatial resolutions as well as those which have the same spatial resolution.

Digital merging multiresolution images has been used in efforts to further enhance the results of an IHS transform. In order to more effectively use the IHS transform, the selection of a proper intensity or brightness component is very critical to the quality of color display (Boynton, 1979). A low intensity component could result in severe image degradations (Judd and Wyszecki, 1975; Haydn et al., 1982). In the case of a low intensity value, corrections are needed for the hue and saturation components (Judd and Wyszecki, 1975) or for the intensity component (Boynton, 1979; Haydn et al., 1982; Gillespie et al., 1986). However, by applying such correction procedures, the final image is very difficult to interpret because the original colors can be altered significantly (Zobrist et al., 1979).

The importance of finding the most effective method to generate the intensity component for the IHS transform for merging multiresolution datasets has been recognized by some researchers, including Carper et al. (1990). Instead of adopting the direct replacement of the panchromatic image for the intensity component, Carper et al. (1990) conducted some experiments on different merging methods in order to find the best intensity component. In addition to many previous studies that relied on imagery data acquired on different

dates or even in different years, simultaneously-acquired SPOT 10-m panchromatic and 20-m multispectral images were used. This was done to eliminate the contribution of temporal information which could introduce some difficulty to the assessment of the benefits of an IHS transform. Carper et al. (1990) proposed the following set of merging algorithms to calculate the intensity components.

$$I_a = (PAN + HRV_3)/2 \quad [3-5]$$

$$I_b = (PAN * PAN * HRV_3)^{1/3} \quad [3-6]$$

$$I_c = (2 * PAN + HRV_3)/3 \quad [3-7]$$

$$I_d = (PAN * HRV_3)^{1/2} \quad [3-8]$$

$$I_o = (HRV_1 + HRV_2 + HRV_3)/3 \quad [3-9]$$

where  $I$ , with alphabetical subscripts for method index, is the calculated intensity component to replace the original intensity component  $I_o$  transformed from the 20-m multispectral images, PAN is the SPOT panchromatic image, and HRV is the multispectral data with numerical subscripts for waveband index. The study concluded that the weighted average method ( $I_c$ ) consistently produced results as good as or better than the others. The effectiveness of this weighted average method ( $I_c$ ) was attributed to the greater histogram similarity between the calculated ( $I_c$ ) and the original ( $I_o$ ) intensity components. However, some points in the results were left



undiscussed. For instance, while the histogram of  $I_c$  correlated extremely well to that of the panchromatic image except with a moderate shift to higher values, it did not have any resemblance to that of the original  $HRV_3$  image. This indicated that the coefficient (2/3) for the PAN image in equation [3-7] significantly exaggerated the effect of the panchromatic image in the  $I_c$  component, implying not only a duplication of the panchromatic information, but also a significant loss of radiometric information for the  $HRV_3$  image in the merging process. In addition, the great similarity between the histograms of intensity  $I_c$  and the panchromatic image suggested that a direct replacement of the intensity component ( $I_o$ ) by the panchromatic image, as used in many other studies, is workable in an IHS transform.

In response to a broad array of diverse approaches which have been used to merge multiresolution datasets, several methods to combine multiresolution images were evaluated by Chavez et al. (1991) using statistical, visual, and graphical comparisons. More specifically, those different combining methods included the IHS transform, the PCA method, and the high-pass (spatial) filtering (HPF). For the Landsat TM and SPOT panchromatic datasets used in the study, a contrast-stretching procedure was applied to the SPOT panchromatic image in an attempt to increase (arbitrarily scale up) the radiometric variance. Then, in the IHS method, the intensity component transformed from Landsat TM images was simply

replaced by the contrast-stretched panchromatic image during the IHS reverse transformation. In the PCA method, the stretched panchromatic image was assumed to be similar to the first principal component transformed from the Landsat TM images of all six wavebands (excluding the TIR waveband), while in the HPF method, a high-pass filter was applied to the contrast-stretched panchromatic image to extract the high frequency spatial information which was merged to each of the six Landsat TM images through a pixel-by-pixel addition method.

Color composites generated by all three methods were subjected to visual comparisons. Statistical correlation analyses were conducted between the first principal component of Landsat TM six-waveband data, the IHS intensity component and the contrast-stretched panchromatic image. Spectral signatures from five selected land-use types were graphically compared between the original Landsat TM data and the merged datasets by the IHS transform and HPF method. Chavez et al. (1991) concluded that, though the IHS method produced the best color composite among the three methods, it distorted the spectral characteristics of the merged images the most. For the HPF method, the merged images possessed the spectral characteristics comparable to those of the original Landsat TM data. The distortion of spectral information by the IHS method was attributed to the fact that the customary assumption of similarity between the IHS intensity component



and the panchromatic image is not always valid. When one examines the implicit spectral requirements (in a decreasing order of spectral bandwidth for the I, H, and S components) by the IHS transform as discussed by Haydn et al. (1982), it is not surprising to recognize that the distortions of spectral integrity would be inevitable in the transformed I, H, and S components. Note that the requirement for decreasing spectral bandwidths for the I, H, and S components would generally result in the numerical values of those components being in the same order. In using the IHS transformed data for post-merging applications other than color composites, these distortions of spectral information cause a serious concern about the utility and effectiveness of a merged dataset for multispectral analyses.

#### Other Enhancement Methods

There were some other cases in which multiresolution merging was used for purposes other than image enhancement. It is worthwhile to discuss these methods because of their pertinence to the subject of merging multiresolution datasets. The practical importance of digitally merging multiresolution datasets for image data compression purpose was investigated by Schowengerdt (1980). He contended that the data volume for storage and transmission can be significantly reduced if a high spatial resolution multispectral dataset can be constructed by combining a high spatial resolution image with

a relatively low spatial resolution multispectral dataset. With that argument in mind, the spatial resolution of the Landsat MSS images of wavebands four (green), six (NIR), and seven (NIR) with the original 80-m spatial resolution was artificially degraded by a linear factor of three to a 240-m spatial resolution dataset. The original 80-m resolution image of waveband five (red) remained unchanged and was used as the high spatial resolution image. Assuming that an image consists of both spectral and spatial components, the following merging equations were proposed

$$MI_i = MSS_i + k_i * H_5 \quad [3-10]$$

and

$$k_i = \sigma_i / \sigma_5 \quad [3-11]$$

where  $MI_i$  is the reconstructed image,  $i$  (and subscript 5) is waveband index,  $H_5$  is the high frequency spatial information, and  $\sigma$  is the image-wide standard deviation. The high frequency spatial component ( $H_5$ ) was obtained by a subtraction between the low-pass and the high-pass filtered images of waveband five. New images with a 80-m spatial resolution were reconstructed through pixel-by-pixel manipulations using equations [3-10] and [3-11]. Visual evaluation of the reconstructed images indicated that a great deal of high frequency information (edges) could be restored except for vegetation-dominated areas where a reverse tonal appearance

was indicated. Waveband five was selected as the high spatial resolution image because it had the greatest contrast. This selection of waveband five would make the  $k_i$  values by equation [3-11] smaller than 1.0 because  $\sigma_5$  is the largest. Consequently, equation [3-10] implicitly emphasizes the multispectral images, making it possible for the merged datasets to maintain the spectral characteristics of the original multispectral data.

The utility of an IHS transform for image data compression was also studied by Haydn et al. (1982) using Landsat MSS wavebands four (green), five (red), and seven (NIR). The hue and saturation components transformed from the three Landsat MSS images were each arbitrarily degraded. The spatial resolution was reduced by linear factors of two, four, and six which corresponded to data compression factors of four, sixteen, and thirty-six, respectively. Color composites were regenerated for each data compression factor using the degraded H and S components along with the original I component. Visual comparisons of the regenerated color composites to that of the three original wavebands did not indicate substantial quality deterioration except for the case which had a data compression factor of thirty-six or a 6x linear resolution factor.

A half-pixel shifting method to improve the effective spatial resolution of remote sensing data was studied by Dye and Wood (1989). They argued that, for a given pixel in a

scene imaged twice over a time period, both its numerical value and geographic location would not be identical because of the potential offset (error) in sampling the pixel by the sensor. Therefore, if one of the two images in a dataset is artificially offset half a pixel before the two images are combined together, the resultant merged image will increase its spatial resolution by a linear factor of two. From the viewpoint of data sampling technique, this method is very interesting. However, in the remote sensing monitoring of land-use activities, the concept may not be valid or even logical when considering the time lapse in image acquisition and the spectrally dynamic changes in natural environments. In a study using artificial as well as satellite images, Albertz and Zelianeos (1990) pointed out the following requirements necessary for this half-pixel shifting method to be successful: (1) the scene must be imaged several times--preferably more than four; (2) there will be no significant changes in the scene environments (spectrally static objects); and (3) image geo-referencing or co-registration must be very accurate in order to have the precise half-pixel offset.

With the advent of geographic information systems (GIS) techniques, various types of geographical data including existing map data and multi-date imagery data have been integrated during an image processing scheme. However, the main purpose of such image processing efforts is to detect changes rather than to improve the spatial and radiometric



qualities of the final results. To improve agricultural land-use classification, Lo et al. (1986) combined two Landsat MSS scenes acquired in different growing seasons. The two scenes were co-registered and some waveband ratioing was undertaken before invoking land-use classification procedures. Using this multitemporal approach, the land-use classification by an unsupervised classification scheme was improved from 84% to 86%. However, it is arguable that the information accumulated from the two scenes and the use of more spectral wavebands would definitely be a factor contributing to the improvement of classification results. A similar study for corn-soybean field classifications was conducted by Badhwar et al. (1982) using Landsat MSS data.

There are many other examples that involved the use of satellite imagery data and thematic overlay techniques. For instance, the study by Walsh et al. (1990) combined Landsat TM images with digital elevation model (DEM) data to study the hydrological processes in rugged terrain environments, and that by Shih (1988) who combined Landsat MSS data with the digitized version of the United States Geological Survey (USGS) land use/land cover maps within a GIS environment for land-use classification comparisons.

#### Summary: Assessment of Problems

Many studies have been made to develop image processing techniques to combine multiresolution images for remote

sensing applications. Opportunities exist to improve the interpretability of satellite image datasets for the management and monitoring of natural resources and the environment. In summary, these efforts have demonstrated the following aspects.

1. The IHS transform is a powerful and effective method for generating true color composites of good quality under a broad range of data characteristics. The effectiveness of the IHS transform has indicated a virtually universal adaptability to any geographic datasets. As compared to the direct RGB color display system, the IHS transform is superior because it can overcome the incompatibility of spectral information content of satellite multispectral images. This makes the IHS transform more likely to produce well balanced color composites that are more suitable for image interpretation. However, the effectiveness of the IHS transform has misled many to believe that it is a powerful image processing technique that can actually sharpen the image data. Unfortunately, it is not. The process is only for the display of colors for human aesthetic pleasure. The merged images by the IHS transform are not useful for multispectral analyses because of the inferior radiometric quality and corrupted spectral integrity.

2. Many combining methods have been developed that vary significantly in the basic principle as well as in the complexity of merging algorithms. These methods can be



categorized as: (1) linear combination of images, (2) principal component analysis, (3) regression technique which is similar to linear combination, and (4) multiplication or product (including square-root of product). Though arbitrary and largely dependent on speculation, these methods provide knowledge about merging multiresolution images. The studies by Schowengerdt (1980), Cliche et al. (1985), Price (1987), Carper et al. (1990), and Chavez et al. (1991) suggest that combining multiresolution images by linear combination of images would have a greater potential for multiresolution processing. The multiplication and principal component analysis methods are perceived as ineffective.

3. The lack of understanding of the principle of multiresolution processing is ubiquitous, resulting in wide speculation for merging algorithms. The fundamental problem is that the effects of combining multiresolution images on the radiometric, spatial, and spectral qualities of a merged dataset were not well understood when a merging algorithm was introduced. Frequently, efforts resulted in radiometrically inferior and spectrally corrupted merged datasets. A good merger should take full advantage of the spatial and spectral benefits of the multiresolution images to create a merged dataset.

4. The main attention of research efforts was given to image color display rather than to the radiometric and spatial enhancement and, the spectral integrity of merged datasets.

In remote sensing applications, achieving the best color display is necessary and often very useful for many applications, but it is not the ultimate nor the only goal of combining multiresolution datasets. Instead, the merged images should be sharpened radiometrically while the spectral integrity is preserved to enhance the utility of merged datasets.

5. Visual assessment, which is necessary for evaluating the quality of color composites, is adopted in most cases as the only technique for determining the qualities of merged datasets. However, the subjectivity and great variability of the technique make many of the efforts inconclusive.

6. One other problem not discussed in the literature is the accuracy of image co-registration. In order to merge multiresolution images correctly, an accurate co-registration is required, particularly for high spatial resolution datasets as well as for images which are not taken simultaneously. For instance, if two images are not co-registered accurately, a pixel of one land-use type will be merged with a different land-use type and the merged pixel belongs to neither of the original land-use elements. This makes the merged dataset very difficult or even impossible to interpret and analyze. Therefore, both the precision of intermediate references (e.g. maps) and the methods of entering (or digitizing) reference coordinates must also be addressed (ASPRS, 1990; Bolstad et al, 1990; and Tan and Shih 1991b). For the current map

standard, which is 0.5 mm (1/47 inch) times the reciprocal of map scale (APSRs, 1990; Bolstad et al., 1991), the geographical error for the USGS 7.5 minute series maps (1:24,000) is about 13 m and the digitizing process could introduce additional errors of significant magnitude (Tan and Shih, 1991b). Therefore, it will be necessary to utilize high-precision techniques such as the global positioning system (GPS) to bypass the intermediate reference (map) as well as manual digitizing operations in order to achieve a high accuracy registration or to use datasets acquired by a satellite sensor equipped with onboard co-registration capability.

7. To merge multi-date images creates another problem in evaluating the techniques of multiresolution processing. Because of the dynamic change of scene environments, it is difficult to analyze the merged data due to the intermingling of image spectral information with the temporal effects. This is particularly important for agricultural lands, as well as natural environments, because they can change rapidly within a short period of time. When multi-date scenes are combined, the merged dataset will naturally contain more information than any of the original ones. Therefore, it will be difficult to objectively assess the possible improvement as well as to evaluate the processing techniques. While the temporal effects could be used for improving land-use

classifications (Badhwar et al. 1982; Lo et al., 1986), it does create difficulties in evaluating the technique.

Fortunately, future satellite sensor systems can provide simultaneous multiresolution sensing capabilities as well as onboard image co-registration techniques (Spotlight, 1991; EOSAT, 1992a; 1992b). Therefore, the problems with multirate merging and image co-registration will no longer be a concern to the user community of future satellite remote sensing data.

## CHAPTER 4

### PRINCIPLE OF MERGING IMAGES

This chapter is focused on the principle of merging satellite remote sensing images. After the fundamental principle is presented and discussed, three merging methods are examined. However, the demonstrations and discussions of the effectiveness of the merging methods are provided in chapter 5 using actual satellite images.

#### Principle of Merging Images

Merging multiresolution images requires the use of arithmetical manipulations to digitally combine the image data. An effective merging approach will take full advantage of the spectral, spatial, and radiometric merits of the images to be combined to generate merged image data with enhanced qualities. To develop successful merging methods for remote sensing applications of multiresolution image datasets, an adequate understanding of the fundamental principle for digital manipulations of image data is essential. Therefore, to assist such efforts in exploring this principle, it is advantageous to conceptualize remote sensing image data so that the factors affecting the spatial, radiometric, and spectral qualities of merged images can be identified, evaluated, and assessed.



### Assumptions

A digital image can be considered as a set of repetitive digital numbers that are constrained to a spatial arrangement which is determined by the relations of objects present in the scene. In virtually all image processing efforts, this spatial arrangement is not important because it serves only to reveal where an object or activity is identified rather than to indicate how and why the decision is made in the process. Therefore, a digital image is similar to a random variable. The numerical values of a remote sensing image, which are often called digital counts (DC), have a distribution depicted by the image histogram.

The radiometric variance of an image is an important indicator of the image radiometric quality, and like a random variable, it can be assessed by the variance of image data. For a given scene environment, a larger radiometric variance indicates that scene activities are recorded in more detail. Throughout this dissertation, the term "radiometric variance" will exclusively refer to those image data that have not been subjected to procedures such as spatial filtering and contrast-stretching discussed in chapter 3.

The assumption that an image is similar to a random variable will allow the statistical variation analyses of random variable manipulations to be applicable to image data. From previous research efforts by Cliche et al. (1985); Price (1987); and Carper et al. (1990), the method of linear



combination of images was considered to have the greatest potential for multiresolution processing. Therefore, attention will be given to these combining methods, which will include summation and differencing of image data. To better understand the benefits as well as to assess the drawbacks from manipulating remote sensing images, the arithmetical functions of summation and differencing of random variables for statistical variation analyses will be briefly reviewed. Such a review is necessary in order to understand the existing merging techniques as well as to develop new merging methods so that remote sensing images can be manipulated more productively. For the purpose of clarity, continuing discussions will be limited to the circumstance of merging two random variables or images, though three or more variables can be manipulated at one time. Also, images with the same spatial resolution will be examined first before proceeding to the discussion of multiresolution merging.

#### Arithmetic of Random Variables

It is necessary to examine the arithmetical functions of random variables to effectively investigate the various forms of digital manipulations of image data and to assess the results of such manipulations. According to Mood et al. (1974) and Mendenhall et al. (1986), combining (both summing up and differencing) two random variables  $X_1$  and  $X_2$  with means  $\mu_1$  and  $\mu_2$  and variances  $\sigma_1^2$  and  $\sigma_2^2$ , respectively, will create

a merged variable (Y) which is expressed in a general form of

$$Y = \alpha X_1 \pm \beta X_2. \quad [4-1]$$

This new variable Y will have a mean value ( $\mu_y$ )

$$\mu_y = \alpha \mu_1 \pm \beta \mu_2 \quad [4-2]$$

and a variance ( $\sigma_y^2$ )

$$\sigma_y^2 = \alpha^2 \sigma_1^2 + \beta^2 \sigma_2^2 \pm 2 \alpha \beta \text{cov}(X_1, X_2) \quad [4-3]$$

where  $\alpha$  ( $>0$ ) and  $\beta$  ( $>0$ ) are numerical constants and  $\text{cov}(X_1, X_2)$  is the covariance between  $X_1$  and  $X_2$ . In digitally combining images, Y is the merged image,  $X_1$  and  $X_2$  represent images one and two to be combined, and the corresponding constants  $\alpha$  and  $\beta$  are often called weighting factors or merging coefficients. The covariance  $\text{cov}(X_1, X_2)$  term in equation [4-3] can be written as (Mendenhall et al., 1986)

$$\text{cov}(X_1, X_2) = r \sigma_1 \sigma_2 \quad [4-4]$$

where  $\sigma_1$  and  $\sigma_2$  are the standard deviations and  $r$  is the correlation coefficient for  $X_1$  and  $X_2$ . The value of  $r$  can be negative or positive depending on the actual relationship between variables  $X_1$  and  $X_2$ . Substituting the covariance of equation [4-4] into equation [4-3] will yield

$$\sigma_y^2 = \alpha^2 \sigma_1^2 + \beta^2 \sigma_2^2 \pm 2 \alpha \beta r \sigma_1 \sigma_2 \quad [4-5]$$

which is the equation for calculating/estimating the variance of a merged variable based on the merging coefficients, the

variances (or standard deviations), and the correlation coefficient for  $X_1$  and  $X_2$ .

For a merged image, the quality factor of greatest concern is the contrast (or gray shades), and the contrast of an image is directly related to the variance of image radiometric data. For instance, an image will have no contrast if its radiometric variance is zero. Therefore, attention in the continuing discussion will be given to the variance ( $\sigma_y^2$ ) of merged variable  $Y$ . From equation [4-5], the factors that collectively affect the radiometric variance or contrast of a merged image are the weighting coefficients  $\alpha$  and  $\beta$ , the correlation coefficient ( $r$ ), and the variances ( $\sigma_1^2$  and  $\sigma_2^2$ ) of the two images to be combined.

To assist the efforts in examining the effects of these various factors on the variance ( $\sigma_y^2$ ) of merged variable  $Y$ , it would be advantageous to reduce the number of the involved elements in equation [4-5]. One method to achieve that is to normalize the variances of  $X_1$  and  $X_2$  to unity (1.0) using the following equation

$$\underline{\sigma}_1^2 + \underline{\sigma}_2^2 = 1 \quad [4-6]$$

where  $\underline{\sigma}_1^2$  and  $\underline{\sigma}_2^2$  are the normalized variances for  $X_1$  and  $X_2$ , respectively. If the condition  $\sigma_1^2 + \sigma_2^2 \neq 0$  is satisfied,  $\underline{\sigma}_1^2$  and  $\underline{\sigma}_2^2$  are defined, respectively, as

$$\underline{\sigma}_1^2 = \frac{\sigma_1^2}{\sigma_1^2 + \sigma_2^2} \quad [4-7]$$

and

$$\underline{\sigma}_2^2 = \frac{\sigma_2^2}{\sigma_1^2 + \sigma_2^2}. \quad [4-8]$$

For easy comparisons, let  $\sigma_y^2$  also be normalized to  $(\sigma_1^2 + \sigma_2^2)$  by the following equation

$$\underline{\sigma}_y^2 = \frac{\sigma_y^2}{\sigma_1^2 + \sigma_2^2} \quad [4-9]$$

where  $\underline{\sigma}_y^2$  is the normalized variance of Y. Note that the normalized values are a relative measure for the variances of  $X_1$ ,  $X_2$ , and Y. Dividing equation [4-5] by  $(\sigma_1^2 + \sigma_2^2)$  and making rearrangements through the use of equations [4-6], [4-7], [4-8], and [4-9] will yield

$$\begin{aligned} \underline{\sigma}_y^2 = & \alpha^2 \underline{\sigma}_1^2 + \beta^2 (1 - \underline{\sigma}_1^2) \\ & \pm 2 \alpha \beta r \underline{\sigma}_1 \sqrt{(1 - \underline{\sigma}_1^2)}. \end{aligned} \quad [4-10a]$$

Because the variances of  $X_1$  and  $X_2$  are normalized to unity, equation [4-10a] can also be written as

$$\begin{aligned} \underline{\sigma}_y^2 = & \alpha^2 (1 - \underline{\sigma}_2^2) + \beta^2 \underline{\sigma}_2^2 \\ & \pm 2 \alpha \beta r \underline{\sigma}_2 \sqrt{(1 - \underline{\sigma}_2^2)} \end{aligned} \quad [4-10b]$$

where

$$\underline{\sigma}_1 = \sqrt{(\underline{\sigma}_1^2)} \quad [4-11a]$$

$$\underline{\sigma}_2 = \sqrt{(\underline{\sigma}_2^2)}. \quad [4-11b]$$

Three benefits result from normalizing the variances of  $X_1$  and  $X_2$ . These benefits are (1) reduction of the number of the involved factors in equation [4-5]; (2) relief from getting involved with actual image data for conceptual discussions; and (3) easy comparison of the variance of the merged variable with those of the original variables. It becomes clear that equation [4-10a] (or [4-10b]) is the basic relation that reflects the effects of the various factors ( $\alpha$ ,  $\beta$ ,  $r$ , and  $\sigma$ ) on the radiometric variance or contrast ( $\sigma_y^2$ ) of a merged image.

A comparison of the relations between equations [4-1] and both [4-10a] and [4-10b] reveals that the only distinction between summation and differencing of two variables is the  $\pm$  sign for the last terms in equations [4-10a] and [4-10b]. Therefore, in the context of evaluating the variance of the merged variable, differencing two negatively correlated variables ( $r < 0$ ) is technically identical to summing up two positively correlated ones ( $r > 0$ ). Because merged image data must be positive, differencing two images may require the addition of a positive constant ( $C$ ) to the end of equation [4-1] such that

$$Y = \alpha X_1 - \beta X_2 + C \quad [4-12]$$

in order to avoid negative image data. However, from the relations of equation [4-10], the constant  $C$  in equation [4-12], which is usually determined by a pre-merging scanning of



the given image data, will not affect the radiometric variance of the differenced image.

In practical applications where two images are given, the radiometric variances ( $\sigma_1^2$  and  $\sigma_2^2$ ) and the correlation coefficient ( $r$ ) are known. The only factors that need to be determined for equation [4-1] are the merging coefficients  $\alpha$  and  $\beta$ . From the relations of equation [4-10] and based on the given factors  $\sigma_1^2$ ,  $\sigma_2^2$ , and  $r$ , the selection of appropriate merging coefficients  $\alpha$  and  $\beta$  for equation [4-1] is the key factor that affects the radiometric variance of merged image data. To assess the impacts of these merging coefficients ( $\alpha$  and  $\beta$ ) on the radiometric variance of merged images, three approaches for digitally combining images will be discussed. In addition, of the two images ( $X_1$  and  $X_2$ ) to be combined,  $X_1$  will be denoted as the primary image and  $X_2$  as the secondary image in order to distinguish their relative importance in the merging process. When actual image data are used, the primary image ( $X_1$ ) will be assumed to contain primary information while the secondary image ( $X_2$ ) is used as the supplementary data for improving the primary image.

#### Confining Method

The first method to be discussed is the confining method which is defined mathematically as

$$Y_c = \alpha X_1 + \beta X_2 \quad [4-13]$$

where  $Y_c$  is the merged image by the confining method,  $X_1$  and  $X_2$  are, respectively, the primary and secondary images, and  $\alpha$  and  $\beta$  are weighting coefficients. An unique aspect in combining images is to keep the merged image data within the 0-255 dynamic range (or 8-bit data depth). One approach to accomplish that requirement is to choose the weighting coefficients  $\alpha$  and  $\beta$  in equation [4-13] such that

$$\alpha + \beta = 1 \quad [4-14a]$$

which can be written alternatively in the following forms of

$$\alpha = 1 - \beta \quad [4-14b]$$

and

$$\beta = 1 - \alpha. \quad [4-14c]$$

Because the merged image data is automatically confined to the 0-255 dynamic range, this merging method is called the confining approach.

Let  $\sigma_1^2$  and  $\sigma_2^2$  denote the normalized radiometric variances for the primary ( $X_1$ ) and secondary ( $X_2$ ) images, respectively. Because the general purpose to combine images is to use the complementary secondary image data for improving the primary image, the weighting coefficient  $\beta$  for the secondary image will be of greater interest. For this reason, the relation of equation [4-14b] is preferred and by substituting it into equation [4-13], the following relation

is obtained as

$$Y_c = (1-\beta) X_1 + \beta X_2. \quad [4-15]$$

In comparing equation [4-15] with the relations between equations [4-1] and [4-10a] (or [4-10b]), the normalized variance ( $\sigma_c^2$ ) of merged image  $Y_c$  can be estimated by the following equation

$$\begin{aligned} \sigma_c^2 = (1-\beta)^2 \sigma_1^2 + \beta^2(1-\sigma_1^2) \\ + 2r(1-\beta)\beta \sigma_1 \sqrt{(1-\sigma_1^2)}. \end{aligned} \quad [4-16a]$$

Since the variances of  $X_1$  and  $X_2$  are normalized to unity, equation [4-16a] can also be written as

$$\begin{aligned} \sigma_c^2 = (1-\beta)^2(1-\sigma_2^2) + \beta^2 \sigma_2^2 \\ + 2r(1-\beta)\beta \sigma_2 \sqrt{(1-\sigma_2^2)}. \end{aligned} \quad [4-16b]$$

The following relations for the normalization of variances are also needed in order to use equation [4-16a] or [4-16b]

$$\sigma_1^2 + \sigma_2^2 = 1 \quad [4-17]$$

$$\sigma_1 = \sqrt{(\sigma_1^2)} \quad [4-18]$$

$$\sigma_2 = \sqrt{(\sigma_2^2)}. \quad [4-19]$$

From equations [4-16a] and [4-16b], the radiometric variance ( $\sigma_c^2$ ) of an image merged by the confining method is influenced only by the secondary image coefficient  $\beta$ . The value  $\beta$  will

have a direct impact on  $\sigma_c^2$  -- a measure of the radiometric quality of a merged image by the confining method. In combining multiresolution images, selecting an appropriate  $\beta$  value is particularly important because it not only affects the radiometric variance, but also indirectly impacts the spectral information of the entire merged dataset. For instance, if a large  $\beta$  is used to merge a panchromatic image to each image in a multi-waveband dataset, all the images in the resultant merged dataset will be very similar to each other.

Assuming that the variances of the primary ( $X_1$ ) and secondary ( $X_2$ ) images are equal or close to each other, the relation of  $\sigma_c^2$  as a function of weighting factor  $\beta$  is depicted in Figure 4-1 for the confining method. Although the graphs in Figure 4-1 can tilt somewhat from one side to the other in response to the variance difference between the primary and secondary images, four important observations can be made for the confining method.

First, the radiometric variance of a merged image by the confining method is likely to be smaller than that of either the primary and secondary image data. A smaller radiometric variance implies that the merged image by the confining method will have low contrast and inferior radiometric data.

Second, the state (positive or negative) as well as the strength of correlation between the primary and secondary image images also has a strong effect on the radiometric

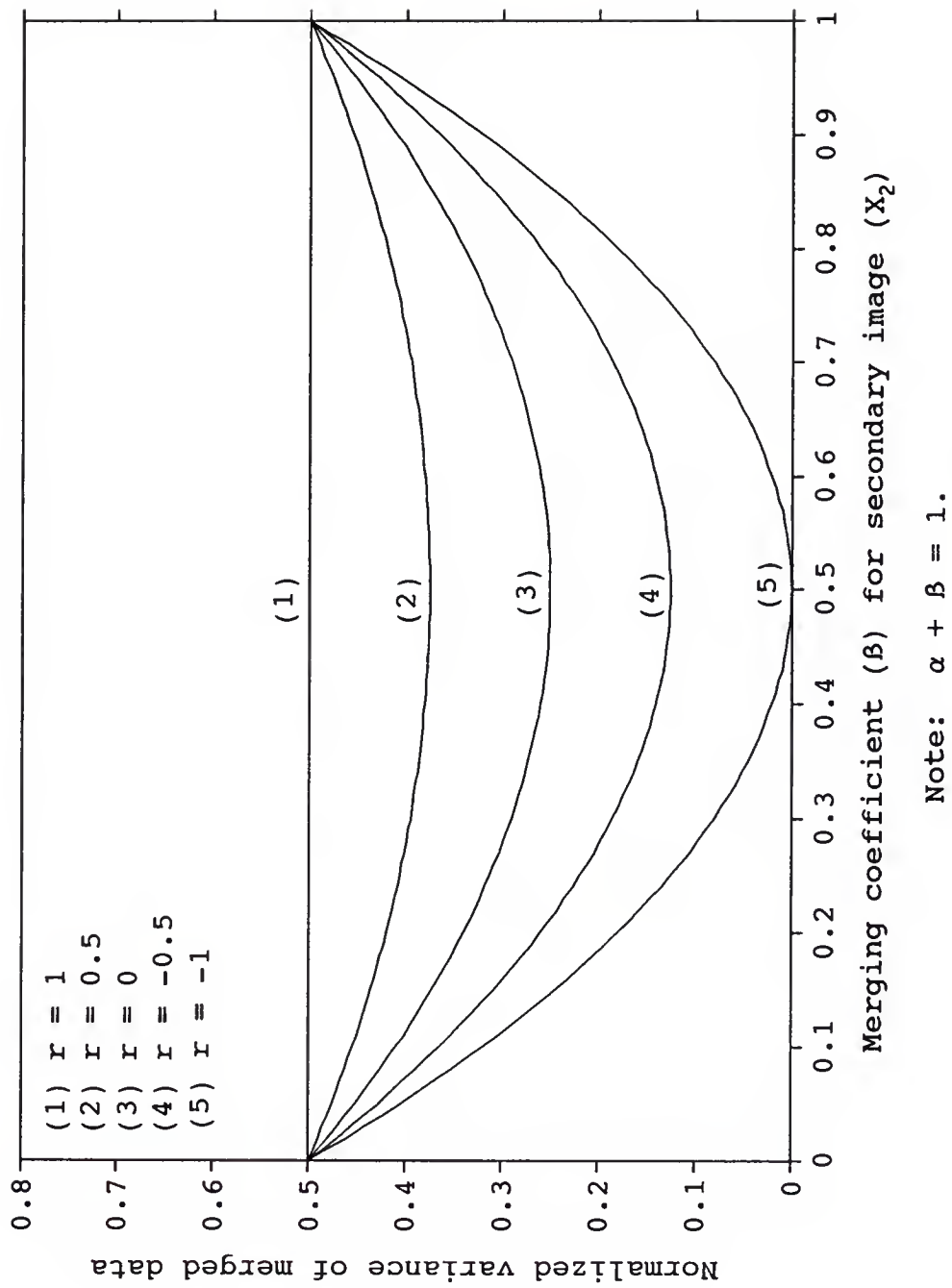


Figure 4-1. Relation of radiometric variance to merging coefficient ( $\beta$ ) and correlation coefficient ( $r$ ) for the confining method.



variance of a merged image. If the primary image is negatively correlated to the secondary image, the loss of radiometric information in the merged image ( $Y_c$ ) will be even more detrimental as shown in graphs (4) and (5) of Figure 4-1. The negative correlation ( $r < 0$ ) creates a negating effect on the variances of the primary image when the secondary image data is digitally merged. Consequently, the resultant merged image will have low or even no contrast depending on the strength of the correlation as well as the use of  $\beta$  values (Figure 4-1). As mentioned earlier, adding up negatively correlated images is similar to subtracting positively correlated ones or vice versa. If two negatively correlated images are differenced instead of summed together as done by Chavez et al. (1983), the loss of radiometric information in the merged image can be alleviated. In this circumstance, the results of graphs (4) and (5) will be changed to those of graphs (2) and (1) in Figure 4-1, respectively.

Third, a  $\beta_c$  exists at which the radiometric variance of merged data will be at minimum. That is, the merged image with  $\beta_c$  value will have least contrast. Therefore, the use of such a  $\beta$  value must be avoided when using the confining method. The value of  $\beta_c$  can be obtained by first taking the derivative of equation [4-16a] (or [4-16b]) with respect to  $\beta$

$$\begin{aligned} \frac{d(\sigma_c^2)}{d\beta} = & -2(1-\beta)\sigma_1^2 + 2\beta(1-\sigma_1^2) \\ & + 2r\sigma_1\sqrt{(1-\sigma_1^2)}(1-2\beta) \end{aligned} \quad [4-20]$$

and then setting the first derivative to equal to zero such as

$$0 = -2(1-\beta_c)\sigma_1^2 + 2\beta_c(1-\sigma_1^2) + 2r\sigma_1 \sqrt{(1-\sigma_1^2)} (1-2\beta_c). \quad [4-21]$$

Through the use of equations [4-7], [4-8], [4-9], and [4-17], the  $\beta_c$  value can be estimated by the following equation

$$\beta_c = \frac{\sigma_1^2 - r\sigma_1 \sigma_2}{\sigma_1^2 + \sigma_2^2 - 2r\sigma_1 \sigma_2} \quad [4-22]$$

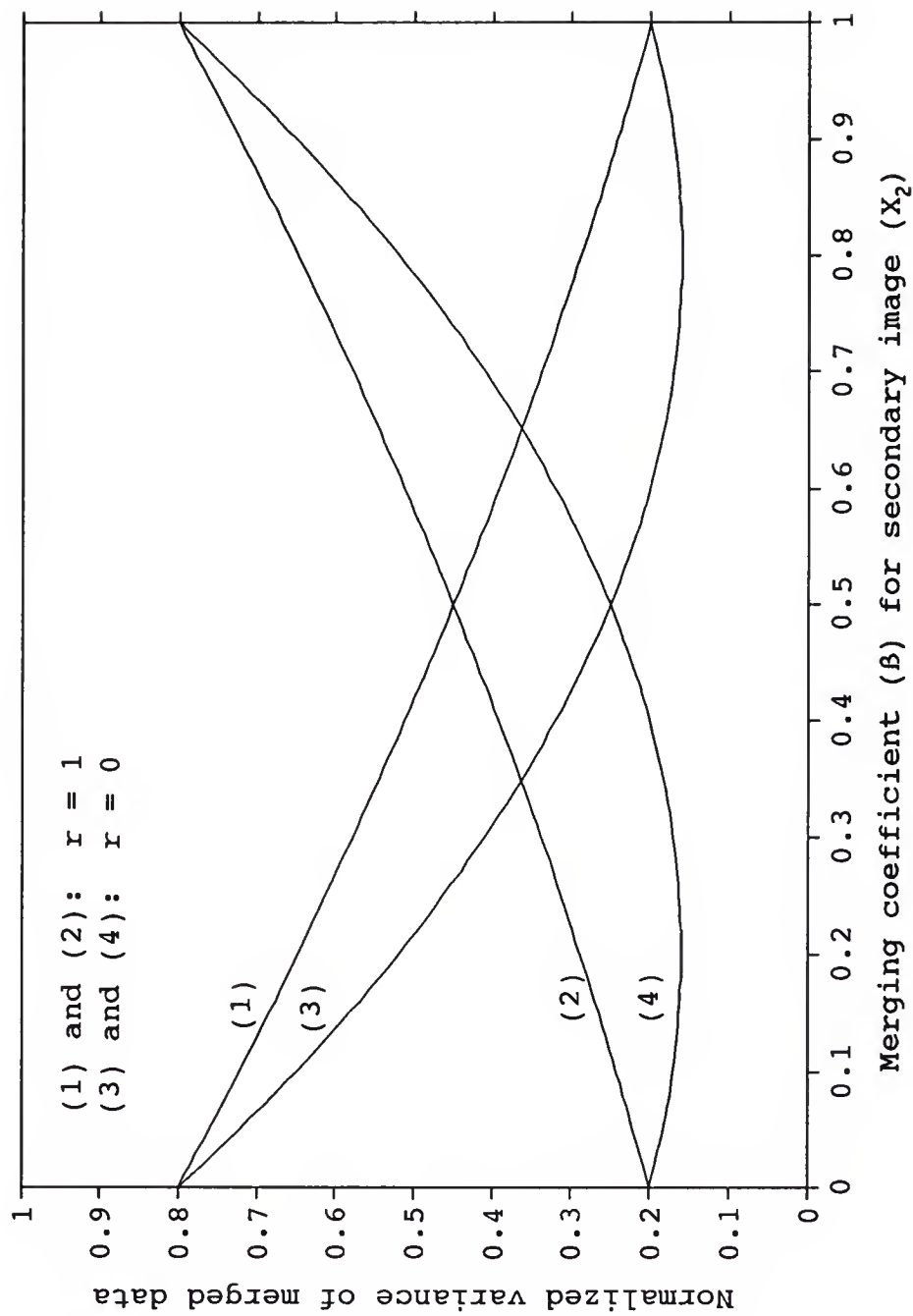
where  $\sigma_1^2$  and  $\sigma_2^2$  are the variances ( $\sigma_1$  and  $\sigma_2$  are the standard deviations) of the primary and secondary images, respectively. Note that the range of valid values for  $\beta$  is 0 to 1. If  $\beta_c$  is outside the 0-1 range, the minimum radiometric variance of a merged image will not exist within that range. Obtaining the  $\beta_c$  value before merging the images will give a first assessment on the variance of a merged image. For instance, if  $\beta_c \leq 0$ , the radiometric variance of merged data is an increasing function with  $\beta$ , implying that an improvement for image contrast is possible. If  $\beta_c \approx 1.0$ , the variance of merged data will decrease as  $\beta$  increases. As a result, the contrast of the merged image will deteriorate. By substituting  $\beta_c$  into equation [4-15a] (or [4-15b]) and by using the relations of equations [4-7], [4-8], [4-9], and [4-17], the minimum variance ( $\sigma_m^2$ ) for an image merged by the confining method can be estimated as

$$\sigma_m^2 = \frac{\sigma_1^2 \sigma_2^2 (1 - r^2)}{\sigma_1^2 + \sigma_2^2 - 2 r \sigma_1 \sigma_2} \quad [4-23]$$

Caution should be exercised in using equation [4-23] to estimate the minimum radiometric variance of a merged image. If  $\beta_c$  is not within the 0-1 range, the estimated minimum radiometric variance is a false value that cannot exist for a merged image.

Fourth, as  $\beta$  continues to increase beyond the  $\beta_c$  value, the variance of merged image  $Y_c$  is approaching that of the secondary image data. This will make the merged image more and more similar or even identical to the secondary image as a result of large  $\beta$  values, which has been indicated by Carper et al. (1990). In the case of merging a high resolution panchromatic image to a set of multispectral images, all the resultant merged images will be highly correlated among each other because of the excessively redundant panchromatic data. Consequently, the spectral integrity (or signatures) of the merged dataset will be corrupted and the effectiveness of the merged multispectral data for differentiating land-use elements will be reduced.

The variance difference between the primary and secondary images can also have an effect on the radiometric variance of a merged image as shown in Figure 4-2. For instance, if the primary image has a larger variance relative to that of the secondary image, the merged image will have less contrast regardless of the state of correlation. This is illustrated



Note:  $r$  = correlation coefficient.

Figure 4-2. Effect of variance difference on the radiometric quality of merged images for the confining method.

by graphs (1) and (3) of Figure 4-2. If the primary image has a smaller variance, the radiometric information in the merged image will either increase or decrease depending on the magnitude of the variance difference as well as the state of correlation between the two images as shown by graphs (2) and (4) in Figure 4-2. Note that only when the primary image has a very small variance relative to that of the secondary image and the correlation between the two images to be combined is high and positive, will an image merged by the confining method have an enhanced contrast. This indicates that (1) the confining method is not an effective merging approach for digitally combining images and (2) the determination of a  $\beta$  value for the confining method can not be arbitrary nor independent of the factors such as the variance difference and the correlation between the two combining images.

The way by which the merging coefficients are determined ( $\alpha + \beta = 1$ ) for the confining method has one important implication of the compromising effect on the quality of the primary and secondary images. The use of a larger  $\beta$  value to emphasize the effect of the secondary image is made at the concession of the primary image variance because of a smaller  $\alpha$  value. As shown in Figure 4-2, this concession of the primary image data can be beneficial or detrimental. If the secondary image has a relatively larger variance, this compromising effect is beneficial to improve the primary image as shown by graphs (2) and (4) in Figure 4-2. On the other hand, the effect will be



deleterious to the radiometric quality of a merged image as illustrated by graphs (1) and (3) in Figure 4-2.

In summary for the confining approach ( $\alpha+\beta=1$ ), the following observations are as follows. (1) The resultant merged image will likely have a smaller radiometric variance or lower contrast unless the primary image has a very small variance relative to that of the secondary image and the correlation between the two combining images is high and positive. (2) There may exist a  $\beta_c$  value at which the radiometric variance or contrast of the merged image will be minimum, therefore, the selection of  $\beta$  values close or equal to  $\beta_c$  should be avoided. (3) Two images with a negative correlation should be differenced rather than summed in order to minimize the loss of radiometric information. (4) In general, the contrast (or variance) and brightness of an image merged by the confining method can be considered as a compromise for each of these two quality factors between the primary and secondary images.

#### Preserving Method

For most satellite imagery, the spread of image digital data does not extend throughout the entire 0-255 dynamic range. For a typical agricultural scene, the data spread is about 40% of the 0-255 range in Landsat imagery (Price, 1984) while a much smaller range is often found for SPOT images. Therefore, the utility of the 8-bit data depth for these

images has not been fully utilized. In merging satellite images, such a deficiency can be turned into an advantage by maintaining the primary image unchanged ( $\alpha=1$ ) while the secondary image data is merged. Hence, this method is called the preserving approach.

By using the preserving approach to combine images, the following merging algorithm is used

$$Y_p = X_1 + \beta X_2 \quad [4-24]$$

where  $\beta$  is weighting coefficient,  $Y_p$  is the merged image, and  $X_1$  and  $X_2$  have been defined previously. Let  $\underline{\sigma}_1^2$  and  $\underline{\sigma}_2^2$  denote the normalized variances for the primary and secondary images, respectively. A comparison of the relations between equations [4-1] and [4-10a] (or [4-10b]) indicates that the normalized variance ( $\underline{\sigma}_p^2$ ) of an image merged by the preserving method can be estimated by

$$\underline{\sigma}_p^2 = \underline{\sigma}_1^2 + \beta^2(1-\underline{\sigma}_1^2) + 2r\beta \underline{\sigma}_1 \sqrt{(1-\underline{\sigma}_1^2)}. \quad [4-25a]$$

Since the variances of the primary ( $X_1$ ) and secondary ( $X_2$ ) images are normalized to unity, equation [4-25a] can also be written as

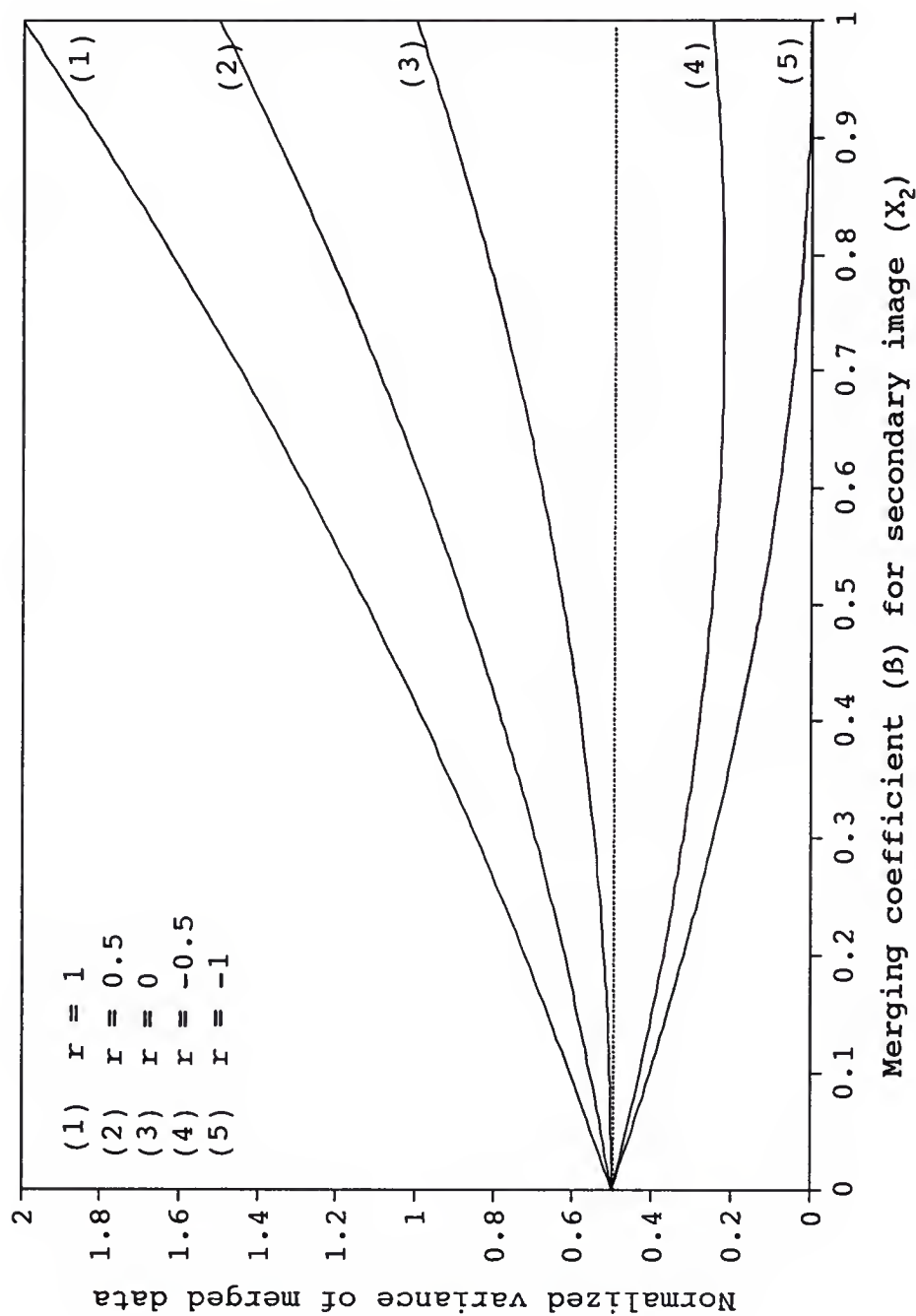
$$\underline{\sigma}_p^2 = (1-\underline{\sigma}_2^2) + \beta^2 \underline{\sigma}_2^2 + 2r\beta \underline{\sigma}_2 \sqrt{(1-\underline{\sigma}_2^2)}. \quad [4-25b]$$

In both equations [4-25a] and [4-25b],  $\beta$  is the weighting coefficient and  $r$  is the correlation coefficient for the primary ( $X_1$ ) and secondary ( $X_2$ ) images. Note that the variance

of merged image  $Y_p$  is normalized to  $\sigma_1^2 + \sigma_2^2$ . Also, the relations of equations [4-17], [4-18], and [4-19] are needed when using equation [4-25a] (or [4-25b]) for assessing the radiometric variance of a merged image. As mentioned earlier, the only distinction between summation and differencing of two images is the  $\pm$  sign for the last term of equation [4-25a] (or [4-25b]). Thus, differencing two negatively correlated images ( $r < 0$ ) is identical to summing up two positively correlated ones ( $r > 0$ ).

Figure 4-3 shows the normalized variance  $\sigma_p^2$  of merged images by the preserving method as a function of both the merging coefficient ( $\beta$ ) and the correlation coefficient ( $r$ ). When the primary and secondary images are not negatively correlated, the variance of an image merged by the preserving method is an increasing function with merging coefficient  $\beta$  as shown in graphs (1) through (3) of Figure 4-3. This implies that the radiometric variance (contrast) of an image merged by the preserving method will surely improve, provided that the correlation coefficient is  $r \geq 0$ . Unlike the confining method, which tends to make a compromise between the secondary and secondary images, the preserving method does not subdue (because  $\alpha = 1$ ) the radiometric variance of the primary image during the merging process. Consequently, the merged data are always enhanced even when the images to be combined are not correlated ( $r = 0$ ) as shown in graph (3) of Figure 4-3.

The results from combining two negatively correlated images are also shown by graphs (4) and (5) of Figure 4-3.



Note:  $\alpha=1$ , and  $\beta>0$ .

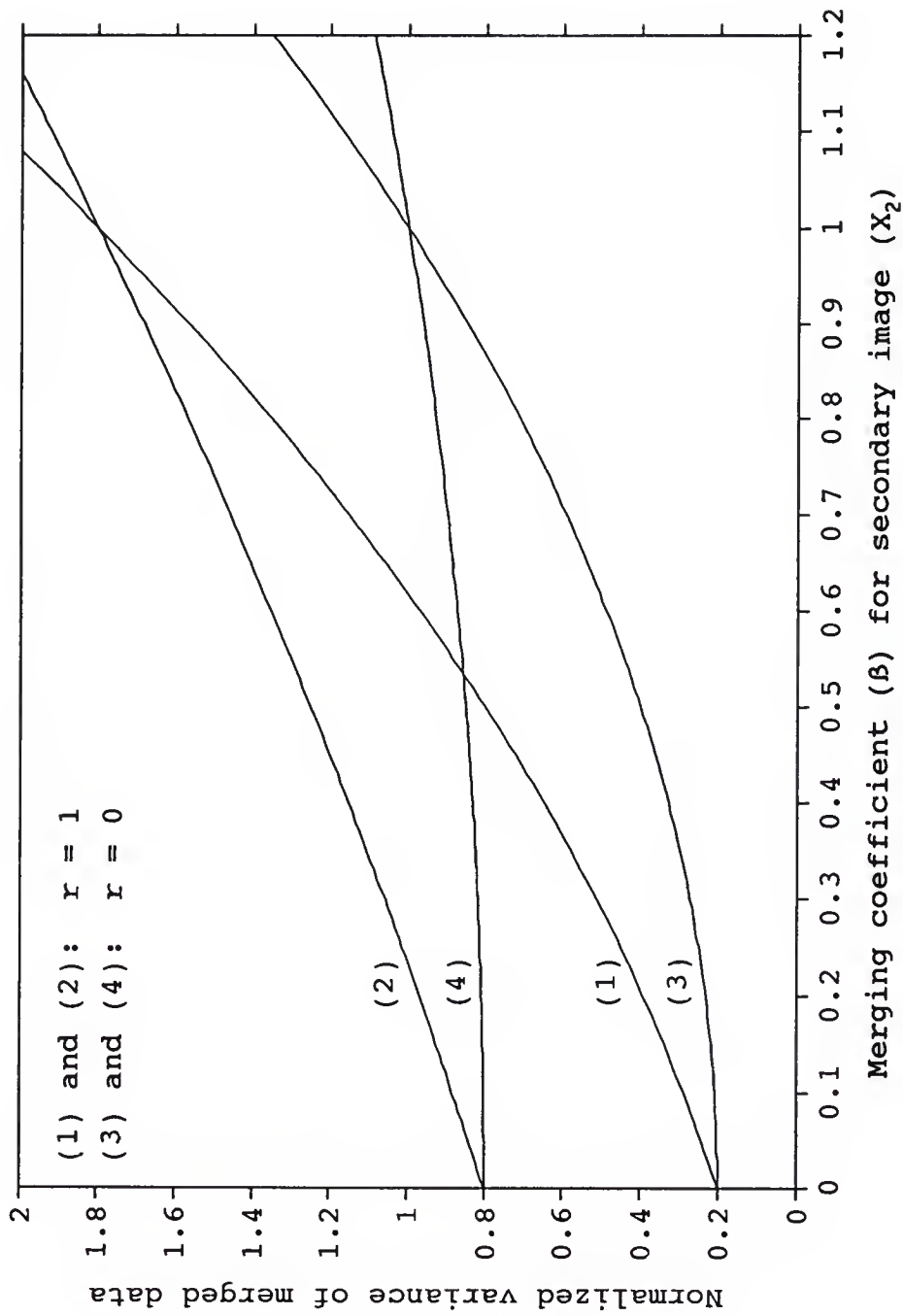
Figure 4-3. Relation of radiometric variance to merging coefficient ( $\beta$ ) and correlation coefficient ( $r$ ) for the preserving method.

Apparently, any improvement on the radiometric variance of merged image  $Y_p$  is unlikely, particularly when the correlation coefficient  $r \approx -1$ . However, such negatively correlated images can be differenced. This will reverse the results to those of summing up two positively correlated images as depicted by graphs (1) and (2) of Figure 4-3. This differencing approach will alleviate or even avoid the loss of image contrast in the merged data.

The radiometric variance difference between the primary and secondary images also has an effect on the radiometric variance of a merged image (Figure 4-4). However, the effect does not cause a negative impact on the radiometric variance of merged data. The image contrast will always improve, and the extent of improvement is inversely related to the magnitude of the variance of the primary image. When the radiometric variance of the primary image is relatively small, the improvement on the merged image is more notable as illustrated by graphs (1) and (3) of Figure 4-4. If the radiometric variance of the primary image is relatively large, the radiometric improvement might not be so apparent, particularly when the correlation between the two combining images is near zero ( $r \approx 0$ ) as shown by graph (4) of Figure 4-4.

It needs to be pointed out that large values of  $\beta$  can not be used for the preserving approach. Otherwise, a scaling factor must be introduced to equation [4-24] in order to keep the merged image data within the 0-255 range. In this case, the





Note:  $r$  = correlation coefficient.

Figure 4-4. Effect of variance difference on the radiometric quality of merged images for the preserving method.

use of an additional scaling factor will make the preserving method less effective or even similar to the confining method.

In summary, several observations are made for the preserving approach: (1) if the correlation coefficient ( $r$ ) between the primary and secondary images is non-negative ( $r \geq 0$ ), the image contrast in the merged data will surely be enhanced by the preserving method; (2) as compared to that of the confining method ( $\alpha + \beta = 1$ ), the effect of the variance difference between the two combining images will not create a negative impact on the radiometric variance of a merged image by the preserving method, provided that the correlation is non-negative ( $r \geq 0$ ); (3) the preserving method, which does not subdue ( $\alpha = 1$ ) the primary image in the digital merging process, will make it less likely that the spectral signatures of the original multispectral dataset will be altered or corrupted in a merged dataset; (4) two images with a strong negative correlation ( $r \approx -1$ ) should be differenced instead of summed together in order to avoid a potential loss of radiometric information in the merged image; and (5) the preserving method has both a much smaller sensitivity to the strength of correlation and a larger range of  $\beta$  values to use because a minimum variance does not exist provided that  $r \geq 0$ .

#### Differencing Method

From previous discussions on both the confining and the preserving methods, it is known that, in order to enhance the

radiometric variance of merged image data from negatively correlated wavebands ( $r < 0$ ), the differencing method must be used. To ensure that the merged data will be positive, a constant must be added to the merged data. Therefore, the following relation will be used as the merging equation for two negatively correlated images

$$Y_d = X_1 - \beta X_2 + C \quad [4-26]$$

where  $\beta$  ( $>0$ ) is a weighting coefficient,  $C$  ( $>0$ ) is a constant to avoid negative merged data,  $Y_d$  is the merged (differenced) image, and  $X_1$  and  $X_2$  have been defined previously.

Let  $\sigma_1^2$  and  $\sigma_2^2$  denote the normalized variances for the primary and secondary images, respectively. By comparing equation [4-26] with the relationship between equations [4-1] and [4-10a] (or [4-10b]), the normalized radiometric variance ( $\sigma_d^2$ ) of a merged image by equation [4-26] can be estimated by

$$\sigma_d^2 = (1 - \sigma_2^2) + \beta^2 \sigma_2^2 - 2r\beta \sigma_2 \sqrt{(1 - \sigma_2^2)}. \quad [4-27a]$$

Since the variances of primary and secondary images are normalized to unity, equation [4-27a] can also be written as

$$\sigma_d^2 = \sigma_1^2 + \beta^2(1 - \sigma_1^2) - 2r\beta \sigma_1 \sqrt{(1 - \sigma_1^2)}. \quad [4-27b]$$

In both equations [4-27a] and [4-27b],  $r$  is the correlation coefficient for the primary and secondary images and  $\beta$  is a weighting coefficient. Note that the variance of the merged image is normalized to the sum of the variances ( $\sigma_1^2 + \sigma_2^2$ ) of

the primary and secondary images. Again, the relations of normalization equations [4-17], [4-18], and [4-19] are needed in order to use equation [4-27a] (or [4-27b]) for estimating the radiometric variance of a pre-differenced image.

Because the last term in equation [4-27a] (or [4-27b]) is negative and the correlation coefficient ( $r$ ) is also negative, the relation of equation [4-27a] (or [4-27b]) is identical to that of equation [4-25a] (or [4-25b]) of the preserving method discussed previously. Therefore, additional information for the effects of  $\beta$  values, correlation coefficient, and variance difference on the radiometric variance of merged data can be found in the previous section for the preserving method with reference to both Figures 4-3 and 4-4.

In order for an image merged by the differencing approach to have an improved radiometric variance, it is essential that the last two terms in equation [4-27a] (or [4-27b]) be  $\geq 0$ . That is

$$\beta^2 \sigma_2^2 - 2r\beta \sigma_1 \sigma_2 \geq 0. \quad [4-28]$$

Hence, if both  $\beta \neq 0$  and  $\sigma_2 \neq 0$ , a critical  $\beta_d$  value for the differencing method can be obtained as

$$\beta_d \geq \frac{2 r \sigma_1}{\sigma_2}. \quad [4-29]$$

According to the relations of equations [4-17] through [4-19], equation [4-29] can be rewritten as ( $\sigma_2 \neq 0$ )

$$\beta_d \geq 2 \text{ r } \sigma_1/\sigma_2 \quad [4-30]$$

where  $\sigma_1$  and  $\sigma_2$  are the standard deviations for the primary ( $X_1$ ) and secondary ( $X_2$ ) images, respectively. If a  $\beta$  value is greater than  $\beta_d$ , the variance of a merged image by the differencing method will increase. Otherwise, the merged (differenced) image will have a decreased radiometric variance.

It must be pointed out that the relative magnitudes of the combining image data can have a serious impact on the tonal appearance of the merged image. Assuming that the primary image ( $X_1$ ) has relatively higher values (brighter) than the secondary image ( $X_2$ ), a subtraction by  $\beta X_2$  in equation [4-26] will be less likely to create negative values in the merged data. Therefore, a small constant is needed for equation [4-26]. This will maintain the tonal gradations of the primary image, and as a result the bright areas in the primary image remain bright while the dark areas remain dark in the merged data. When the secondary image has relatively larger values, the component of  $\beta X_2$  in equation 4-26] will not be small in comparison to the primary image ( $X_1$ ) data. This will likely create negative values of large magnitude in the merged data, requiring the use of a large constant in equation [4-26] to offset these negative values. Consequently, the areas with low values (e.g. water bodies) will have relatively large image values in the merged data because of the use of a large constant in equation [4-26]. This could make these dark



areas appear bright in the merged image ( $Y_d$ ), suggesting that the tonal gradations of the original primary image have been altered. Thus, it must be cautioned that the differencing method may invert the merged image.

#### Summary: Principle of Merging Images

The principle of merging images has been discussed under the assumption that an image is similar to a random variable with regard to digital manipulations for statistical variation analyses. Three fundamental approaches, which include the confining, the preserving, and the differencing methods, have been put forth for digitally merging image data.

Understanding these methods for digitally merging images is essential for manipulating remote sensing data. Such an understanding will render useful guidelines for evaluating the existing methods as well as for developing new effective approaches in future image processing efforts for remote sensing applications.

When two images are digitally combined, the radiometric improvements on the merged image will depend on three factors which include (1) the selection of a merging method or merging algorithm; (2) the correlation ( $r$ ) between the two combining images; and (3) the variance difference ( $\sigma_1$  and  $\sigma_2$ ) between the primary and secondary images. The confining approach should be avoided because of its ineffectiveness for radiometric enhancement. Unfortunately, this merging approach is the most

widely used method (Cliche et al., 1985; Carper et al., 1990). The preserving method is recommended for merging positively correlated images while the differencing approach is for those with a strong negative correlation. In addition, the image with a brighter appearance should be chosen as the primary image ( $X_1$ ) for the differencing method in order to avoid a potential of altering the tonal appearance in the merged (differenced) image.

A summary for the effectiveness of the three merging approaches is provided in Table 4-1 for an easy comparison. Actual satellite images will be utilized in chapter 5 to demonstrate the results discussed throughout this chapter.

Table 4-1. Summary of the characteristics of different merging approaches.

When	Radiometric improvement on merged image		
	Confining	Preserving	Differencing
i : $r \geq 0$ and			
$\sigma_1 \gg \sigma_2$	No	Yes	No
$\sigma_1 \approx \sigma_2$	No	Yes	No
$\sigma_1 \ll \sigma_2$	Yes(if $r \approx 1$ )	Yes	No
ii: $r < 0$ and			
$\sigma_1 \gg \sigma_2$	No	No	Yes
$\sigma_1 \approx \sigma_2$	No	No	Yes
$\sigma_1 \ll \sigma_2$	No	No	Yes

Note:  $r$  = correlation coefficient.

$\sigma_1$  = standard deviation of primary image.

$\sigma_2$  = standard deviation of secondary image.

## CHAPTER 5 DEMONSTRATION OF MERGING METHODS

The main objective in this chapter was to verify and demonstrate the results of the three merging methods discussed in chapter 4. To begin the process, the radiometric variance and mean brightness of merged images by the three methods were examined using the results from an actual satellite dataset. The visual appearance in both image contrast and brightness for the merged images were also evaluated.

### Satellite Image Data

A satellite scene by the advanced very high resolution radiometer (AVHRR) on a National Oceanographic and Atmospheric Administration (NOAA) series satellite was acquired for this demonstration. The satellite scene had five images recorded at the 14:05h U.S. eastern standard time on December 14, 1989 by the AVHRR sensor onboard the NOAA-11 satellite. The NOAA satellite scene consisted of two reflective (red and near-infrared or NIR) and three thermal infrared (TIR) spectral wavebands with wavelength characteristics shown in Table 5-1 (Kidwell, 1991). The scene had a local area coverage (LAC) of the entire south-eastern region of the United States and all the images of the five spectral wavebands have the same spatial resolution of about 1,000 m (Kidwell, 1991).

Table 5-1. Wavelength characteristics of NOAA-11 AVHRR LAC images.

Waveband#	Wavelength range ( $\mu\text{m}$ )	Spatial resolution
1 <sup>a</sup>	0.58 - 0.68 (red)	1000 m
2 <sup>a</sup>	0.725 - 1.10 (NIR <sup>b</sup> )	1000 m
3	3.55 - 3.93 (TIR <sup>c</sup> )	1000 m
4	10.30 - 11.30 (TIR <sup>c</sup> )	1000 m
5	11.50 - 12.50 (TIR <sup>c</sup> )	1000 m

Source: Kidwell, 1991.

<sup>a</sup> -- used in this study.

<sup>b</sup> -- near infrared.

<sup>c</sup> -- thermal infrared.



The original NOAA-11 LAC scene contained image data in a 10-bit data-depth format where every three pixels were packed to a 32-bit word (Kidwell, 1991). A program, which runs on a PC computer environment, was developed (Appendix C) to unpack as well as to rescale (linearly) these 10-bit data to a 8-bit data format for compatibility with PC-based image processing systems as well as display device. For this research, the LAC scene was clipped to the region of the Florida peninsula (Figure 5-1) and only the red and NIR images of the clipped scene were used. The images of the TIR wavebands were excluded to avoid confusions from merging thermal data. In the discussions that follow, a NOAA-11 LAC image is simply referred to the clipped data unless otherwise stated. The main usage of this clipped LAC scene was for the verifications of the three different merging methods discussed in chapter 4. For ease of explanation, the red waveband was arbitrarily named as LAC1 while the NIR waveband was denoted as LAC2. The mean, standard deviation, normalized variance, maximum, and minimum values of the LAC1 (red waveband) and LAC2 (NIR waveband) images are presented in Table 5-2. The two selected LAC images were positively correlated with a correlation coefficient ( $r$ ) of 0.577.

Because of the noted difference in the radiometric variances between the two LAC images (Table 5-2), the use of LAC1 and LAC2 for the primary and secondary images was alternated for each of the three merging methods. In case I,

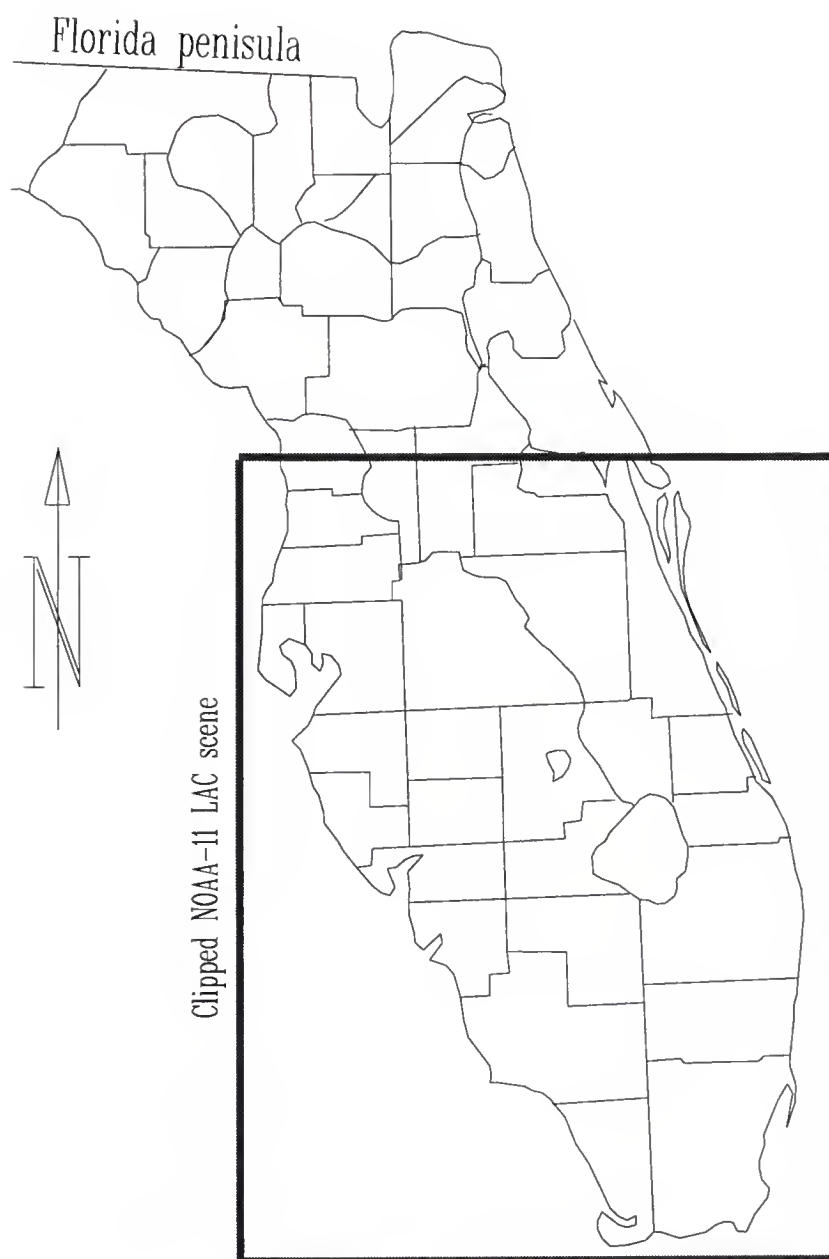


Figure 5-1. Location of clipped NOAA-11 AVHRR LAC images.

Tables 5-2. Standard deviation ( $\sigma$ ), normalized variance ( $\sigma^2$ ), mean ( $\mu$ ), maximum and minimum values of NOAA-11 AVHRR LAC images.

Waveband	$\mu$	$\sigma$	$\sigma^2$	max	min
LAC1 (0.58-0.68 $\mu\text{m}$ )	20.54	5.108	0.2286	138	14
LAC2 (0.725-1.10 $\mu\text{m}$ )	26.35	9.383	0.7714	125	11

LAC2 was used the primary image and LAC1 as the secondary image, and in case II, LAC1 and LAC2 were used, respectively, as the primary and secondary images. The purpose of this alternative use for the LAC1 and LAC2 images was to assess the effect of variance difference between the combining images on the radiometric variance of merged data. In the differencing method, the constants (C) used in equation [4-26] are provided in Table 5-3 for both case I and case II. These constant values, which were determined by a scanning of the original image data, were used to avoid negative merged image data in the differenced LAC images for the corresponding  $\beta$  values.

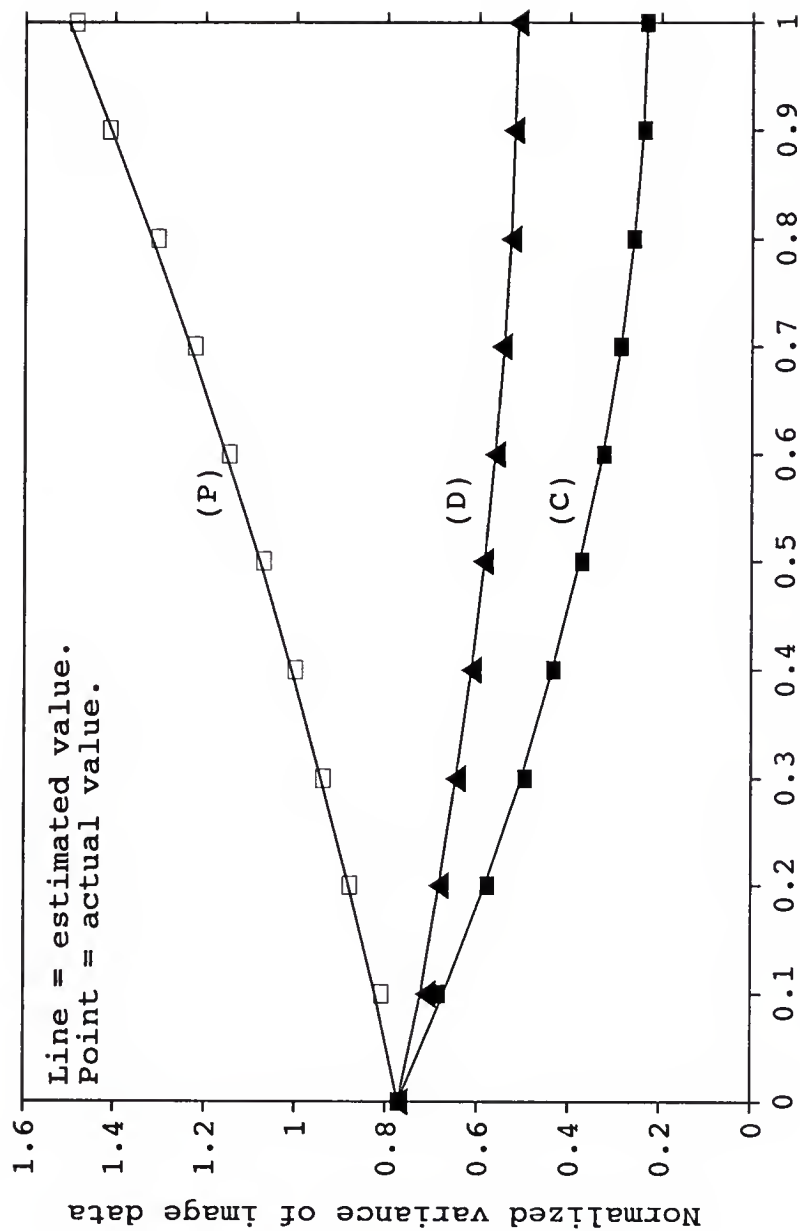
#### Variance of Merged LAC Images

The normalized radiometric variances of merged LAC images by the three methods are presented in Figures 5-2 (case I) and 5-3 (case II). In addition, the mean values (brightness) of these merged LAC images are presented in Figures 5-4 and 5-5 for case I and case II, respectively. The points in these four figures are the results computed from the actual merged image data, while the lines represent the estimates obtained through the equations in chapter 4. While the estimates of radiometric variance were obtained through equations [4-15], [4-25], and [4-27] along with the normalized variances (Table 5-2) and a correlation coefficient ( $r$ ) of 0.577, the mean digital count (Figures 5-4 and 5-5) were estimated using equations [4-13], [4-24], and [4-26] for each corresponding

Table 5-3. Offset constant (C) used in the differencing method for merging LAC images.

Case	$\beta$ value									
	0.1	0.2	0.3	0.4	0.5	0.6	0.7	0.8	0.9	1.0
I	-	-	-	-	3	7	11	15	20	24
II	-	-	-	-	-	3	5	8	10	13

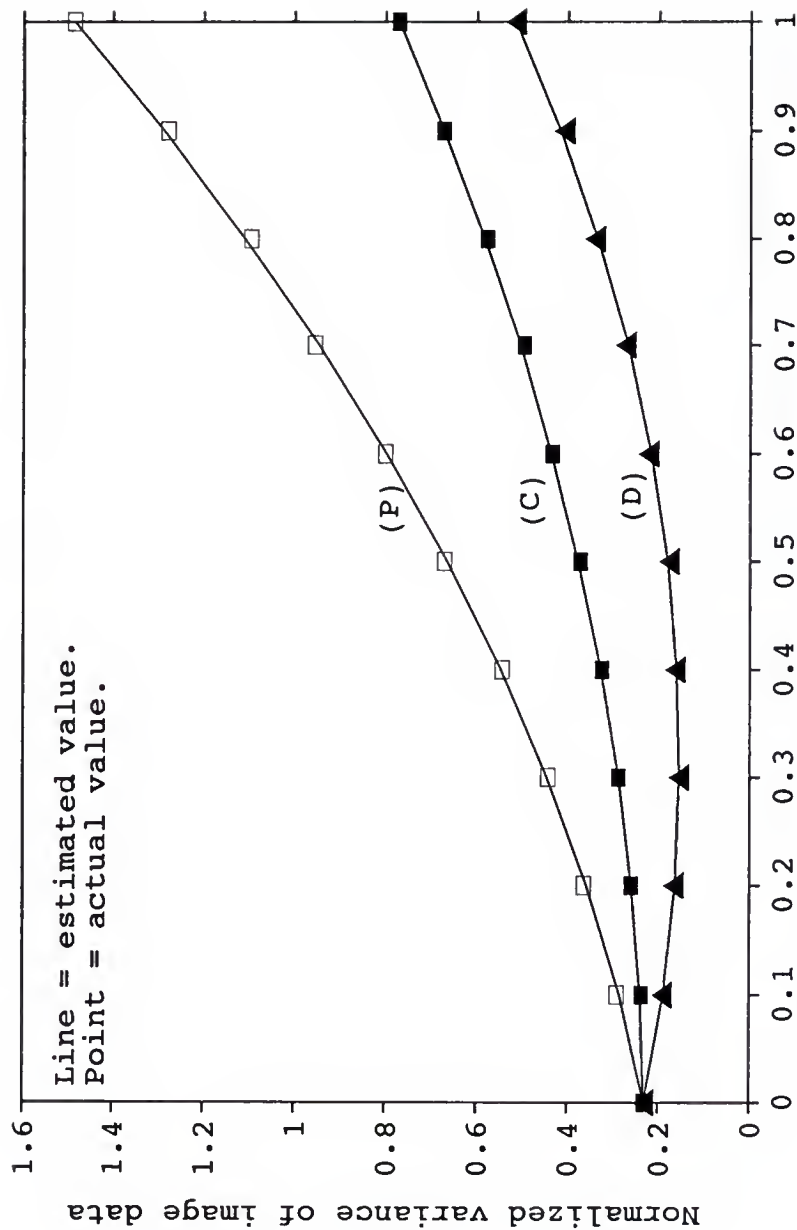




Merging coefficient ( $\beta$ ) for secondary image

Note: i. Primary image is LAC2; secondary image is LAC1.  
ii. Methods: (C) --confining; (D) --differencing; and (P) --preserving.

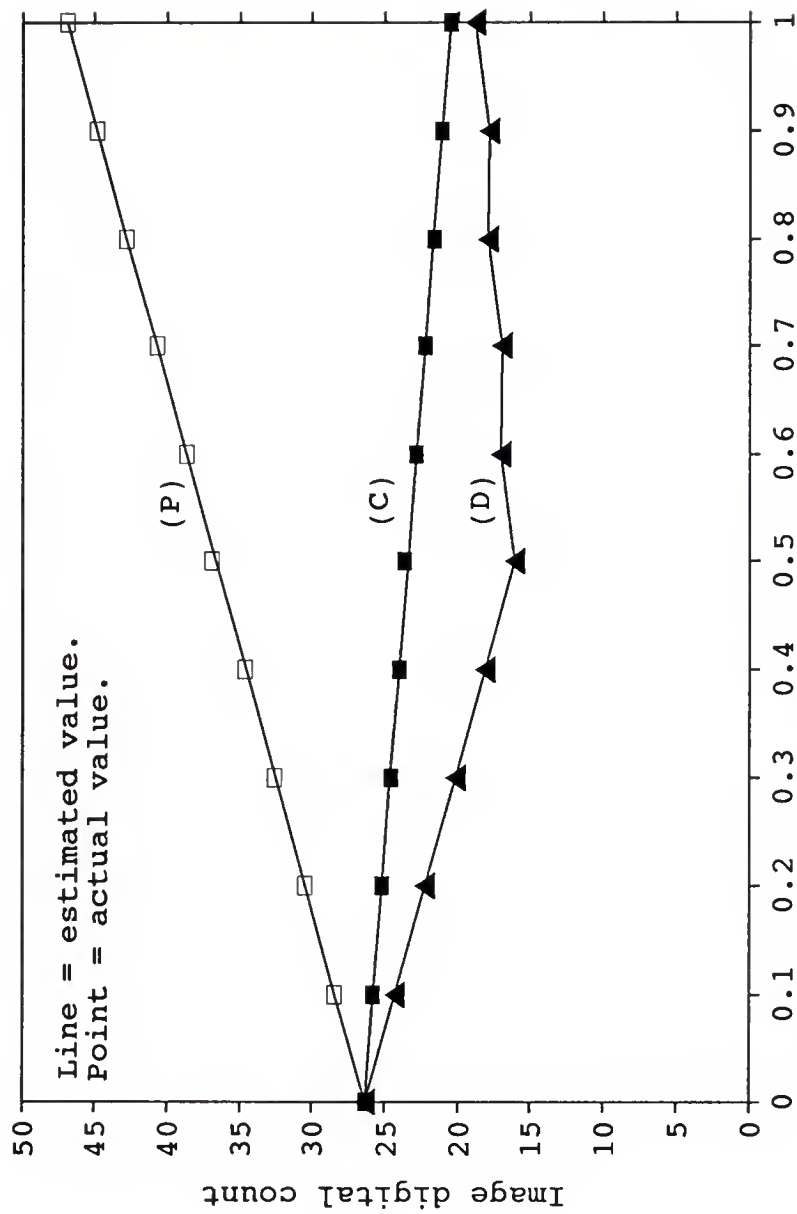
Figure 5-2. Comparison between actual and estimated radiometric variance for merged LAC images (case I).



Merging coefficient ( $\beta$ ) for secondary image

Note: i. Primary image is LAC1; secondary image is LAC2.  
ii. Methods: (C) --confining; (D) --differencing; and (P) --preserving.

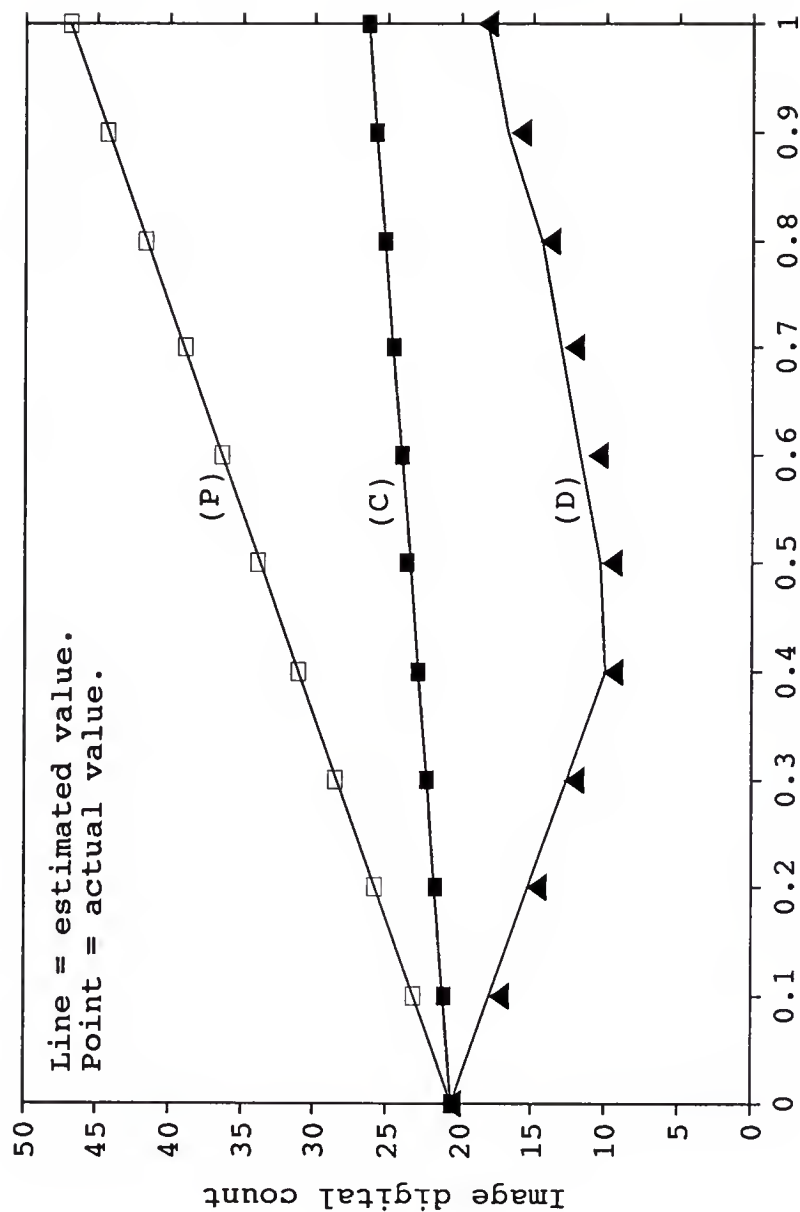
Figure 5-3. Comparison between actual and estimated radiometric variance for merged LAC images (case II).



Merging coefficient ( $\beta$ ) for secondary image

Note: i. Primary image is LAC2; secondary image is LAC1.  
ii. Methods: (C) --confining; (D) --differencing; and (P) --preserving.

Figure 5-4. Comparison between actual and estimated mean digital count for merged LAC images (case I).



Merging coefficient ( $\beta$ ) for secondary image

Note: i. Primary image is LAC1; secondary image is LAC2.  
ii. Methods: (C) --confining; (D) --differencing; and (P) --preserving.

Figure 5-5. Comparison between actual and estimated mean digital count for merged LAC images (case II).

merging method. The letters P, C, and D in Figures 5-2 through 5-5 denote the preserving method, the confining method, and the differencing method, respectively. From the results shown in Figures 5-2 through 5-5 for all the three methods and  $\beta$  values used, four observations are in order.

First, the principle of statistical variation analyses for combining random variables can be applied in assessing the radiometric quality (variance and brightness) of a pre-merged image. This provides the basis for understanding the various forms of digital manipulations of satellite image data and for assessing the effectiveness of an image processing effort in remote sensing applications. In practical applications when two images are given, the values of correlation, radiometric variance, and mean digital (brightness) for the images to be merged are known. Therefore, the overall quality in both radiometric variance (contrast) and brightness of a merged image can be evaluated based on the merging method and coefficient ( $\beta$ ). This pre-merging evaluation will lead to more efficient approaches because unproductive efforts can be eliminated.

Second, an image contains many subvariables representing the various land-use types distributed throughout the entire scene. Note that the subvariables do not usually possess the same correlation, radiometric variances, and mean data values in the images of a multispectral dataset. When a merging algorithm is used to digitally combine the entire images, the

changes in both radiometric variance and brightness might not be the same among the land-use elements. While some land-use elements will benefit with an improvement in radiometric information, others could have a quality detraction. Even for those land-use elements with an enhancement, the extent of improvement in both contrast and brightness will not be identical. Therefore, digitally merging satellite images is not simply a mathematical procedure. It is a transformation of radiometric information from the combining images into the merged data. Unfortunately, such a radiometric transformation was overlooked in previous efforts in image data merging.

Third, the non-uniform changes in radiometric quality across an entire scene can be beneficial or detrimental to an image processing effort. Therefore, an adequate understanding of the principle of digitally manipulating images is critical to selecting effective merging methods for image enhancement. Because of the importance of such a radiometric transformation in merging images, an increasing amount of knowledge for the spectral data characteristics of satellite images acquired by various sensing systems will further enhance the utility of remote sensing data.

Fourth, though the results observed here are based on the linear combination (summation and subtraction) operations of image data, the fundamental principle can be extended to assessing the effectiveness of more elaborate merging algorithms such as waveband ratioing method. A pre-merging



assessment will allow the feasibility of a particular image processing effort to be effectively evaluated before vigorous attempts are made to actually combine the image data. Because the primary objective of this study is for multiresolution merging, only a brief discussion of the ratioing method will be presented later in this chapter to examine the technicality of image data ratioing.

As illustrated in graphs (P) of Figures 5-2 and 5-3, the preserving method was able to improve the radiometric variance of all merged images in both case I and case II. In addition, the merged images for each  $\beta$  value also had higher values than the corresponding primary image as shown in graphs (P) of Figures 5-4 and 5-5. The improvement in radiometric variance and mean brightness indicates that those merged images would be brighter and have more contrast than their primary data. The radiometric enhancement will render a greater differentiation of a satellite scene for land-use classification applications using the merged data. When the variance of the secondary image was larger than that of the primary image (case II), the relative improvement to a merged image was more substantial. This signifies an importance of improving the radiometric quality of the high spatial resolution (panchromatic) image in a multiresolution dataset. The primary cause for increasing the radiometric variance and brightness in the merged data is the appendive effect created by the preserving approach.

For the confining approach, the radiometric quality of a merged image would depend on the relative radiometric variance and brightness of the primary image due to the compromising effect. For example, in case I when the primary image (LAC2) had higher values and a larger variance than the secondary image (LAC1), the resultant merged images each had a smaller radiometric variance and lower values as shown in graphs (C) of Figures 5-2 and 5-4. However, when the radiometric variance and the data value of the primary image were smaller than those of the secondary image data (case II), the merged images were improved with slightly larger radiometric variances and higher image values as indicated by graphs (C) of Figures 5-3 and 5-5, respectively. The main impact of the confining approach is its compromising effect which tends to equalize both the contrast and brightness of the primary image with those of the secondary data.

To find out whether the confining method will improve or degrade the radiometric variance of a merged image, one approach is to calculate the  $\beta_c$  value using equation [4-22]. By definition, the  $\beta_c$  value is the merging coefficient at which a merged image by the confining method will have the least radiometric variance (chapter 4). If  $\beta_c \leq 0$ , the radiometric variance of a merged image is on the ascending side of a parabolic function for the whole (0-1) range of  $\beta$  values. When  $\beta_c \approx 1.0$ , it will be certain that the merged image will have a smaller radiometric variance (less contrast).

Using equation [4-22] with the values in Table 5-2 and a correlation coefficient of  $r=0.577$ , the  $\beta_c$  values for case I and case II were estimated at 1.04 and -0.03, respectively. Hence, the confining approach would degrade a merged image in case I ( $\beta_c=1.04$ ), yet improve it in case II ( $\beta_c=-0.03$ ).

The radiometric variances and mean values of merged LAC image data by the differencing approach are shown in graphs (D) of Figures 5-2 through 5-5. Similarly to the confining approach, an enhancement or a detracting on the radiometric variance of a merged image by the differencing method can be assessed by a comparison between the  $\beta$  used and the critical  $\beta_d$  values from equation [4-30]. Using the values in Table 5-2 and a correlation coefficient  $r=0.577$ , the  $\beta_d$  value was 2.12 and 0.63 for case I and case II, respectively. As shown in graph (D) of Figure 5-3 (case I), a merged image always had a smaller radiometric variance than the primary image unless the merging coefficient ( $\beta$ ) would take a value greater than 2.12, which would be very unlikely for the differencing method. In case II, however, the radiometric variance of merged images became slightly larger than that of the primary image (LAC2) when  $\beta$  took values greater than 0.63 as shown in graph (D) of Figure 5-2, though it was decreasing initially due to the positive correlation between the two LAC images.

#### Comparison of Merged LAC Images

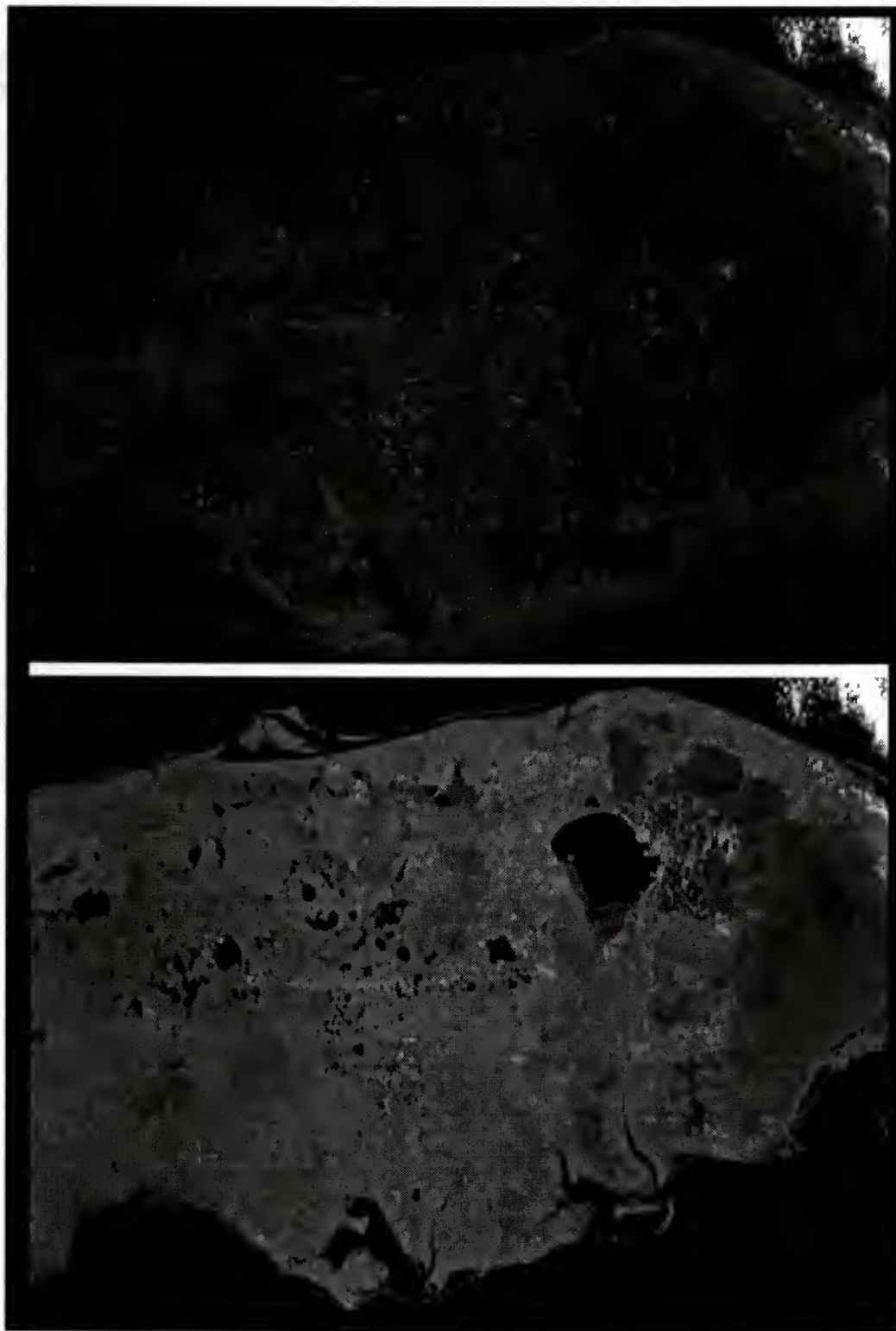
From the above discussions on the radiometric quality (variance and means) of merged images, this section attempts

to further demonstrate those results using image displays. The image contrast, brightness, and tonal gradations of the merged LAC images were evaluated through visual comparisons between the primary image and the merged data. To reduce the subjectivity of evaluation and to avoid color preference, black-and-white displays were used. In addition, all the images to be evaluated have not been subjected to any digital enhancement procedures (e.g. spatial filtering and contrast stretching) which would alter the brightness and contrast. The displays are strictly the results of unaltered merged image data (gray shade data). Note that the evaluations were based on the overall quality of image appearance and only three merged images at  $\beta$  values of 0.2, 0.4, and 0.6 were selected for each case.

The original LAC1 and LAC2 images are presented in Figure 5-6. Obviously, these two LAC images have very different qualities in terms of contrast and brightness. Because of its larger radiometric variance and greater mean data value (Table 5-2), the LAC2 (NIR) image has more contrast as well as a brighter appearance than the LAC1 (red).

For case I of the preserving method, the three selected merged images at  $\beta=0.2$ , 0.4, and 0.6 are presented in Figure 5-7. One unambiguous indication in Figure 5-7 is that the increase in radiometric quality in a merged image corresponds to the increase in visual quality (contrast and brightness). The increasing radiometric variances for  $\beta=0.2$ , 0.4, and 0.6

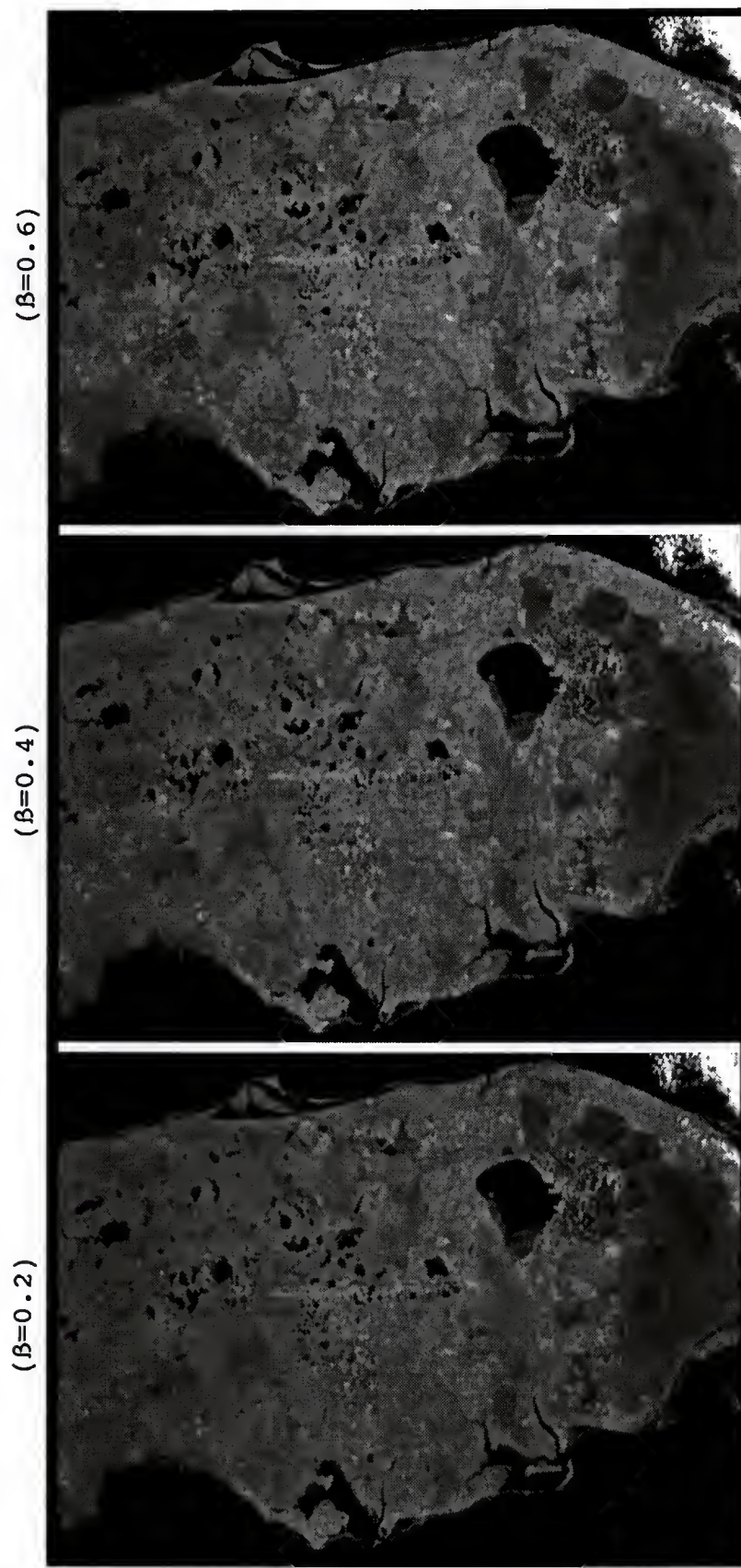




LAC2 (NIR)

LAC1 (red)

Figure 5-6. Original clipped NOAA-11 LAC images of red and NIR wavebands.



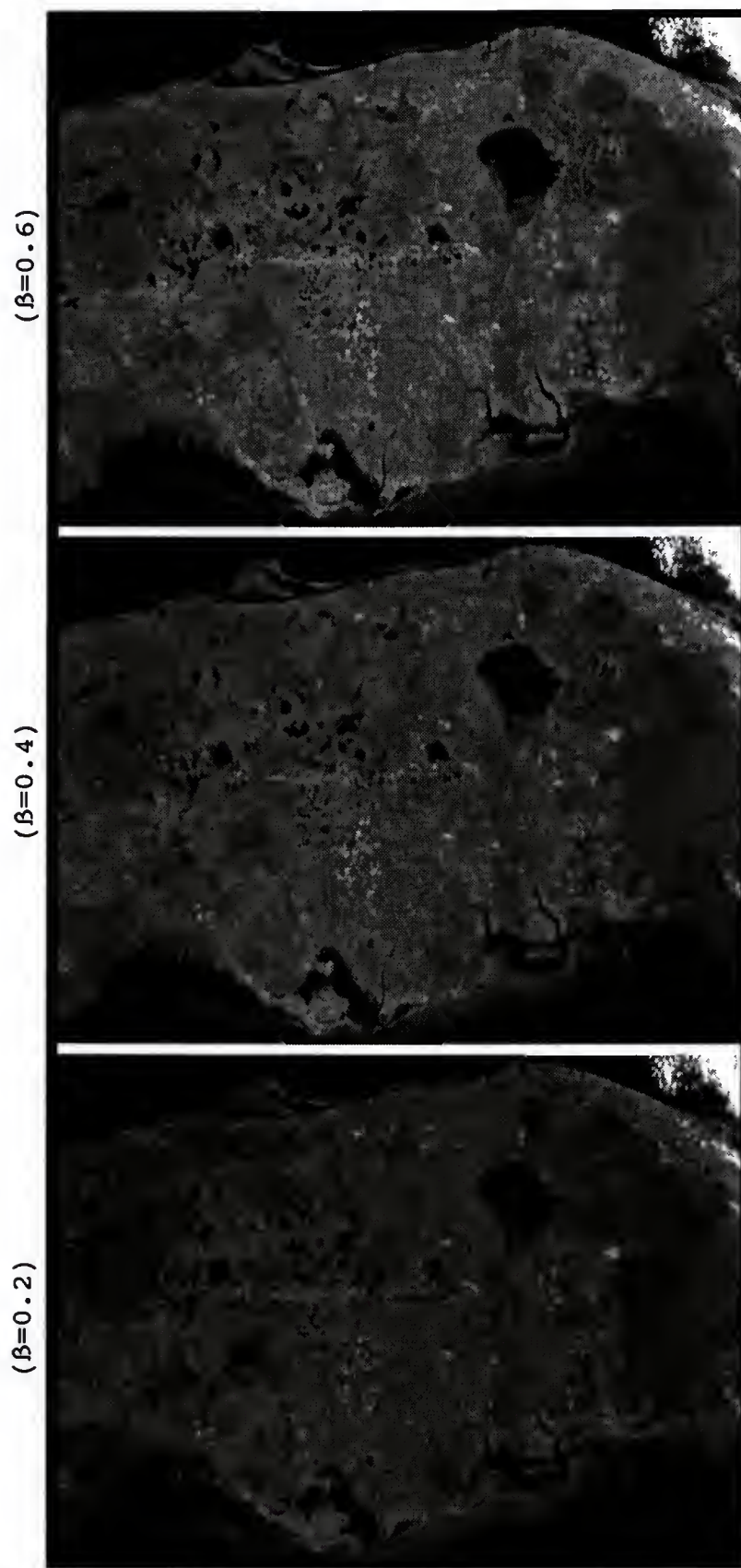
Note: Primary image = LAC2 (NIR).  
 Secondary image = LAC1 (red).

Figure 5-7. Merged LAC images by the preserving method (case I).



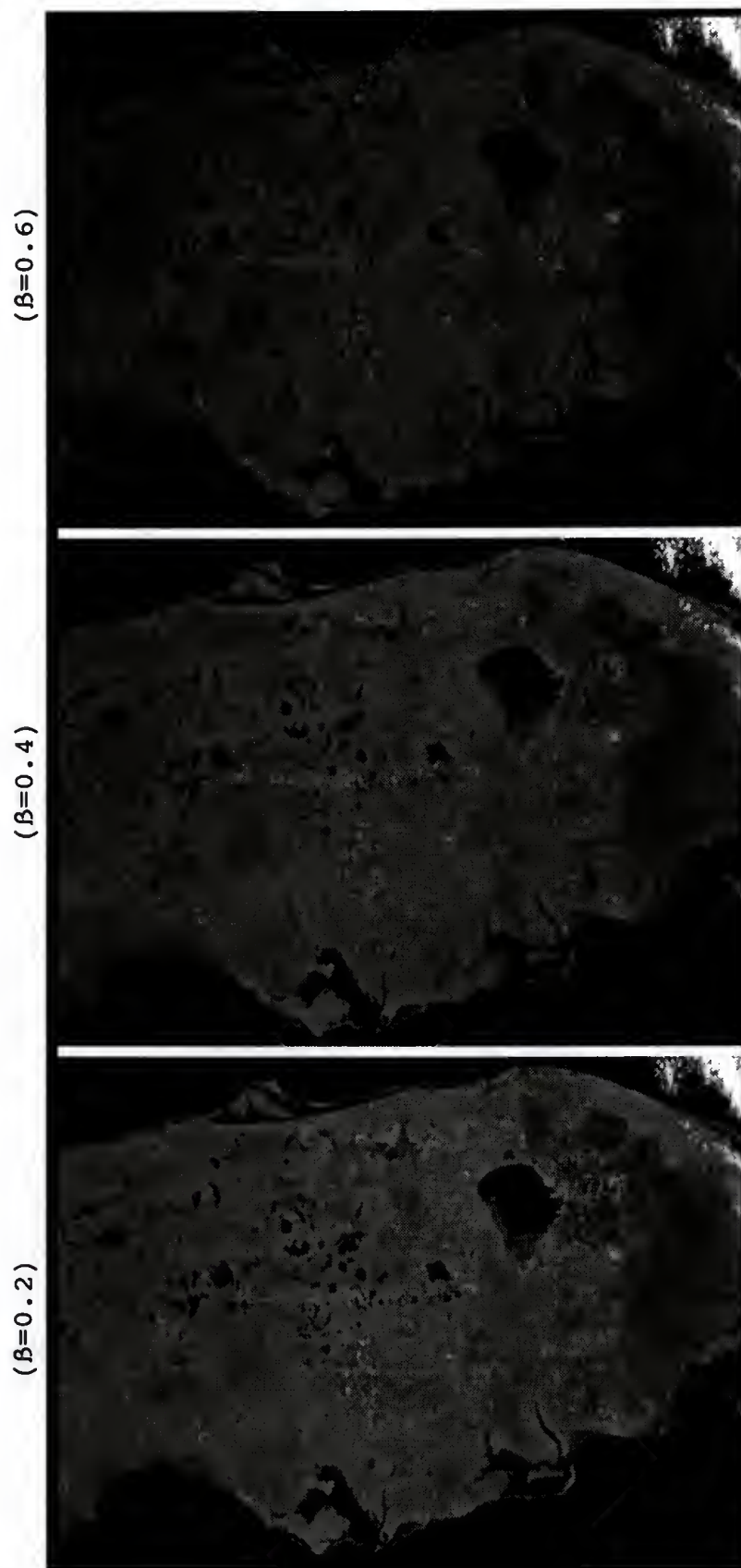
resulted in more and more contrast in the merged image data. The merged images also became increasingly brighter as  $\beta$  increases. For case II, the corresponding merged images are presented in Figure 5-8 where similar improvements on image contrast and brightness were observed, even when the primary image had a much smaller radiometric variance (Table 5-2). In comparison with case I, the improvements in case II were more substantial because its secondary image (LAC2) had a larger variance. Though the enhancement was less apparent at small  $\beta$  values (0.2), all merged images by the preserving method have evidenced improvements in image contrast and brightness when compared to the corresponding primary image. The reason for such a consistent enhancement is that, given the positive correlation ( $r=0.577$ ), the preserving method was able to preserve the primary image when the secondary image data were merged, and as a result, the merged images each had increased radiometric quality.

For both case I and case II of the confining method, the merged images are presented in Figures 5-9 and 5-10. Recall that the confining approach is in essence a compromising method that attempts to equalize the contrast and brightness between the primary and secondary images. Because of this compromising effect, a merged image will have less contrast if the primary image has a larger variance. In addition, a brighter primary image will result in a relatively darker merged image. For example, when the primary image in case I



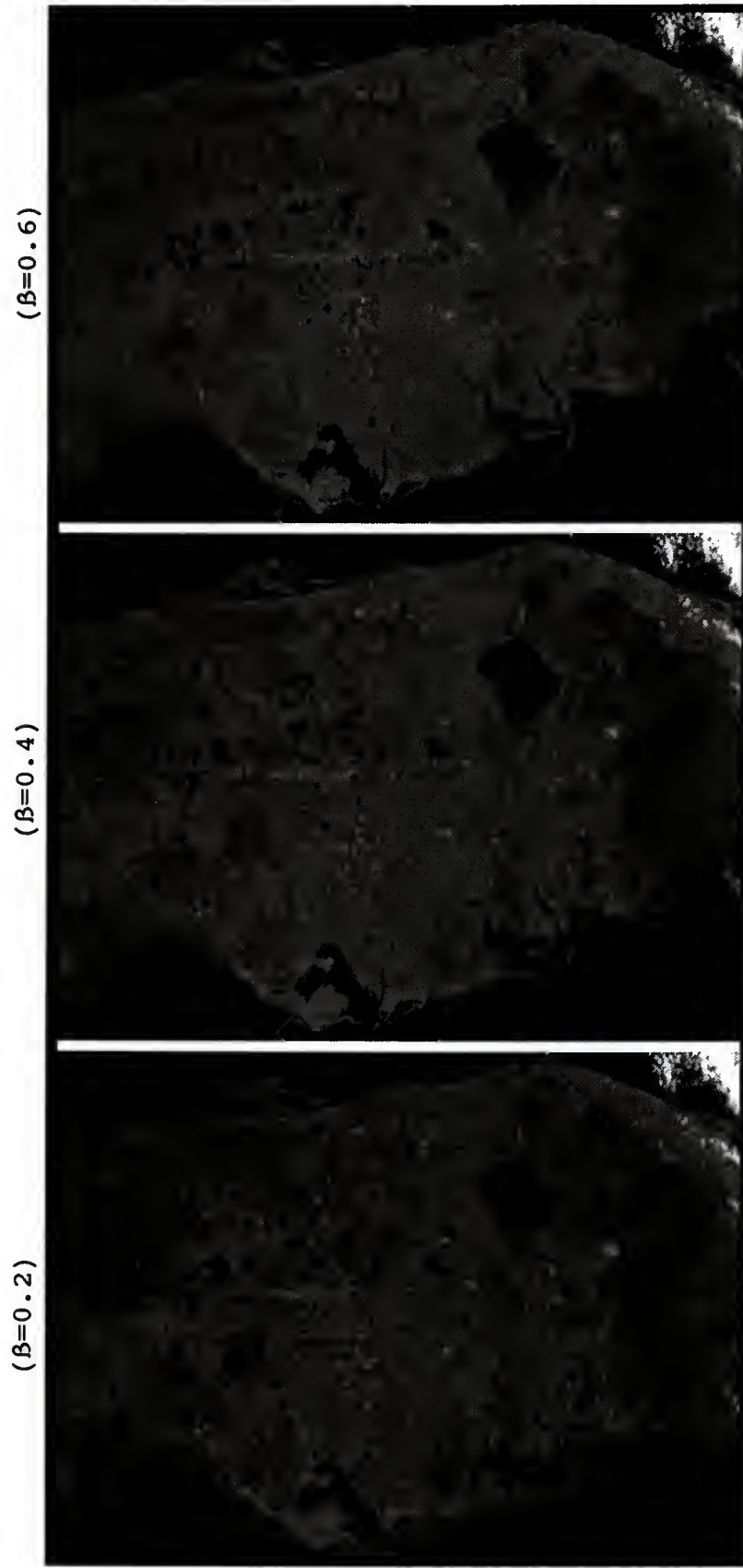
Note: Primary image = LAC1 (red).  
Secondary image = LAC2 (NIR).

Figure 5-8. Merged LAC images by the preserving method (case II).



Note: Primary image = LAC2 (NIR).  
Secondary image = LAC1 (red).

Figure 5-9. Merged LAC images by the confining method (case I).



Note: Primary image = LAC1 (red).  
 Secondary image = LAC2 (NIR).

Figure 5-10. Merged LAC images by the cinfining method (case II).

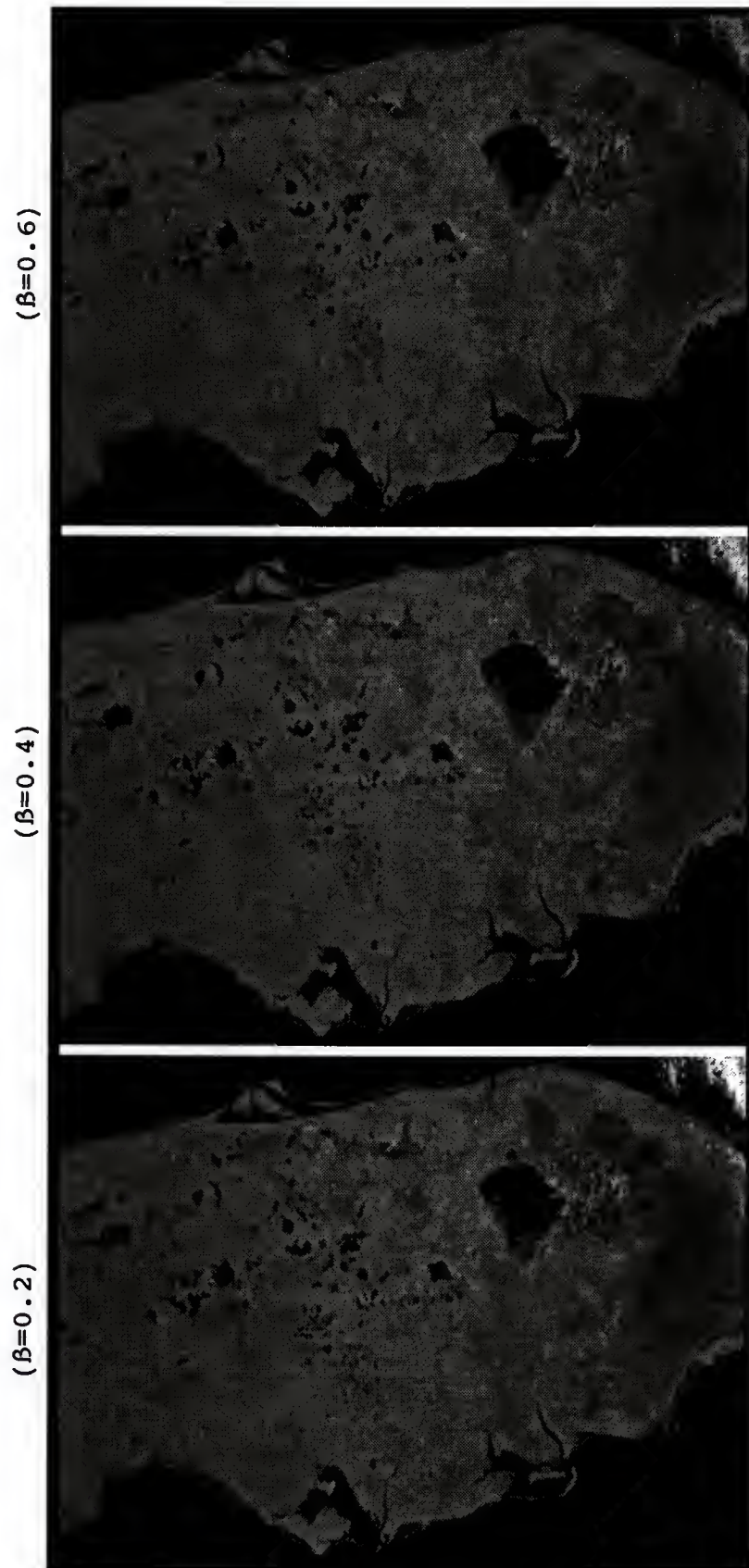


(LAC2) had a larger variance and greater brightness as compared to the secondary image data (LAC1), the merged images became increasingly darker and had less contrast (Figure 5-9) as the merging coefficient  $\beta$  increased from 0.2 to 0.6. However, a slightly improvement in both image contrast and brightness is observed for the merged images in case II when the primary image was relatively darker and had a smaller variance (Figure 5-10). One method to evaluate the effectiveness of the confining method is to examine the critical  $\beta_c$  value, which was calculated as 1.04 and -0.03 for case I and case II, respectively. Apparently, the confining approach decreased the contrast of a merged LAC image in case I (Figure 5-9), but slightly improved it in case II as shown in Figure 5-10.

For the differencing method, the merged LAC images with  $\beta$  values of 0.2, 0.4, and 0.6 for both case I and case II are presented in Figures 5-11 and 5-12. Note that two completely different sets of merged images were generated when the differencing approach was utilized. Recall from Table 5-2 and Figure 5-6 that the LAC1 image not only had a much smaller variance, but also was much darker (a smaller mean value) in comparison to the LAC2 image. In addition, the two LAC images were also positively correlated ( $r=0.577$ ).

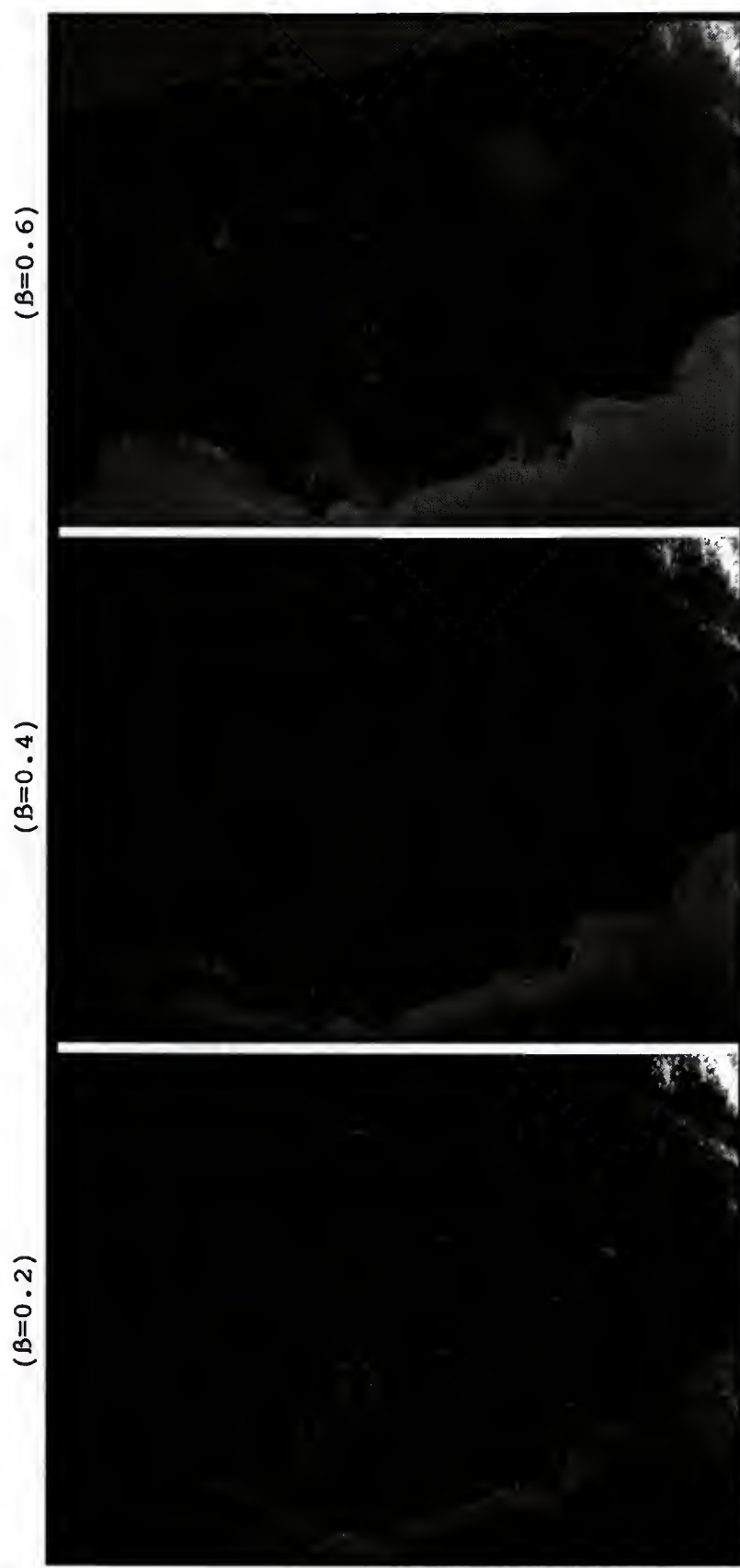
Because of the positive correlation between the two LAC images, the differencing method should not be utilized to merge the LAC images in practical applications. However, the





Note: Primary image = LAC2 (NIR).  
Secondary image = LAC1 (red).

Figure 5-11. Merged LAC images by the differencing method (case I).



Note: Primary image = LAC1 (red).  
Secondary image = LAC2 (NIR).

Figure 5-12. Merged LAC images by the differencing method (case II).

purpose for the discussions here is to understand the merging process as it affects the radiometric quality of merged images. In case I when the LAC2 image was differenced by the LAC1 data, the results (Figure 5-11) showed that the merged image was not seriously impacted because the original LAC2 image had both a brighter appearance and a relative larger variance. As a result, all the merged (differenced) images (Figure 5-11) maintained a great deal of tonal similarity to the primary image (LAC2). However, the results were completely different when the primary image (LAC1) had both a smaller mean and variance (case II). At  $\beta=0.2$ , the merged image appearance began to fade out and significant image contrast was lost as a result of a smaller radiometric variance in the merged data (Figure 5-12). When a slightly larger  $\beta$  value (0.4) was used, a reverse tonal began to surface in the merged image. For instance, the dark appearance of water bodies (e.g. Lake Okeechobee and sea water) became slightly bright or similar to those of land areas. At  $\beta$  value of 0.6, the tonal gradations of the entire image were completely reversed, making dark water bodies show up as bright and bright areas (lands) appear as dark in the merged image. While the positive correlation was responsible for the decrease in merged image contrast, the reversed tonal appearance was caused by the greater brightness of the secondary image data (LAC2), which required the use of a larger positive constant (Table 5-3) in the differencing equation.

A mosaic of all the nine selected merged images for the preserving, confining, and differencing methods is presented in Figure 5-13 as a summary for the three selected  $\beta$  values of 0.2, 0.4, and 0.6. These images are shown in a way that the changes of radiometric quality in the horizontal direction indicate the effects of increasing  $\beta$  values for a given method, while those in the vertical direction are related to the effects of the different merging methods. Similarly, the nine merged images for case II of the preserving, confining, and differencing methods at  $\beta$  values of 0.2, 0.4, and 0.6 are shown in Figure 5-14 with the same image arrangements as in Figure 5-13.

From all the merged images in the two mosaics of Figures 5-13 and 5-14, three conclusions are as follows. First, the preserving approach is a very effective method to generate merged images with the greatest improvement in radiometric quality. The radiometrically enhanced images will be more useful for greater differentiations of land-use elements in multispectral analyses using the merged image data. Second, the confining approach is subordinate to the preserving method in every aspect. The images merged by the confining approach can have either an enhancement or a detracting in radiometric quality, depending on the data characteristics of both the primary and the secondary images. Even when a radiometric enhancement is revealed, the extent of improvement will not be comparable to that by the preserving approach. Third, the



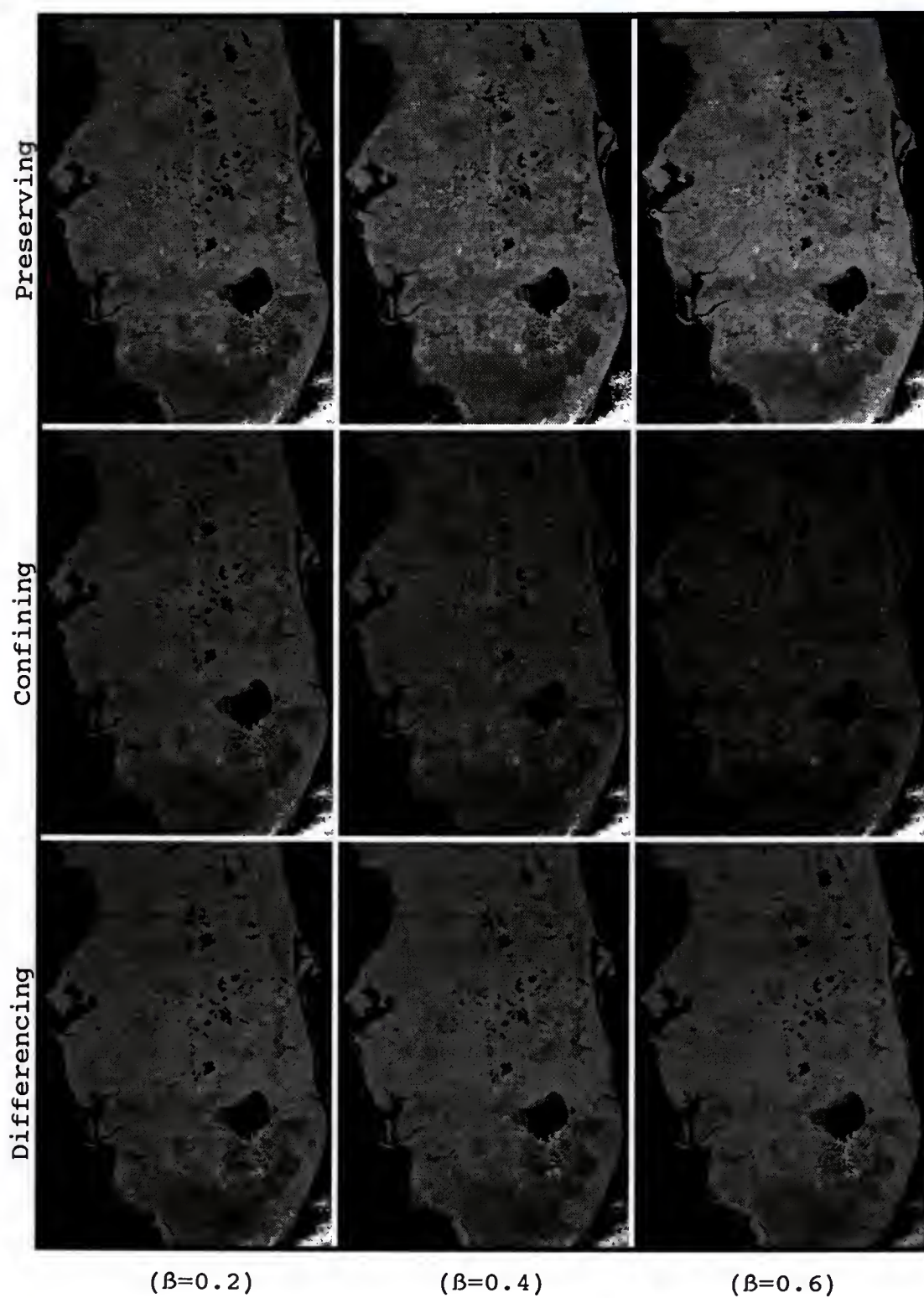


Figure 5-13. Summary (mosaic) of merged LAC images for three methods in case I.



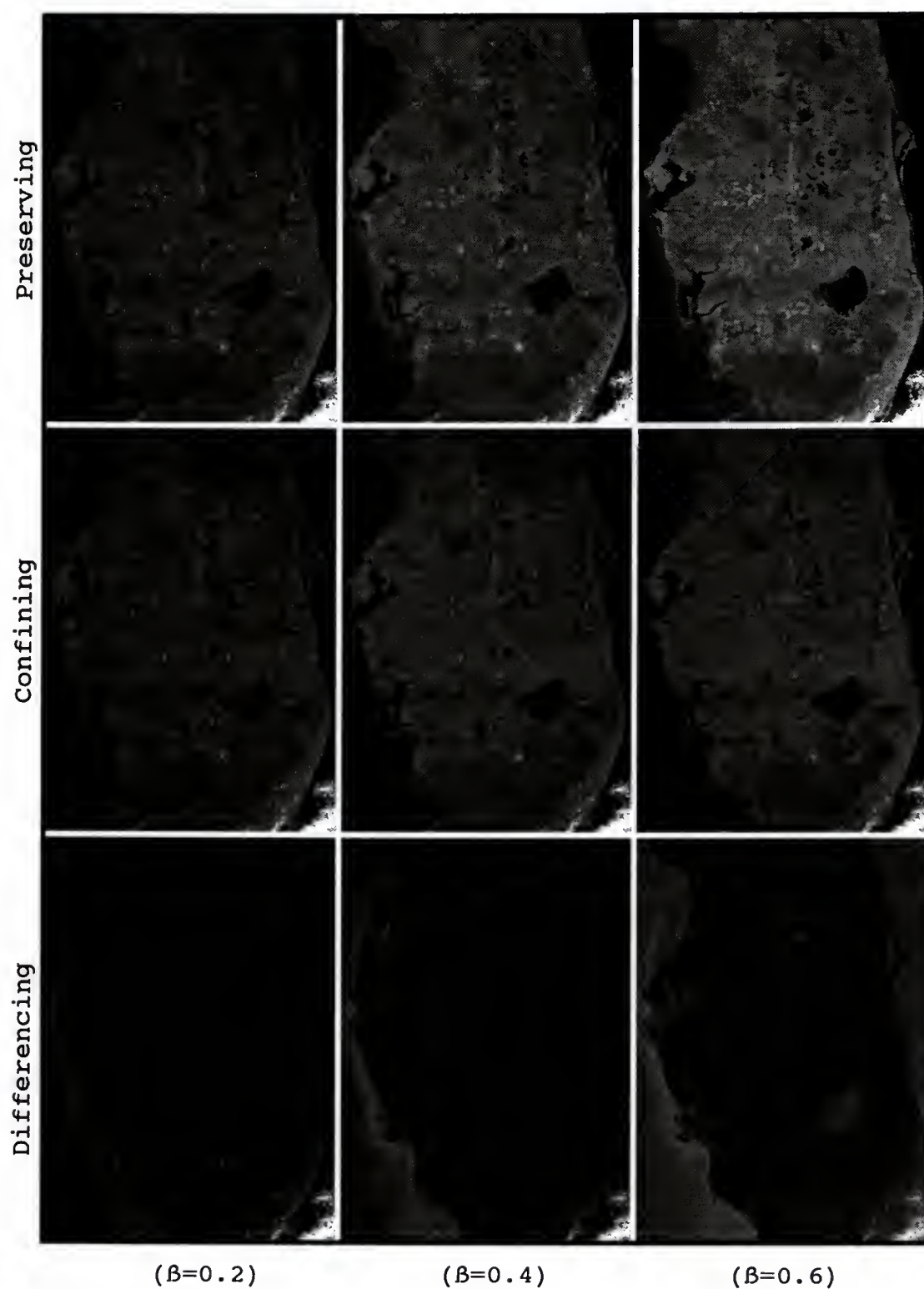


Figure 5-14. Summary (mosaic) of merged LAC images for three methods in case II.

differencing approach must be used with great caution because of the possibility of inverting the merged image, particularly when the primary image has relatively values. The efficacy of the differencing method is limited to the circumstances when the images to be combined have a strong negative correlation.

### Ratioing of Satellite Images

The ratioing of satellite images (often called waveband ratioing) is a widely adopted approach for image enhancement (Lillesand and Kiefer, 1979; Lo et al., 1986; Huete and Jackson, 1988; Kidwell 1991). Because successful applications of the ratioing technique often depend on a trail-and-error process with many failed efforts, this section attempts to examine and understand the mechanics of waveband ratioing by using the principle of random variable manipulations. According to Mood et al. (1974), the ratio  $Y_r$  of variables  $X_1$  and  $X_2$  ( $X_2 \neq 0$ ) can be expressed as

$$Y_r = \frac{X_1}{X_2} \quad [5-1]$$

for which the mean value ( $\mu_r$ ) of ratioed variable  $Y_r$  can be estimated by

$$\mu_r = \frac{\mu_1}{\mu_2} - \frac{\text{cov}(X_1, X_2)}{\mu_2^2} + \frac{\mu_1}{\mu_2^3} \sigma_2^2 \quad [5-2]$$

while the variance ( $\sigma_r^2$ ) can be approximated as

$$\sigma_r^2 = \left(\frac{\mu_1}{\mu_2}\right)^2 \left[ \frac{\sigma_1^2}{\mu_1^2} + \frac{\sigma_2^2}{\mu_2^2} - \frac{2 \text{cov}(X_1, X_2)}{\mu_1 \mu_2} \right] \quad [5-3]$$

where  $\mu_1$  ( $\neq 0$ ) and  $\mu_2$  ( $\neq 0$ ) are the means, and  $\sigma_1^2$  and  $\sigma_2^2$  are the variances for variables  $X_1$  and  $X_2$ . In ratioing images,  $X_1$  and  $X_2$  are the numerator and denominator images, respectively. The covariance  $\text{cov}(X_1, X_2)$  term in both equations [5-2] and [5-3] can be rewritten in the following form (Mood et al., 1974)

$$\text{cov}(X_1, X_2) = r \sigma_1 \sigma_2 \quad [5-4]$$

where  $\sigma_1$  and  $\sigma_2$  are the standard deviations and  $r$  is the correlation coefficient for  $X_1$  and  $X_2$ . Substituting equation [5-4] into equations [5-2] and [5-3] yields

$$\mu_r = \frac{\mu_1}{\mu_2} - \frac{r \sigma_1 \sigma_2}{\mu_2^2} + \frac{\mu_1}{\mu_2^3} \sigma_2^2 \quad [5-5]$$

for the mean ( $\mu_r$ ) and

$$\sigma_r^2 = \left(\frac{\mu_1}{\mu_2}\right)^2 \left( \frac{\sigma_1^2}{\mu_1^2} + \frac{\sigma_2^2}{\mu_2^2} - \frac{2 r \sigma_1 \sigma_2}{\mu_1 \mu_2} \right) \quad [5-6]$$

for the variance ( $\sigma_r^2$ ) of ratioed variable  $Y_r$ . Note that the  $\sigma/\mu$  ( $\mu \neq 0$ ) terms in equations [5-5] and [5-6] are in fact the coefficient of variation  $\text{CV} = \sigma/\mu$  (where  $\mu \neq 0$ ). Thus, using the  $\text{CV}$  values, both equations [5-5] and [5-6] can be rewritten as

$$\mu_r = \frac{\mu_1}{\mu_2} (1 + \text{CV}_2^2 - r \text{CV}_1 \text{CV}_2) \quad [5-7]$$

and

$$\sigma_r^2 = \left(\frac{\mu_1}{\mu_2}\right)^2 (\underline{CV}_1^2 + \underline{CV}_2^2 - 2 r \underline{CV}_1 \underline{CV}_2) \quad [5-8]$$

for the mean value and the variance of  $Y_r$ , respectively. To assist in the discussions for ratioing remote sensing image data, let  $F_v$  be defined by the following

$$F_v = \underline{CV}_1^2 + \underline{CV}_2^2 - 2 r \underline{CV}_1 \underline{CV}_2 \quad [5-9]$$

as the variability factor, and  $R_b$  as the brightness ratio

$$R_b = \mu_1/\mu_2 \quad [5-10]$$

where  $\mu_2 \neq 0$ . Note that  $R_b$  is a measure of the relative magnitudes of brightness between the numerator ( $X_1$ ) and the denominator ( $X_2$ ) images, while  $F_v$  provides a collective assessment of the data variability and relation in  $X_1$  and  $X_2$ . As indicated by equations [5-1] and [5-9],  $F_v$  is a constant when two images are given ( $\sigma_1$ ,  $\sigma_2$ , and  $r$  are known). Its value does not change when the numerator and denominator images are alternated. However,  $R_b$  can be significantly different if the numerator image is replaced by the denominator data.

Substituting both  $R_b$  and  $F_v$  into equations [5-7] and [5-8] yields the followings

$$\mu_r = R_b (1 + \underline{CV}_2^2 - r \underline{CV}_1 \underline{CV}_2) \quad [5-11]$$

$$\sigma_r^2 = R_b^2 F_v \quad [5-12]$$

for the mean and variance of ratioed image  $Y_r$ . A clear indication from equations [5-11] and [5-12] is that both the variance and mean brightness of ratioed image  $Y_r$  is a function of  $R_b$ . In fact, the radiometric variance ( $\sigma_r^2$ ) is related to the square of  $R_b$ . This signifies that the selection of an numerator image is critical for the effectiveness of waveband ratioing.

One unique aspect in ratioing satellite images is to scale the fractional ratioed results (Equation [5-1]) to a range (typically 0-255) of integers. This makes it arbitrary to compare both the radiometric variance ( $\sigma_r^2$ ) and mean brightness ( $\mu_r$ ) to those of the two original images ( $X_1$  and  $X_2$ ). Since the scaling factor is applied to the entire scene, the concepts of  $R_b$  and  $F_v$  can be extended to the various land-use elements when assessing the feasibility of waveband ratioing.

In remote sensing applications when two images are to be ratioed, the value of  $F_v$  for each and every land-use element is determined regardless of the selection of the numerator (or denominator) image. However, the  $R_b$  values among the land-use elements in a satellite scene can be significantly different depending on which of the two ratioing images is used as the numerator ( $X_1$ ) for equation [5-1]. Note that a relative large  $R_b$  value provides an advantage in attaining a potential radiometric enhancement, while a small value is the indication of difficulty in achieving any enhancement. For instance, in



order to enhance vegetation lands, the ratioing image with greater values for vegetation areas should be chosen as the numerator image to achieve a relative large  $R_b$  value for increased radiometric variance and brightness. If the ratioing image that possesses the larger mean value (brighter) for vegetative areas is used as the denominator image, the  $R_b$  value will be small, making it difficult or even impossible for vegetation land use to stand out in the resultant ratioed image. This points out that one important consideration in a ratioing approach is to select the numerator image with which the land-use elements of interest can have relative large  $R_v$  values.

The variability factor ( $F_v$ ) is a function of both the correlation coefficient ( $r$ ) and the coefficients of variation. If the correlation between images  $X_1$  and  $X_2$  approaches positive unity ( $r=1.0$ ),  $F_v$  can be expressed as

$$F_v = (\underline{CV}_1 - \underline{CV}_2)^2 \quad [5-13]$$

which is the square of the difference between the coefficients of variation  $\underline{CV}_1$  and  $\underline{CV}_2$ . Consequently, the values of  $F_v$  will be very small for those land-use elements with a strong positive correlation between  $X_1$  and  $X_2$ . If  $r \approx -1.0$ , the value of  $F_v$  can be written as

$$F_v = (\underline{CV}_1 + \underline{CV}_2)^2 \quad [5-14]$$

which is the square of the sum of coefficients of variation

$\underline{CV}_1$  and  $\underline{CV}_2$ . When  $r = 0$ , equation [5-9] becomes

$$F_v = \underline{CV}_1^2 + \underline{CV}_2^2 \quad [5-15]$$

which is essentially the sum of the squares of the coefficient of variation. From equations [5-13], [5-14], and [5-15], the indication is that the correlation between the two ratioing images plays a very important role in the feasibility of waveband ratioing. If a strong positive correlation exists for a land-use element such as urban structures, the  $F_v$  value will be very small, implying a great difficulty in obtaining an enhancement by the ratioing method. However, a strong negative correlation (or even  $r=0$ ) will allow a land-use element in question to have a relative large  $F_v$  value, creating the potential for that land-use element to have an increased radiometric variance in the resultant ratioed image. In addition, a negative or zero correlation ( $r \leq 0$ ) would also make the land-use type in question appear brighter because the  $(-r \underline{CV}_1 \underline{CV}_2)$  component in equation [5-11] is non-negative. It becomes clear that it will not be feasible to use the ratioing method in an effort to enhance the radiometric variances of those land-use types that have a strong positive correlation between the two ratioing images. To state alternatively, a radiometric enhancement by the ratioing method can be achieved only for those land-use types whose correlations are weak or negative in the images to be ratioed.

It is worthwhile of pointing out that both the numerator and denominator images ( $X_1$  and  $X_2$ ) can be manipulated by other

merging approaches (preserving, differencing, etc.) in a way that the land-use elements of interest can attain relatively large  $R_b$  and  $F_v$  values. One example of this manipulation is the normalized difference vegetation index (Huete and Jackson, 1988; Kidwell, 1991) for vegetation enhancement. Therefore, given the understanding of the ratioing principle, an increasing amount of knowledge about image spectral characteristics for various land-use types in different wavelength ranges as well as sensing systems will extend the ratioing approach to greater applications of remote sensing data. Since the primary objective of this study is in multiresolution processing, further efforts will not be undertaken for demonstrating the ratioing approach.

In summary of the waveband ratioing approach, two comments are in order. First, the selection of the numerator image is critical for the effectiveness of a ratioing method for remote sensing applications. If the radiometric qualities of a land-use element are to be enhanced, the ratioing image which has relatively large digital (brighter) values for the land-use element in question should be used as the numerator image to attain a relative large  $R_b$  value. Otherwise, it should be used as the denominator image to detract the radiometric qualities of the land-use element. Second, the feasibility of ratioing images for image enhancement depends on the correlation between the ratioing images. Successful applications of the ratioing method can be achieved only for

the land-use elements which have a negative or very weak correlation ( $r \leq 0$ ) between the ratioing images.

### Multiresolution Enhancement

Since merging actual multiresolution satellite datasets was carried out in chapters 6 and 7, this section focuses on the factors that are unique to merging multiresolution images. This arrangement was intended to address those unique aspects before efforts were made to demonstrate the process of multiresolution merging using a SPOT satellite dataset.

The spatial resolution difference in a multiresolution dataset requires the resampling of all image data to the same pixel size before being merged. One concern is the validity of applying the merging principle discussed previously to the resampled image data. In the statistical context, if the elements of a random variable are each duplicated for a certain number of times, the new variable will still attain the characteristics of a random variable. Similarly, if the pixels of a low spatial resolution image are each resampled for a certain number of times, the resampled image will still have the characteristics of a random variable. Hence, the principle of merging images can be applied to multiresolution image datasets after a resampling procedure.

Multiresolution merging can be considered as an unique process in that there is no alternative in the selection of the primary and secondary images from the multiresolution



data. Each of the multispectral images is used as the primary image while the high spatial resolution panchromatic image serves as the secondary image data. Stated another way, the high spatial resolution image is merged to each of the low spatial resolution multispectral images. Consequently, the panchromatic information becomes a mutual component in the resultant merged dataset. This will cause a concern with elevating the between-waveband correlations in the merged dataset. An increase in between-waveband correlation will reduce the effectiveness of a merged dataset in multispectral analyses to differentiate the land-use elements. Therefore, the use of a larger value for the merging coefficient ( $\beta$ ) must be cautioned.

The difference in spatial resolution between the panchromatic and multispectral images must also be considered. For instance, if the spatial resolutions have a linear ratio of two, one low spatial resolution pixel in the multispectral images will encompass four sub-pixels in the panchromatic image (Figure 1-1). If the four sub-pixels represent four different land-use objects, the minimum difference in the digital numbers of the four sub-pixels is 0, 1, 2, and 3 (or any four contiguous integers within the 0-255 range). In order for all of these four land-use objects to show up in a merged image, a merging coefficient ( $\beta$ ) of 1.0 is required because of the truncation of integer image data. If a  $\beta$  value of 0.5 is utilized, up to two of the four land-use objects



corresponding to a low resolution pixel will not show up in a merged image. In other words, up to 50% of the panchromatic spatial information could be lost in the merging process for a  $\beta$  value of 0.5. If a  $\beta$  value is chosen to be greater than 0.5, more spatial details can be expected. However, this can cause an increase in the between-waveband correlations as well as the possibility of introducing a scaling factor to scale back the radiometric variances in the merged dataset. On the other hand, a smaller  $\beta$  value will lead to greater loss of spatial information. Practically, it is difficult to expect all panchromatic spatial information to be merged with the multispectral image in a multiresolution processing, particularly when the radiometric resolution of the panchromatic image is low. If the spatial resolution ratio is greater than two (one low resolution pixel has more than four sub-pixels), more spatial objects could lose their presence in a merged dataset. This constraint in spatial resolution difference, which was also observed by Price (1984), underlines a limitation to multiresolution processing as well as a challenge to the development of future multiresolution sensing systems.

A haze-correction procedure is recommended for the entire multiresolution dataset. This correction eliminates the radiance (a small fraction of digital count) caused by the atmosphere rather than by scene reflectance. It is usually performed by subtracting the value of each pixel with the

image-wide minimum digital number (typically of water areas). This procedure can be applied to the panchromatic image in a straight forward fashion. For the multispectral images, the procedure must be done somewhat differently in order to preserve the integrity of spectral information in the original multispectral dataset. The correction factor has to be based on the minimum of the minimum values for all the multispectral images. For instance, if the minimum values of three multispectral images are found to be 23, 35, and 48, the value of 23 must be used for all three multispectral images. Spatial filtering and contrast-stretching procedures are not recommended for pre-merging processing because they alter the original image data.

#### Summary: Appraisal of Merging Methods

Results from merging an actual NOAA LAC satellite dataset conveys evidence that the principle of statistical variation analyses for random variable manipulations can be applied in the assessment of the radiometric quality (variance and brightness) of pre-merged images. This understanding provides the basis for both evaluating the effectiveness of existing image processing efforts in digitally combining images and for developing new merging approaches for more effective use of satellite image datasets for remote sensing applications.

The preserving method is the preferred approach for merging satellite images because of its effectiveness in

enhancing the radiometric quality of merged image data. The confining approach is deemed as ineffective, while the differencing method for radiometric improvement is limited to circumstances when the images to be merged possess a strong negative correlation. In a multiresolution dataset, the panchromatic image usually has a broad waveband that extends to parts or even the entire ranges of the multispectral wavebands (e.g. SPOT datasets). This spectral waveband characteristic, for which non-negative correlations are usually observed between the panchromatic and multispectral images, will make the use of the preserving approach particularly suitable for merging multiresolution datasets. For this same reason, however, the use of the differencing approach will be detrimental to the radiometric quality of multiresolution merged images.

When a merging method is chosen such as the preserving approach, the value of merging coefficient ( $\beta$ ) will play a vital role in affecting the overall quality (radiometric, spatial, and spectral) of a multiresolution merged dataset. In the context of both radiometric and spatial enhancement, a large value of merging coefficient  $\beta$  will be beneficial. However, the use of an excessively large  $\beta$  value could corrupt the integrity of multispectral information because of the possibility of increasing the between-waveband correlations among the merged images. The corrupted spectral signatures will diminish the usefulness of the merged dataset for remote

sensing applications involving multispectral analyses. On the other hand, a too small  $\beta$  value will not be effective in improving the spatial detail nor enhancing the radiometric quality in the merged data. Therefore, when the radiometric, spatial, and spectral considerations for a merged dataset are put in perspective, the effective  $\beta$  values can be considered as in the range of 0.5 to less than 1.0. In addition, consideration must also be given to the ratio of linear resolutions between the panchromatic and multispectral images. If the linear spatial resolution ratio is greater than three, any notable improvements in spatial detail will be difficult in the merged dataset.

The feasibility of waveband ratioing for satellite image enhancement depends on the correlation between the two images to be ratioed. Successful applications can be achieved only for the land-use elements which have a negative or very weak correlation ( $r \leq 0$ ) between the two ratioing images. In addition, selecting the numerator image is critical for the effectiveness of a ratioing method. If the radiometric qualities of a land-use element are to be enhanced, the image which has relatively large digital (brighter) values for the land-use element in question should be used as the numerator image to attain a relative large brightness ratio ( $R_b$ ). Otherwise, it should be used as the denominator image to detract the radiometric qualities of both variance and brightness.



## CHAPTER 6

### MATERIALS AND METHODOLOGY FOR MULTIRESOLUTION LAND-USE CLASSIFICATION

This chapter presents the materials and methodologies which include sources of image dataset, and processing equipment and systems, procedures for multiresolution data merging, photogrammetric estimation of citrus canopy cover, and land-use classification analyses. In addition, a special attention was given to citrus land use, mainly because of the economic importance of citrus crops to the State of Florida (Jackson and Sauls, 1983, 1984; Shih et al., 1985).

#### Data Source and Equipment

The data sources and equipment utilized include a SPOT HRV multiresolution dataset, an ACIR photography, two computer image processing systems, an Arc/Info GIS (ESRI, 1993), and a photogrammetric stereo plotter for making photogrammetric measurements for the estimation of citrus canopy size.

#### SPOT Image Data and Study Area

A multiresolution scene acquired by the SPOT HRV sensor was used. The SPOT scene (#622-295) has an area coverage of the entire St. Lucie county, Florida (Figure 6-1), and consists of four images that were acquired simultaneously on October 3, 1987. Of the four SPOT images, one is panchromatic



while the others are multispectral with corresponding spatial resolutions of 10 m and 20 m, respectively. The spectral wavelength ( $\mu\text{m}$ ) ranges are 0.51-0.73 for the panchromatic image, and 0.50-0.59 (green), 0.61-0.68 (red), and 0.79-0.89 (NIR) for the multispectral images. The panchromatic waveband encompasses almost the entire bandwidth of the green and red wavebands plus a small portion of the NIR wavelength range (0.7-1.0  $\mu\text{m}$ ). For ease of explanation, the SPOT green, red, NIR, and panchromatic wavebands are denoted as wavebands  $\text{HRV}_1$ ,  $\text{HRV}_2$ ,  $\text{HRV}_3$ , and PAN, respectively.

The SPOT scene was clipped to an area of approximately 95  $\text{km}^2$  (1000 by 950 pixels of 10-m size) located in the north-central portion of St. Lucie county (Figure 6-1). This clipped scene was designated as the study area in which pasture lands and citrus groves were found to be predominant together with some isolated urban lands and residential areas. In the discussions that follow, a SPOT image is simply referred to the clipped area (Figure 6-1). The main usage of this SPOT scene was to study the effects of multiresolution processing on land-use classification and the feasibility of differentiating citrus groves based on canopy size difference. Since the differentiation of citrus canopy cover is the most difficult on satellite images acquired in summer seasons, the use of this SPOT satellite scene will render additional insights into the feasibility of classifying citrus groves using remote sensing datasets.

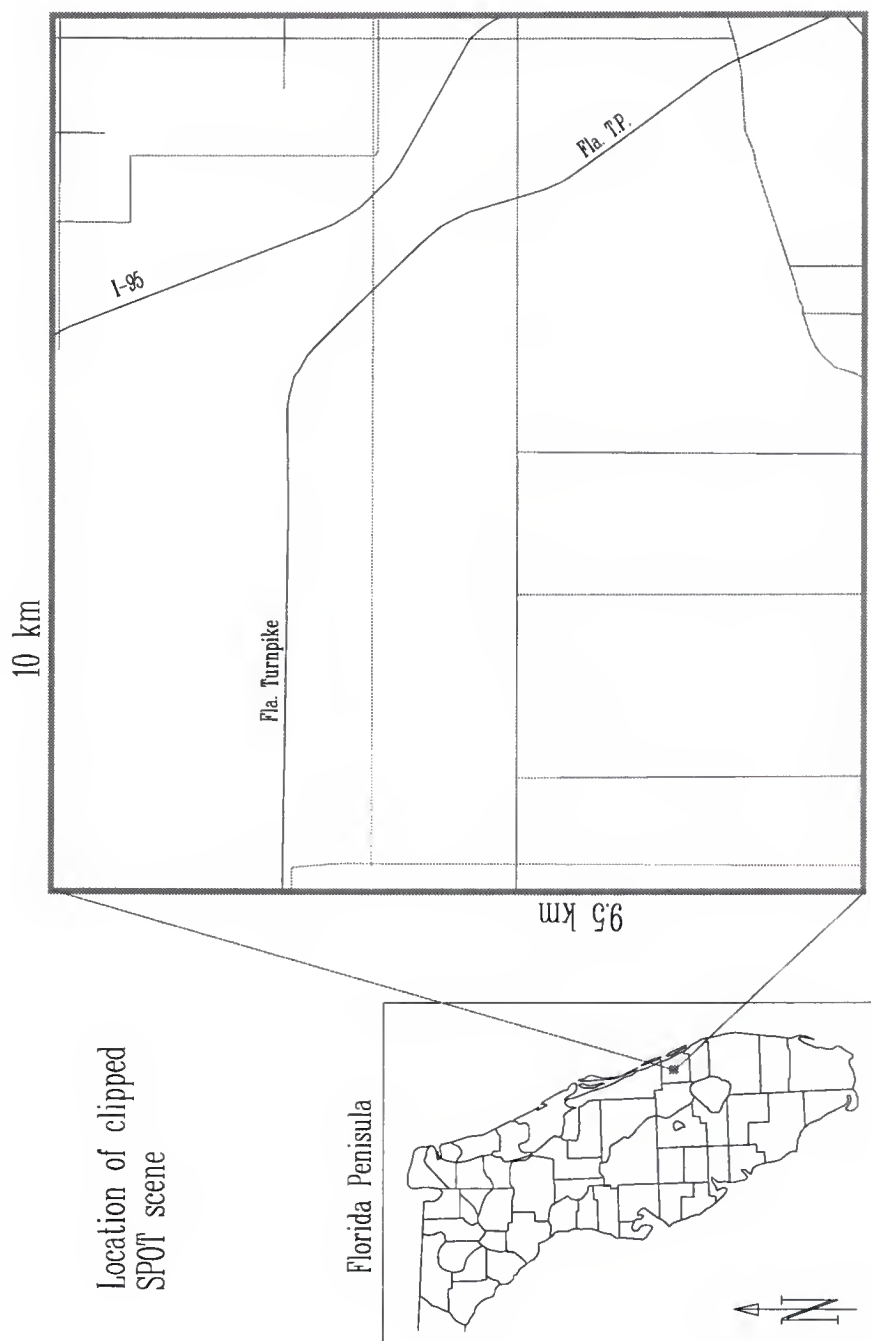


Figure 6-1. Location of clipped SPOT multiresolution dataset and study area.

### ACIR Photography

ACIR photography covering the same area as the clipped SPOT scene was taken on February 5, 1987. The Kodak Aerochrome 2443 color infrared film was used along with a 15.24 cm (6 inch) focal length camera (with a minus-blue filter) flown at a height of 3657 m (12,000 ft). The film was developed into a set of 228.6 x 228.6 mm (9 inch x 9 inch) transparencies with a 1:24,000 scale at which the resolution limit is about 0.25-0.75 m according to the film granularity information provided by the Kodak Company. The main usage of this ACIR photography was to obtain photogrammetric measurements for citrus canopy cover estimations and to provide data for ground-truthing land-use classification results. The estimates of percentage canopy cover were used to assess the feasibility of separating citrus groves based on canopy size difference. Note that there is an eight-month time lapse between taking this ACIR photography and the acquisition of the SPOT scene. However, due to the slow growth of citrus trees, the changes of canopy size were considered as negligible during this eight-month period, particularly the relative changes among the selected fields.

### Image Processing Systems

The primary image processing system utilized in this study was the earth resources data analysis system (ERDAS) located in the Remote Sensing Application Laboratory (RSAL) of

the Department of Agricultural Engineering at the University of Florida. This image processing package contains extensive image processing capabilities for image enhancement, image registration/rectification, land-use classification, GIS analyses, etc. (ERDAS, 1991). The ERDAS system used is the PC version (7.4) for micro computers with a VGA display. In addition to the ERDAS system, the Earth Resources Laboratory Application Software (ELAS) image processing system (PC version) was also used (Graham et al., 1986). The primary usage of ELAS was for land-use classification comparisons as well as for various interactive image display purposes in ground-truthing classified datasets. For more information regarding the two entire image processing systems, the appropriate documentation (Graham et al., 1986; ERDAS, 1991) of the aforementioned software systems should be consulted. The Arc/Info GIS (ESRI, 1993) system located at the same RSAL lab was also utilized for digitizing operations of graphical map data entry, and miscellaneous processing and conversions of image grid data.

#### Photogrammetric Stereo Plotter

A photogrammetric stereo plotter (FMA Model 503290-2 Multi-Format Photo Interpretation Station) was utilized to make photogrammetric measurements from the ACIR photography for citrus canopy cover estimation. The plotter consists of two viewing plates, one adjustable magnifying viewing lens

assembly with a maximum 15 magnification power, a body frame, and two vernier measuring devices (for x and y directions) each with a designed precision of 0.001 mm. For this 1:24,000 ACIR photography, the plotter precision (0.001 mm) can be translated ( $0.001 \times 24,000$  mm) into a 24-mm (or 2.4 cm) horizontal distance on the ground. Photogrammetric measurements were used to obtain field planting geometry (row and tree spacings) and tree crown diameter for the estimation of citrus canopy size.

#### Procedures for Merging SPOT Dataset

Before the SPOT multiresolution images were digitally merged, some pre-merging processing was necessary which included image co-registration and haze corrections. A merging method must be chosen according to the SPOT image data characteristics ( $\sigma$ ,  $\mu$ , and  $r$ ) to generate merged image data from the co-registered multiresolution images for the assessments of radiometric enhancement, spatial improvement, and land-use classification.

#### Pre-merging Processing

The multispectral images with a 20-m spatial resolution were each resampled to a 10-m pixel size through a duplication approach. As a result of this resampling, each of the pixels in an original multispectral image became four identical ones in the resampled dataset. Then, the panchromatic image, which



had a 10-m spatial resolution, was co-registered to the resampled multispectral images. Because of accuracy concerns for topographical maps (Thorpe, 1990; ASPRS, 1990) and map data entry operations (Bolstad et al., 1990; Tan and Shih, 1991b), the image co-registration was done without using an actual geographical reference system (e.g. UTM). A total of 25 mutual points were selected as tie points between the multispectral and panchromatic images. The root-mean-square (RMS) error for these selected points was 6.26 m. The multispectral images were treated as a master to which the panchromatic image was rectified as a slave. Since the between-waveband registrability of the SPOT sensor is 6.0 m (SPOT, 1989), the co-registration of the SPOT images was considered very accurate with a RMS error of 6.26 m.

Haze correction was also applied to the clipped SPOT scene before being merged. From the raw image data of the clipped area, the minimum values for the panchromatic, red, green, and NIR wavebands were 13, 25, 14, and 9, respectively. Therefore, the haze-correction coefficients were chosen as 13 for the panchromatic waveband and 9 (the minimum of 9, 14, and 25) for the three multispectral images. The pixel values each were subtracted by 13 for the panchromatic image and by 9 for all the multispectral images. This specific haze-correction procedure was done to preserve the integrity of spectral information in the original multispectral data. The standard deviations for the green, red, NIR, and panchromatic wavebands

of the haze-corrected SPOT dataset are presented in Table 6-1. Also shown in Table 6-1 are the correlation coefficients ( $r$ ) of the panchromatic waveband to the multispectral images. Note that a haze-correction procedure will not affect the correlation coefficients as well as the radiometric variances of the original image data.

#### Generating Merged Dataset

When merging multiresolution images, a merging approach must be determined based on the image data characteristics of the original multiresolution dataset. According to the information presented in Table 6-1, each of the multispectral images is positively correlated to the panchromatic waveband with respective correlation coefficients ( $r$ ) of 0.826, 0.852, and 0.085 for the green, red, and NIR wavebands. Therefore, the preserving approach is chosen in order to generate radiometrically enhanced merged image data for improving the differentiation of land-use elements.

The value of merging coefficient ( $\beta$ ) for the selected merging method must be determined with due considerations to the radiometric quality and potential spatial improvement as well as the spectral integrity of the final merged dataset. From chapter 5, it was noted that the magnitude of merging coefficient  $\beta$  can have a strong impact on the quality of a multiresolution merged dataset. A large value of  $\beta$  is beneficial to both the radiometric and spatial enhancements.

Table 6-1. Standard deviation ( $\sigma$ ), mean ( $\mu$ ), maximum and minimum values, and correlation coefficients (r) of SPOT multiresolution dataset.

Waveband#	( $\mu$ )	( $\sigma$ )	(r)	Max.	Min.
1 (green)	29.8	6.73	0.826	148	11
2 (red)	18.1	7.41	0.852	157	1
3 (NIR)	65.2	11.51	0.085	141	0
P (pan.)	27.3	9.22	--	238	0

Note: Correlation coefficients (r) are to the panchromatic image which was used as secondary image data.

However, the use of excessively large  $\beta$  values will raise the possibility of altered or even corrupted spectral information for a merged dataset. In multiresolution merging, there is no alternative in the selection of the primary and secondary images from the multiresolution dataset. The multispectral images are each utilized as the primary images and the panchromatic waveband as the secondary image data for every multispectral image. In other words, the panchromatic image was merged to each of the multispectral images. Therefore, a large merging coefficient ( $\beta$ ) will increase the extent of panchromatic information in each of the merged multispectral images, creating the potential for corrupting the integrity of multispectral information in the original data. When the spatial, radiometric, and spectral considerations are put in perspective, a  $\beta$  value of 0.5 was chosen for the preserving method to generate a multiresolution merged dataset from the co-registered SPOT image data. In addition, a normalized difference vegetation index (NDVI) image was also generated using the 20-m NIR (HRV<sub>3</sub>) and 10-m panchromatic (PAN) wavebands to develop a new approach in using SPOT image data for vegetation study. This NDVI image is named as NDVI<sub>p</sub> in order to distinguish it from the customary NDVI image (Kidwell, 1991) usually created from the HRV<sub>3</sub> (NIR) and HRV<sub>2</sub> (red) wavebands. The NDVI<sub>p</sub> for a SPOT dataset is defined as

$$\text{NDVI}_p = \frac{\text{NIR} - \text{PAN}}{\text{NIR} + \text{PAN}}. \quad [6-1]$$

The purpose of generating the  $NDVI_p$  image was to assess its effectiveness in differentiating vegetation such as citrus canopy covers. There were three datasets (Table 6-2) used for further analyses including land-use classification assessment. These datasets are denoted as (1) OMD--original multispectral dataset of the 20-m multispectral images of the green, red, and NIR wavebands; (2) MMD--multiresolution merged dataset by the preserving approach with  $\beta=0.5$  for each image; and (3) MMND--multiresolution merged and  $NDVI_p$  dataset which is similar to MMD except that the merged NIR image was replaced by the  $NDVI_p$  data.

#### Evaluation of Merged Data

The evaluation of merged image data includes the assessment of radiometric and spatial improvements, the integrity of spectral information, and more importantly the feasibility for improving land-use classification. However, the procedures for assessing the effectiveness of merged datasets in improving land-use classification will be discussed in the final section of this chapter.

To evaluate the radiometric quality of merged images, the standard deviations ( $\sigma$ ) of image data in OMD, MMD, and MMND were obtained through the ERDAS image processing system and then compared with those of the original data. In addition, the estimates of standard deviation were also calculated based on the corresponding equations in chapter 4, and then compared



Table 6-2. Multiresolution datasets and corresponding merging equations.

Dataset	Waveband	Merging equation
OMD	1 (green)	$HRV_1$ (original)
	2 (red)	$HRV_2$ (original)
	3 (NIR)	$HRV_3$ (original)
MMD	1 (green)	$HRV_1 + 0.5PAN$
	2 (red)	$HRV_2 + 0.5PAN$
	3 (NIR)	$HRV_3 + 0.5PAN$
MMND	1 (green)	$HRV_1 + 0.5PAN$
	2 (red)	$HRV_2 + 0.5PAN$
	3 ( $NDVI_p$ )	$(HRV_3 - PAN) / (HRV_3 + PAN)$

- Note: 1. OMD = original multispectral dataset which includes the original three 20-m multispectral images.
2. MMD = multiresolution merged dataset generated by the preserving approach with  $\beta=0.5$  for each image.
3. MMND = multiresolution merged and  $NDVI_p$  dataset which is similar to MMD except that the merged NIR image is replaced by the  $NDVI_p$  data.
4.  $HRV_i$  and PAN are multispectral and panchromatic images, respectively.

to the actual values computed from the merged data digital counts. The assessment of spatial improvement on a merged dataset was based on color composite comparisons to examine the spatial details present in the merged data. For each merged dataset, its color composite was visually compared to that from the original multispectral images, and the image interpretability enhancement through multiresolution merging was evaluated.

Because of its simplicity as well as availability in most image processing systems, the direct RGB display system was used to generate color composites. The green, red, and NIR wavebands in each dataset (Table 6-2) were assigned to the blue, green, and red color primaries, respectively. This color assignment was done to make the appearance of the generated color composites similar to that of an ACIR photography which is the most widely used in photographic remote sensing applications. The IHS transform was not used because of its universal adaptability or insensitivity to a wide range of data quality (Pellemans et al., 1992; Chavez et al., 1991; Carper et al., 1990; Harris et al., 1990; Welch and Ehlers, 1987; Cliche et al., 1985; Daily, 1983; and Hydan et al., 1982), which could introduce ambiguity to the evaluation.

The evaluation of spectral integrity of a merged dataset was based on comparisons of color composite and correlation analyses. If the color composite of a merged dataset shows a

great resemblance to that of original dataset OMD, the spectral information in the original image data is well preserved after the panchromatic image was merged. In addition, a high correlation between a merged image and its original multispectral counterpart can provide the indication of well maintained spectral disposition of original multispectral data. The weakening in the spectral integrity can also be reflected by an increase in between-waveband correlations within a merged dataset.

#### Image Response and Citrus Canopy Cover

The feasibility to separate citrus groves based on canopy cover difference was investigated using the SPOT data. The effect of multiresolution merging on such a differentiation was also evaluated. The percentage canopy covers of citrus groves were estimated photogrammetrically using both the ACIR photography and the stereo plotter.

#### Photogrammetric Measurement

Photogrammetric measurements from the ACIR photography were converted to ground distance by the following equation (Lillesand and Kiefer, 1979)

$$L = D \times h/f \quad [6-2]$$

where L is the actual ground distance (m), h is the flying height (m), f is the focal length of camera lens (mm), and D

is the distance (mm) on the photo which is obtained by

$$D = \sqrt{(x_2 - x_1)^2 + (y_2 - y_1)^2} \quad [6-3]$$

where  $x$  and  $y$  are photo coordinates (mm) for points 1 and 2, which were read directly from the ACIR photography through the stereo plotter. The photogrammetric accuracy of the ACIR photography was tested using highway pavement (Interstate Highway 95, Florida Turnpike, and local roads). The photo measurements of highway pavement width at 22 locations were obtained from the stereo plotter and then converted to ground distance using equations [6-2] and [6-3]. A comparison of the photogrammetric results with the data obtained from the local highway maintenance offices indicated a RMS error of 0.251 m (0.823 ft) which suggested a very accurate estimation for this photogrammetry.

Eighteen citrus groves within the study area (Figure 6-1) were selected through a visual inspection of the ACIR photographs. These 18 groves were uniform in that the number of missing or dead trees was few or zero. Photogrammetric measurements were made only in the central portion of each photograph. This was done to minimize the potential scale distortions resulting from camera lens and flight operations (Lillesand and Kiefer, 1979; Curran, 1985). The radius of the central portion was about 63.5 mm (2.5 inches) centered at the photo principal point. Because of the flat terrain in south Florida, corrections were not needed for the effect of topographic variations on the photogrammetric measurements.

For each selected grove, two to five rows were randomly chosen for taking photogrammetric measurements which included row length for the selected rows, field width at several locations (at least three), and the crown diameter of individual trees in all selected rows. The measurements were used for calculating field planting geometry (row and tree spacings) and the diameter of tree crown.

Tree spacing (a) within a row was obtained by dividing the row length by the number of trees in a row and averaged over the selected rows in a field, excluding three trees from each of the row ends. Similarly, row spacing (b) was obtained by dividing the field width by the number of rows in the grove and averaged over the number of measured locations (at least three locations) along the row length, excluding two rows from each side of the field. The diameter of tree crown (d) was based on the average of all measured trees in a selected grove. In addition, the photogrammetric measurements of tree and row spacings were ground-truthed for accessible selected groves.

#### Canopy Cover Estimation

Two cases were encountered in the estimation of citrus canopy covers using the ACIR photogrammetric measurements. The first case was that tree crowns were within the area bounded by tree spacing (a) and row spacing (b). In this case, percentage citrus canopy cover ( $\theta$ ) for each selected



grove was estimated by the following equation

$$\theta = \frac{\pi(d/2)^2}{a \times b} \times 100\%. \quad [6-4]$$

For mature groves with trees slightly overlapped or tree crown larger than tree spacing, the overlapping areas ( $A_o$ ) on both sides must be excluded. For this case, percentage canopy cover  $\theta$  was estimated by

$$\theta = \frac{\pi(d/2)^2 - A_o}{a \times b} \times 100\% \quad [6-5]$$

and the overlapping areas  $A_o$  ( $m^2$ ) were calculated by the following equations

$$A_o = 0.5[\pi d^2 (\phi/360) - a\sqrt{(d^2 - a^2)}] \quad [6-6]$$

$$\phi = 2 \tan^{-1}[\sqrt{(d^2 - a^2)}/a] \quad (0 \leq \phi \leq 180^\circ) \quad [6-7]$$

where  $a$  is tree spacing (m),  $b$  is row spacing (m), and  $d$  is diameter of tree crown (m).

Locations of the selected citrus groves in the SPOT scene were identified by scan lines and pixels in each of the three datasets including the original one with a 20-m spatial resolution. For each waveband of a dataset, the mean and standard deviation of grove-wide pixel values were obtained, excluding those pixels along field boundaries. The relations

between estimated canopy cover and image spectral response were investigated.

To assess the feasibility of differentiating citrus groves based on differences of canopy cover, the variations of image spectral responses (or pixel values) were analyzed for all selected groves through coincident plots of field-wide image data ( $\mu \pm \sigma$ ). Within a spectral waveband, a data overlap between two groves is the implication that these two groves can not be separated satisfactorily in that waveband because they possess image data of the same magnitude. An increase in the overlapping of image data is the indication of greater difficulty in separating the groves in a land-use classification analysis. In fact, it will be impossible to differentiate two groves if they have severe image data overlaps between all wavebands in a dataset (Lillesand and Kiefer, 1979).

#### Land-use Classification

Land-use classification analyses were performed on the three datasets listed in Table 6-2. The analyses were based on the capability of each dataset to differentiate the scene environment through spectral signature extraction. In addition, a GIS-based discrete land-use classification technique was introduced and applied to the canopy-size classification of citrus groves.

### Précis and Concept

Computerized land-use classification from remote sensing datasets is a two-step pattern recognition procedure which involves a training process and a sorting technique or classification decision rule. In order to classify a scene or dataset, the spectral signature patterns that are related to various land-use types within the scene must be extracted and defined using statistical criterion (e.g. means, variances, and covariances) implemented in an image processing system. This step of defining signature patterns is called the training process whose purpose is to "teach" the computer system to recognize the signature patterns inherent in the multi-waveband data. It is usually done through either a supervised or an unsupervised approach (Lillesand and Kiefer, 1979; ERDAS, 1991). In a supervised training, the analyst directs or supervises the computer in defining the signature patterns with the help of his prior knowledge or existing information about the ground. The process takes place in an interactive fashion between the computer and the analyst. One apparent advantage of a supervised training is that accurate signature patterns can be generated for the land-use types for which there is abundant existing information. However, for those land-use types for which there is not sufficient information, they are usually ignored or treated as background

elements. The emphasis is given mainly to the land-use types with available information. In addition, the analyst is often incapable of identifying the subpatterns within a broad land-use type even though those signature patterns are statistically separable and might possess some significance. Consequently, there is a great possibility that the whole set of signature patterns inherent to a dataset will either be incomplete or subjective in a supervised training.

In contrast to the supervised approach, the unsupervised training is very automated. Based on some input criterion specified by the analyst, the computer system searches through the dataset to unveil all the unique statistical patterns that are inherent in the image data. This training approach will allow the derivation of a complete set of signature patterns while alienating the likely subjectivity of a supervised training. To choose or select the proper criterion (or input parameters), some image processing experience is needed. However, the implementation of modern image processing systems has made such a task much easier by minimizing the number of input parameters. After the spectral signature patterns are defined, a classification decision rule is invoked to sort through or to classify all pixels in an entire dataset. The result of classification is a thematic image that contains the numberings of spectral patterns or classes which are later related to various land-use types through a ground-truthing

procedure. A summary of the commonly used classification decision rules is presented in Appendix D, which includes the parallelepiped classifier, the minimum distance classifier, the mahalanobis distance classifier, and the most widely used maximum likelihood classifier (Lillesand and Kiefer, 1979; ERDAS, 1991).

### Extracting Signature Patterns

One method to assess the effects of multiresolution processing was to evaluate the capability of a merged dataset to unveil the signature patterns for the given scene environment. If a dataset indicates a greater prospect to derive more signature patterns under the same given criterion, it will be advantageous to use the dataset for improving land-use classification results. On the other hand, a dataset would be considered as inferior if its ability to unveil spectral signature patterns is limited. In order to have an objective evaluation, the signature patterns for each dataset have to be complete while the statistical criterion used for a clustering procedure should be identical. In addition, the subjectivity associated with the supervised training method must be avoided to ensure that none of the potential signature patterns inherent in a dataset will be overlooked.

To derive the signature patterns for each dataset, the ERDAS STATCL (statistical clustering) module was used. In an



unsupervised statistical clustering procedure, the most important parameter is the scaled (spectral) distance (ERDAS, 1991; Graham et al., 1986) which defines the separability criteria for all signature patterns of a dataset within a multidimensional space bound by the wavebands. Two signature patterns are considered not separable if their scaled distance is less than the specified value (automatically merged). When the scaled distance is set at a large value, the number of separable signature patterns will become smaller. On the other hand, a small scaled distance will allow a "tight" clustering, making closely related signature patterns become separable (ERDAS, 1991).

The ERDAS STATCL module was used with a large number (80) of conceivable spectral patterns to ensure that none of the potentially separable signature patterns will be forced to merge to the others before the clustering process is completed. Also, several values of scaled distance were used in order to examine the consistency as well as the dependability of a merged dataset. In order for a signature pattern to be statistically reliable, the adequate sample size for each signature pattern must contain at least  $(10-100) \times (n+1)$  pixels where  $n$  is the number of spectral wavebands used (Swain, 1978). For instance, the desired sample size for a three-waveband dataset is about 40-400 pixels. At the completion of the STATCL module, a spectral pattern with a

scaled distance less than the specified value is automatically merged to its closest neighbor. After such a merging based on the specified scaled distance, those patterns with a sample size less than 99 pixels (10 fields in an ERDAS term) were discarded. The input parameters for the STATCL module are summarized in Table 6-3. Similar clustering procedures and parameters were also used in the ELAS image processing system (TMTR module) to derive signature patterns for each dataset for comparisons between the two systems. Since an identical methodology that included clustering module and input parameters was utilized to generate spectral signature patterns for each of the datasets, a larger number of spectral patterns is a clear indication that the dataset will have a greater differentiations among the various land-use elements. When sufficient ground-truth information is available, a larger number of spectral classes will be advantageous to land-use classification efforts for obtaining land-use data with greater detail.

#### GIS-based Discrete Classification

A GIS-based discrete land-use classification technique was introduced in an effort to classify the citrus groves based on differences of canopy cover. The basic concept of a discrete approach is to utilize GIS techniques to guide the entire process of both clustering and classifying to only the

Table 6-3. Parameters used in ERDAS STATCL and ELAS TMTR modules for signature extraction.

---

Presumed number of patterns:	80
Lower bound standard deviation:	0.1
Upper bound standard deviation:	1.2
Coefficient of variation (%):	5
Scaled distance (used):	3, 2, 1
Minimum field threshold:	10
Perform final merge:	Yes

---

land-use types of interest. This will eliminate the pixels of unrelated land-use types in the classification results. In remote sensing land-use classification, confusion often exists that one spectral class entails several different land-use types. For instance, pasture lands can be mixed with brushes while citrus groves mingle with forests, pasture lands, and brushes. This inter-class mingling creates a great difficulty in improving classification results. Though the extent of inter-class confusions depends on many factors such as low radiometric quality of image data, the method to cluster and classify the image data is very critical. If a traditional clustering procedure is applied, the derived signature patterns often consist of pixels related to other land-use categories. When using GIS techniques, both the clustering and classifying processes can be confined within each respective land-use category to extract the potential subclasses. There are several advantages for this discrete classification technique.

First, efforts and resources can be concentrated on the land-use type(s) of greater interest by confining the processes of clustering and classifying to only the land-use category (e.g. citrus land use) being studied. This significantly reduces the time and resources devoured to the less important land-use types.

Second, spectral signature patterns will consist of pixels only from the land-use category that is being

investigated. This eliminates the problems of inter-class confusion and as a result, increases the accuracy of classification results.

Third, the subclasses within each category of land use can be classified and evaluated individually, allowing the problems associated with a given land-use category to be isolated and identified with greater accuracy.

Fourth, as the capability of remote sensing systems continues to improve, information in image datasets becomes less and less generalized while more detailed land-use information is increasingly demanded. The use of this GIS-based discrete approach will make more efforts for improving land-use classification successful.

The discrete classification procedure can be achieved through a collaborate use of GIS techniques and traditional land-use classification procedures. The approach utilizes a supplementary data layer to guide the processes of both signature extraction and classification for all subclasses within their respective category of land use. For instance, when a GIS database containing general citrus land use is used, both the derivation of spectral signatures and the classification of subclasses can be confined within the citrus land use. This will avoid the impurity of spectral signature patterns because the pixels used are only from citrus land use. As a result, the inter-class confusions between citrus



and non-citrus land uses are eliminated, allowing a further classification of citrus land use. This discrete approach will allow the problems related to the land use type of interest to be isolated for further investigation.

The discrete classification technique was demonstrated in the classification of citrus land use. Since a GIS dataset containing the general land use of citrus was not available, it had to be constructed from map data together with the ACIR photography. The field boundaries of all groves in the study area were transferred from the ACIR photography to the USGS 7.5 minute series quadrangle maps and then digitized as a data layer of polygons using the Arc/Info GIS software. The polygon data layer was projected to the UTM coordinate system before being converted (by use of Arc/Info POLYGRID command) to a grid of 10-m cells compatible with the SPOT satellite data. This grid is named as CITRUS data layer.

Through the use of ERDAS NRECTIFY (non-linear rectify) module along with the nearest neighbor resampling method, the three datasets (Table 6-2) were also georeferenced to the UTM coordinate system in order to be geographically compatible with the CITRUS grid data layer. Because an integrated module for the discrete clustering and classification is not available in either the ERDAS or ELAS image processing systems nor does it exist in the Arc/Info GIS system, some additional efforts were required which included clipping the citrus areas

using the CITRUS grid layer and setting all the non-citrus pixels to zero. The resultant datasets each (OMD, MMD, and MMND) allowed the clustering and classifying processes to be directed to only citrus pixels (non-zero pixels) while non-citrus pixels were ignored. If an integrated module for discrete classification was available, these efforts to clip and manipulate the image data could have been avoided. All the areas outside the citrus land use could also have been classified in just one unified procedure.

For its high clustering accuracy, the ERDAS ISODATA module (ERDAS, 1991), which is based on the iterative self-organizing data analysis technique (Tou and Gonzalez, 1974 in ERDAS, 1991), was utilized to derive the spectral signature patterns from all the groves. The STATCL module was not used because of concerns about its clustering process that relies on blocks of pixels (3 x 3 pixel arrays) which could introduce problems to the boundary areas between citrus and non-citrus land-use types. For each of the three datasets, the ISODATA module was instructed to derive seven signature patterns which were later used by the ERDAS MAXCLAS (maximum likelihood) classification module to classify all the citrus pixels in each entire dataset into seven spectral classes. For both the ISODATA and MAXCLAS modules, the non-citrus pixels were ignored and treated as a background class (class zero). The ELAS system was not used because its implementation does not

render the alternative of ignoring pixels with certain values (e.g. zero).

The discrete classification technique is not a supervised classification procedure, though a supplemental GIS dataset is used in the clustering and classifying processes. Within each category of land use, all potential subclasses are clustered and classified using the unsupervised classification method. Therefore, the seven spectral classes for each dataset (OMD, MMD, and MMND) were ground-truthed using canopy cover estimates from the ACIR photography as well as data collected during field visits.

## CHAPTER 7

### DISCUSSIONS AND ANALYSES OF MULTIRESOLUTION LAND-USE CLASSIFICATION

The results from merging the SPOT multiresolution data are discussed in this chapter, which include the radiometric quality of merged datasets, the feasibility for a canopy-size differentiation of citrus groves, and the effect of multiresolution processing on land-use classification.

#### Evaluation of Merged Image

To evaluate the quality of merged images, image standard deviations (or radiometric variances) and color composites of merged image data are examined. Since the primary emphasis of multiresolution processing is to enhance the multispectral data, evaluations and comparisons of merged image/datasets will be made based on the same quality factors of the corresponding original multispectral image.

#### Radiometric Quality

The standard deviations ( $\sigma$ ) and mean brightness values ( $\mu$ ) for the merged SPOT images are summarized in Table 7-1. A substantial increase in image standard deviation was observed for all merged images (Table 7-1). Even for the NIR waveband which had a near-zero correlation ( $r=0.085$ ) to the panchromatic data (Table 6-1), the image standard deviation

Table 7-1. Standard deviations ( $\sigma$ ) and mean brightness values ( $\mu$ ) for multiresolution merged SPOT images.

Wave-band#	Merging-method & coeff.	Mean ( $\mu$ )	Standard deviation ( $\sigma$ )
pan.	raw data	27.3	9.22
green	raw data	29.8	6.73
red	raw data	18.1	7.41
NIR	raw data	65.2	11.51
green	P <sup>a</sup> (0.5)	43.7	10.86
red	P (0.5)	32.0	11.59
NIR	P (0.5)	73.5	12.06
NDVI <sub>p</sub> <sup>b</sup>	-	179.8	18.52

Note: <sup>a</sup> -- Preserving method with  $\beta=0.5$ .

<sup>b</sup> -- NDVI<sub>p</sub> is normalized difference vegetation index using panchromatic waveband.



(radiometric variance) was also increased in the merging process. Note that the radiometric enhancement in all these merged images was not the contemplations of a contrast-stretching or PCA procedure, even though those techniques can be applied for further image enhancement. They are the results of increased image gray shades in the merged data, which are essential to improve the visual qualities for image interpretation and to achieve a greater differentiation of the scene environment for improving land-use classification. In addition, the enhanced radiometric quality also demonstrates the effectiveness of the preserving approach to merge the panchromatic data to the multispectral images for multiresolution processing, which was already observed in the results from the NOAA-11 LAC data discussed in chapter 5.

For the  $NDVI_p$  image, the use of a scaling factor hampers an objective comparison of its radiometric quality with that of the multispectral NIR waveband. The scaling factor used for the fractional ratioed results was functionally equivalent to a linear stretching procedure. In addition, the  $NDVI_p$  method had a special purpose of image enhancement for vegetation. For the three images of MMD, the standard deviations ( $\sigma$ ) computed from the merged image data were found virtually identical to the estimates from equation [4-25]. These results not only extend the applications of the principle of statistical variation analyses of combining random variables to satellite images with different spatial

resolutions, but also provide a feasible means to assess and evaluate the radiometric quality of pre-merged multiresolution datasets.

### Spatial Improvement and Spectral Integrity

The evaluation of spatial enhancement is based on an visual comparison of the color composites between datasets OMD and MMD (Table 6-2). After the panchromatic data is merged, the composite of merged dataset MMD indicated a substantial improvements in spatial detail. As noted in the study by Ehlers (1989), the most obvious enhancement was revealed in linear features which included interstate highway 95, the Florida turnpike, local roads, and field boundaries. The spatial enhancement is attributed to the preserving approach with a  $\beta=0.5$  merging coefficient, which effectively merged the panchromatic spatial information to the multispectral images while increasing the radiometric quality in the merged data.

The spectral integrity in a multispectral dataset is the disposition of image data in the respective multispectral wavebands. Its assessment includes three analyses: (1) a comparison of the color composite of a merged dataset with that of the original multispectral data; (2) a correlation analysis between a merged image and its multispectral counterpart; and (3) a comparison of between-waveband correlations among the images within a dataset. While the color appearance of a composite renders an effective

comparison of the overall spectral quality of a dataset, the correlation analyses provides a further assessment of the spectral disposition of the merged image data.

The color composites of datasets OMD and MMD indicated an outstanding conformity based on a visual assessment. This correlation in visual quality suggests that the multispectral information in merged dataset MMD is comparable to that of original dataset OMD. In addition, the color composite of merged dataset MMD also exhibited a great resemblance to an ACIR photography of good quality, suggesting its usefulness and effectiveness for image interpretation applications. All vegetative areas (e.g. citrus groves, pasture lands, and forest stands) showed up in bright red colors of varying intensities for different vegetation conditions, while roads and urban structures were indicated with white colors as they are usually observed in a typical ACIR photography.

The high correlation between each merged image and its original multispectral counterpart (Table 7-2) suggests that there is no significant alterations of image spectral data between datasets OMD and MMD. In other words, the disposition of spectral information in merged dataset MMD is similar to that of dataset OMD. Though a slight increase in the between-waveband correlations was noted for dataset MMD (Table 7-3), these changes are neither substantial nor deleterious to the original multispectral integrity of dataset OMD. When the factors of radiometric improvement, spatial enhancement, and spectral integrity are put in perspective, the conclusion is

Table 7-2. Summary of correlations between a merged image and its original multispectral counterpart.

Waveband			
Green (HRV <sub>1</sub> )	Red (HRV <sub>2</sub> )	NIR (HRV <sub>3</sub> )	NDVI <sup>a</sup>
0.971	0.978	0.921	0.935 <sup>a</sup>

<sup>a</sup> -- for NDVI and NDVI<sub>p</sub> images.

Table 7-3. Between-waveband correlations (r) within multiresolution merged datasets.

Data-set#	Merging-method	Wave-band	Spectral waveband		
			green	red	NIR
-	raw data	Pan	0.826	0.852	0.085
OMD <sup>a</sup>	raw data	green	-	0.963	0.155
	raw data	red	-	-	0.022
	raw data	NIR	-	-	-
MMD <sup>a</sup>	P <sup>b</sup> (0.5)	green	-	0.986	0.451
	P (0.5)	red	-	-	0.384
	P (0.5)	NIR	-	-	-
(NDVI <sub>p</sub> )					
MMND <sup>a</sup>	P (0.5)	green	-	0.986	-0.610 <sup>c</sup>
	P (0.5)	red	-	-	-0.685 <sup>c</sup>
	NDVI <sub>p</sub>	NDVI <sub>p</sub>	-	-	-

<sup>a</sup> -- Refer to Table 6-2 for dataset definition.

<sup>b</sup> -- Preserving method.

<sup>c</sup> -- NDVI<sub>p</sub> image was used instead of NIR waveband for the correlation analysis.

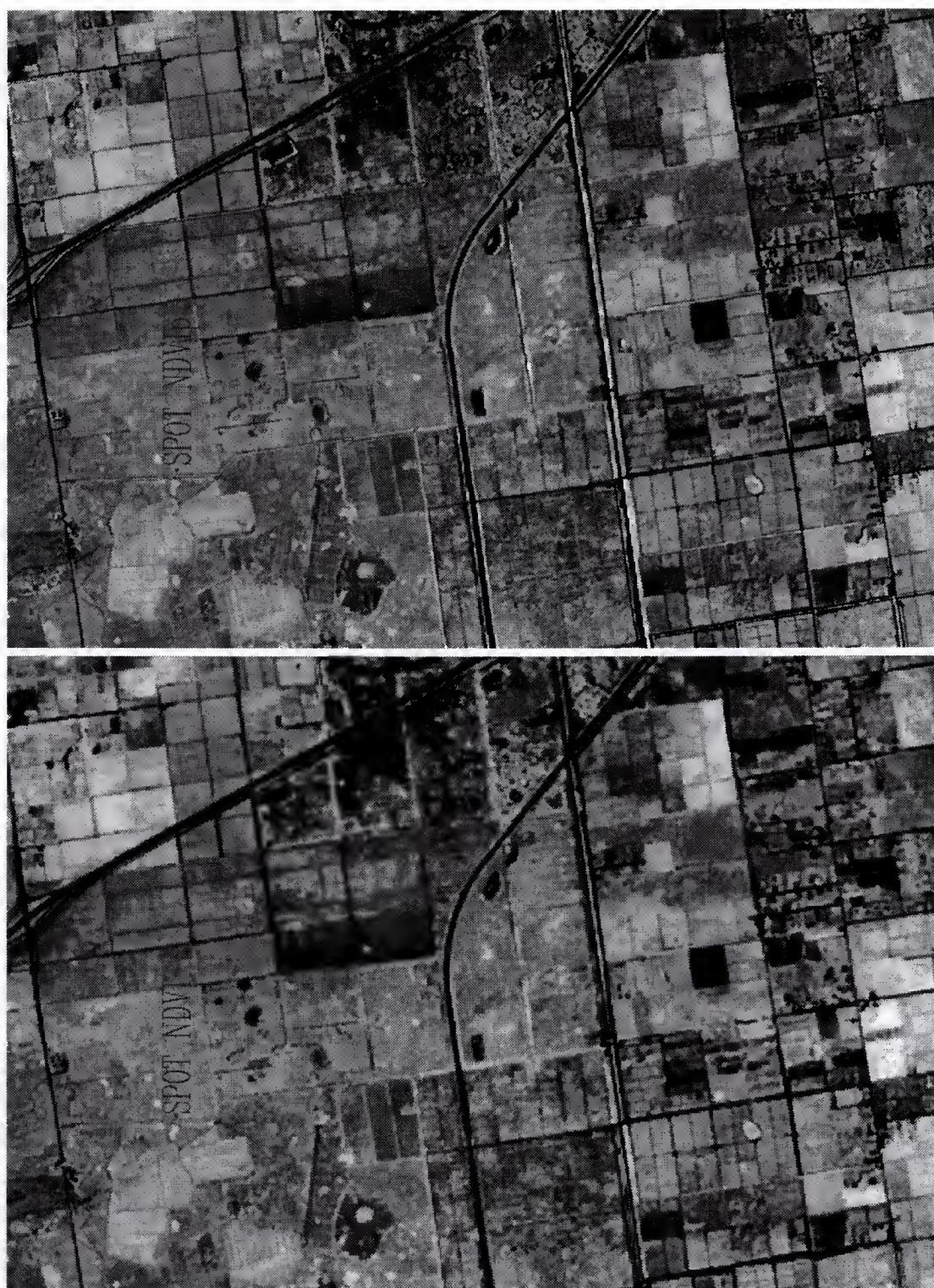


that the preserving approach (with  $\beta=0.5$ ) is an effective method for multiresolution processing of SPOT multiresolution datasets for remote sensing applications.

From a black-and-white display (Figure 7-1), the  $NDVI_p$  image indicated a great resemblance to the customary NDVI image generated from the original 20-m multispectral NIR and red wavebands [Note:  $NDVI=(NIR-Red)/(NIR+Red)$ ]. These two vegetation index images had a ( $r=0.935$ ) high correlation (Table 7-2), implying that the information of one image is very similar to the other. In both the  $NDVI_p$  and NDVI images, vegetative areas appeared as bright (large NDVI values) and had a greater image contrast, while urban lands/structures and water bodies including marshes showed a black appearance with little contrast. This demonstrates not only the capable enhancement of vegetative lands by the  $NDVI_p$  method, but also the comparable  $NDVI_p$  effectiveness to that of the original NDVI method. The benefit of substituting the red waveband by the panchromatic data was the added spatial enhancement while maintaining the effectiveness of the original NDVI image. The enhanced spatial details makes the  $NDVI_p$  approach more appealing for vegetation studies.

In summary for the radiometric assessment of the SPOT multiresolution merged dataset, three observations were made. First, the preserving approach with  $\beta=0.5$  is a very effective method to generate multiresolution merged SPOT datasets with improved radiometric quality and to produce spatially enhanced





$$\text{NDVI} = (\text{NIR} - \text{Red}) / (\text{NIR} + \text{Red})$$

$$\text{NDVI}_p = (\text{NIR} - \text{PAN}) / (\text{NIR} + \text{PAN})$$

Figure 7-1. Comparison of SPOT 20-m NDVI and 10-m NDVI<sub>p</sub> images.



color composites for image interpretation applications. The well preserved spectral information in the merged data will allow the merged datasets for further applications such as land-use classification. Second, the effectiveness of the  $NDVI_p$  method for vegetation enhancement is comparable to that of the customary NDVI method using the original 20-m NIR and red wavebands. The added improvement in spatial detail by replacing the red waveband with the panchromatic image makes the  $NDVI_p$  method more appealing for vegetation studies. Third, the radiometric quality of pre-merged multiresolution SPOT datasets can be accurately assessed by using the principle of statistical variation analyses for random variable manipulations discussed in chapter 4.

#### Image Response and Citrus Canopy Cover

The focus of this section is to discuss the effect of citrus canopy cover on image spectral response as well as the feasibility of a canopy-size differentiation for citrus groves. The specific points included the photogrammetric estimation of citrus canopy cover, the relations between SPOT image response and citrus canopy cover, the differentiation of citrus groves based on canopy cover differences, and the effect of multiresolution processing.

#### Estimation of Citrus Canopy Cover

For the 18 selected citrus groves, the percentage canopy covers ranged from about 20% to 75% based on photogrammetric

estimations. Groves with canopy cover less than 20% have trees too small to measure on the ACIR photography with a 1:24,000 scale and were not selected. Canopy cover estimation for young groves (small canopy cover) requires photographs of a larger scale (e.g., 1:2,400). However, the irregular tree shape in young groves can create further problems for making reliable measurements. On the other hand, citrus trees in mature groves are over-growing into each other's canopies. When a grove is over-grown, it becomes impossible to identify the separation between trees for making measurements of tree spacing and tree crown size (diameter). As a result, canopy covers outside the 20 to 75% range are considered to be difficult to estimate photogrammetrically. However, since the ground-based estimation of citrus canopy cover is extremely difficult, the photogrammetric approach might be the only practical solution to the problem of citrus canopy cover estimation. In addition, the ground-truthing in four accessible groves indicated very accurate measurements for tree and row spacings with a RMS error of 0.35 m which is within the spatial resolution limits of the ACIR photography.

It should be noted that the scale of the photography will have a direct effect on the accuracy of photogrammetric measurements. A large scale (e.g., 1:2,400) is desirable for better accuracy, but aerial photography at large scales is expensive, particularly when a large coverage area is needed. Also, it is important to recognize that the benefit of photo

enlargement or magnification is limited by the spatial resolution constraints of the original photographs/films. Therefore, the selection of a photo scale for citrus canopy cover estimation must be based on consideration of the actual tree crown (object) diameter (size) and the equipment capability (precision). Generally, ACIR photographs with a scale from 1:24,000 to 1:2,400 can be considered as appropriate for citrus canopy cover estimation.

#### Relation of Image Response to Canopy Cover

The relations between citrus canopy cover and image response for the green and red wavebands of the original 20-m multispectral dataset OMD are shown in Figures 7-2 and 7-3. The difference of citrus canopy cover does have an effect on the SPOT spectral responses of the green and red wavebands (Figures 7-2 and 7-3). However, the effect was not profound enough to result in well defined relationships. In other words, citrus canopy size does not have a solitary correlation with the SPOT spectral responses of the green and red wavebands. Also observed in Figures 7-2 and 7-3 is an inverse relationship between canopy size and spectral response for the green and red wavebands. The primary cause for such inverse relationships, which were also observed for wheat crops by Idso et al. (1977), was due to the relatively higher spectral reflectance of underlying soils. In partial canopy groves, the spectral response of a pixel depends on the collective



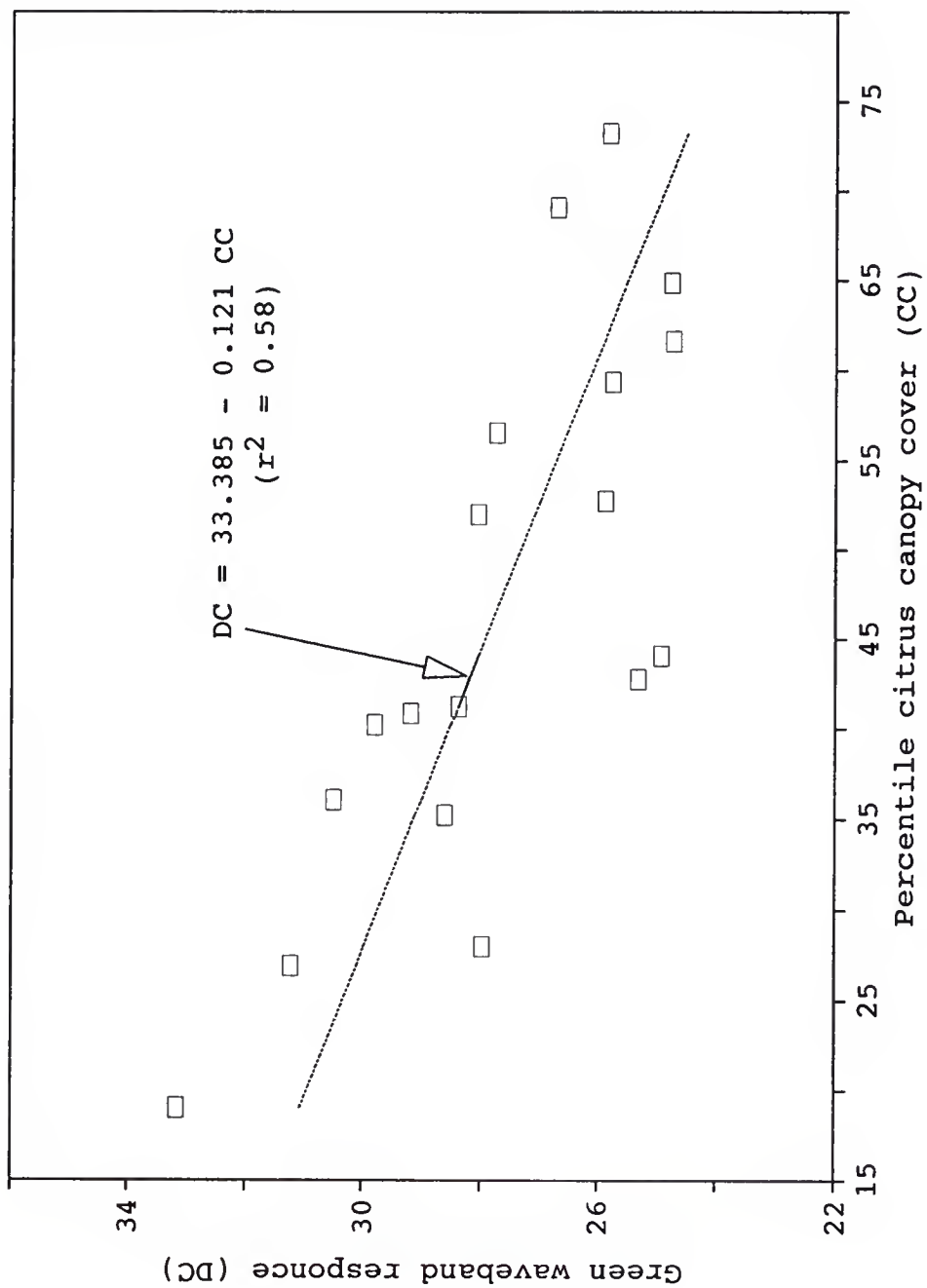


Figure 7-2. Effect of citrus canopy cover on SPOT green waveband response.

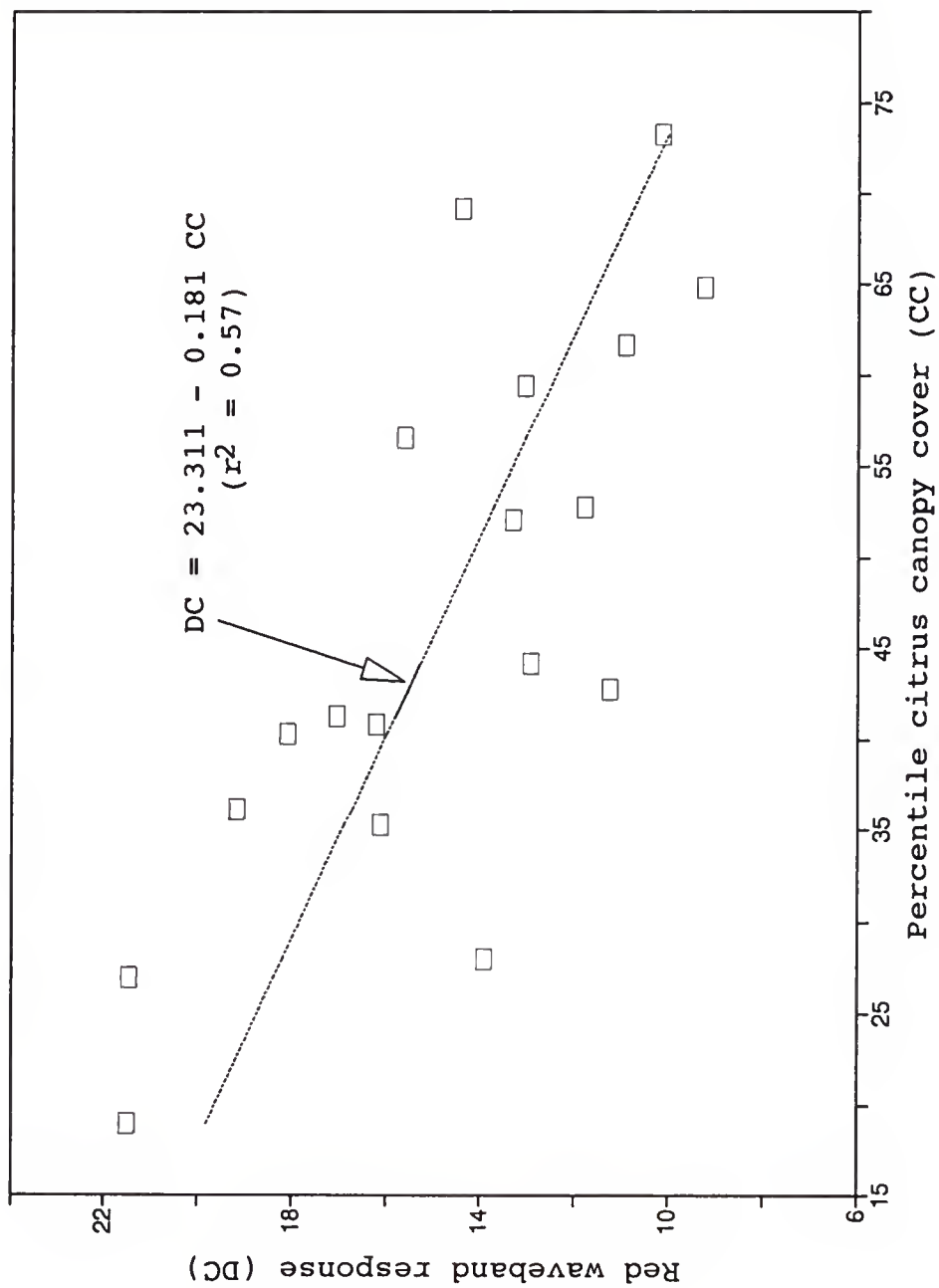


Figure 7-3. Effect of citrus canopy cover on SPOT red waveband response.

effect of both exposed soils and canopy covers. As compared to vegetation, exposed soils (especially sandy soils in south Florida orchards) tend to have significantly strong reflectance in the visible (e.g. green and red) wavelength ranges, particularly when soil moisture content is low (Lillesand and Kiefer, 1979; Shih, 1988; and Rees, 1990). An increase in canopy cover would shut out more high-reflectance exposed soils from the sensor's instantaneous viewing area. This will reduce the overall reflected radiance from the target (pixel). As a result of increased canopy cover, a smaller value of spectral response (digital count) was recorded in the image. In citrus groves in south Florida, bare soils between trees as well as in traffic tracks are examples that have relatively higher spectral reflectance than trees in the green (0.50-0.60  $\mu\text{m}$ ) and red (0.60-0.70  $\mu\text{m}$ ) wavelength ranges. For the SPOT panchromatic waveband, which encompasses both the green and red wavebands while extending to a small portion of the NIR wavelength range (generally regarded as 0.7-1.0  $\mu\text{m}$ ), its spectral response to citrus canopy cover maintained the general characteristics of both the green and red wavebands (Figure 7-4).

Unlike those of the green and red wavebands, the spectral response of the NIR waveband did not indicate to correlate to citrus canopy cover (Figure 7-5). For the NIR waveband, the lack of a perceivable relationship of spectral response to citrus canopy size can be caused by many factors including

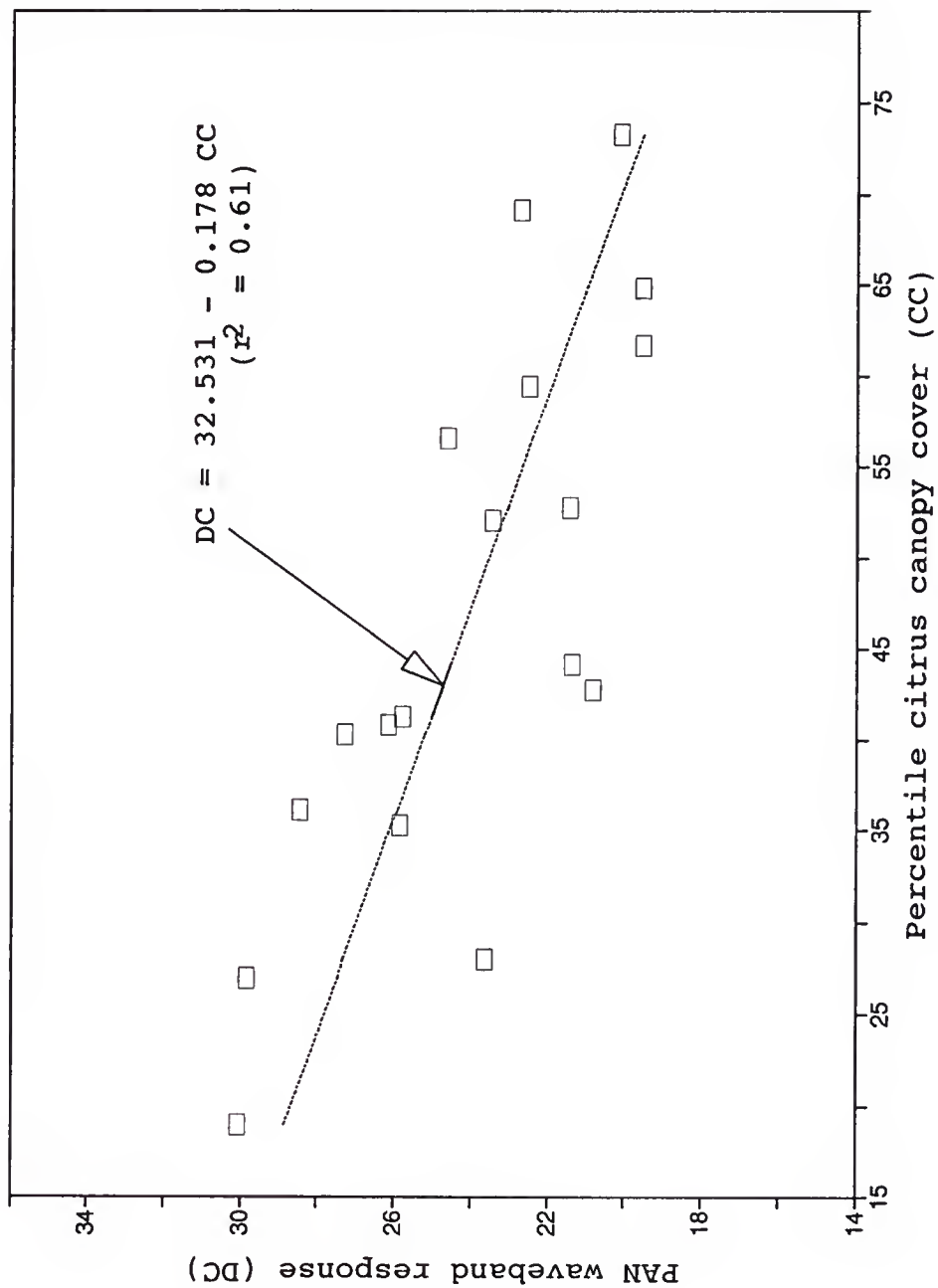


Figure 7-4. Effect of citrus canopy cover on SPOT panchromatic waveband response.

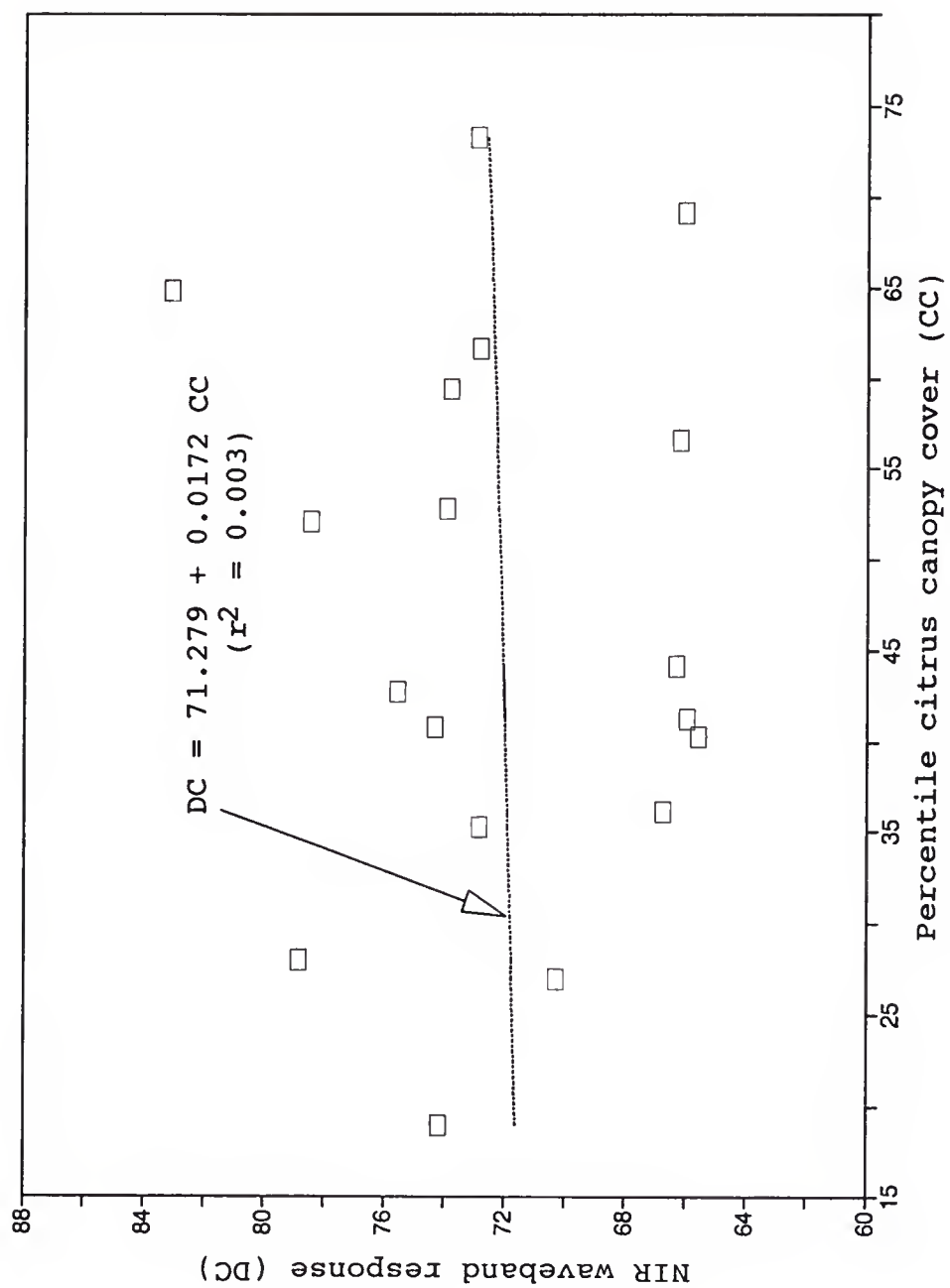


Figure 7-5. Effect of citrus canopy cover on SPOT NIR waveband response.



canopy itself and underlying soils. In a study of cotton crops spectra, Huete and Jackson (1988) found that there is a strong interaction between canopy cover and underlying soils for partial canopy fields. For instance, the NIR spectral reflectance of exposed soils is generally lower than that of vegetation (Lillesand and Kiefer, 1979; Rees, 1990). In a land-use classification study, Shih (1988) found that barren soils had a lower NIR response than agricultural lands including citrus groves in south Florida. Therefore, an increase in citrus canopy cover would increase the reflected radiance from the sensor's viewing area, resulting in a larger image value. However, the spectral response of the NIR waveband is not influenced by canopy cover alone. In the NIR wavelength range, the reflectance of citrus trees (vegetation) is predominately related to tree health/growth conditions. While a healthy citrus tree exhibits very high reflectance, a stressed one will not (Shih et al., 1985). In addition, the stage of growth, cultural practices (e.g. hedging, topping, weeding, etc.), and diversity of soil substrates (e.g. dry, wet, dark, or bright) could also contribute individually or collaborately to the variations of the NIR image response for groves with partial canopy cover. Therefore, these factors together will make it extremely difficult for the NIR waveband to have a defined relation to the differences of citrus canopy size.

In summary, the SPOT image response does indicate tangible inverse relations to citrus canopy size for the

green, red, and panchromatic wavebands. However, these relationships are neither strong nor solidary. On the other hand, the SPOT NIR response did not indicate a perceivable relation to citrus canopy cover. In general, the lack of well defined relations between canopy cover and image spectral response is the implication of great variations of both soil and tree conditions over the study area. Recall that the SPOT scene was acquired in early October when the season is generally wet with miscellaneous vegetation still thriving in the fields. In order for a satellite sensor to effectively differentiate the differences of citrus canopy cover, soil conditions must be as less variable (e.g. dry winter months of January and February) as possible over the entire area of study. This will minimize the strong influence of soil substrate variations.

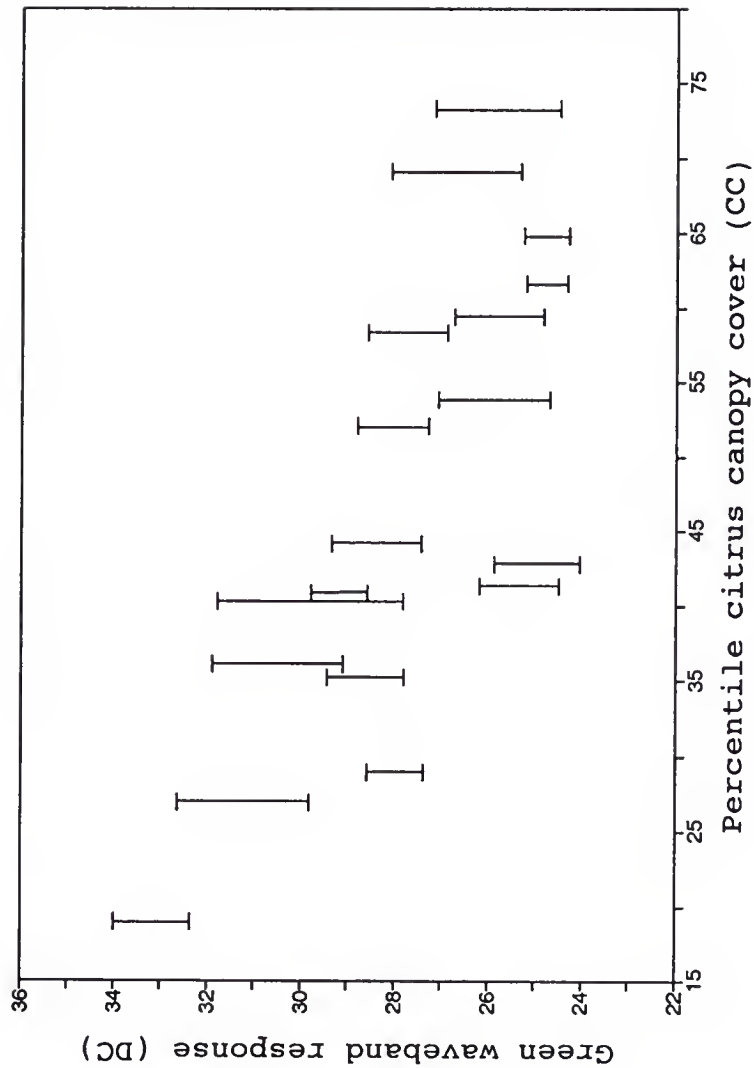
#### Differentiation of Canopy Cover

The feasibility for a canopy-size differentiation of citrus groves based on percentage canopy covers was evaluated using coincident plots of the field-wide image response of the selected groves. In land-use classification analyses, the variations of grove-wide image data will have a direct impact on the separability of groves with different canopy covers. To examine the feasibility of a canopy-size differentiation of citrus groves, the grove-wide image response ( $\sigma \pm \mu$ ) for each

selected field in dataset OMD is illustrated in Figures 7-6, 7-7, and 7-8 for the green, red, and NIR wavebands, respectively.

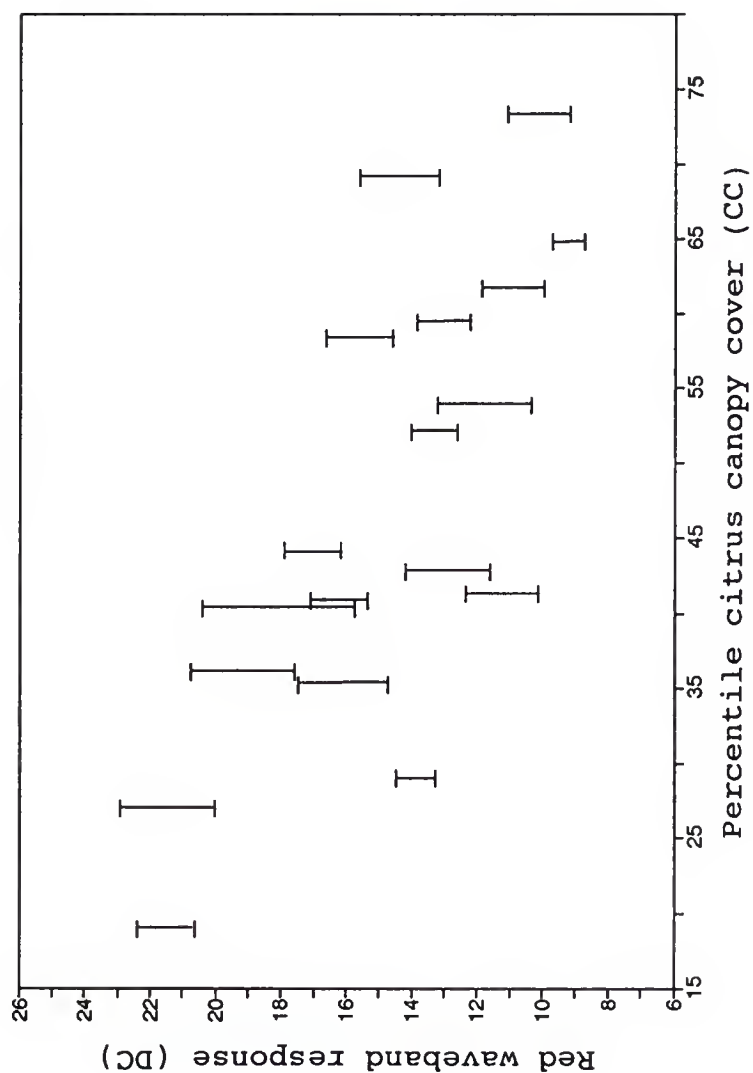
From the results presented in Figures 7-6, 7-7, and 7-8, three comments are in order. First, the number of image gray shades were very limited for the entire 20-75% range of canopy cover. This strong containment of image gray shades, which were respectively about 13, 14, and 26 for the green, red, and NIR wavebands, not only revealed a very limited resolving capability of the SPOT image data for the entire 20-75% canopy cover range, but also implied a great difficulty for a canopy-size differentiation of citrus groves. The limited gray shades together with the lack of well defined relations between canopy cover and image response did not suggest likely separations within the 20-75% canopy cover range.

Significant grove-wide variations of image response created severe data overlaps among the groves with different canopy sizes, and as a result, these data overlaps further complicated the separability problem. If two groves have a data overlap in a waveband, the two groves may not be separated in that waveband because they possess image data of the same magnitude. The more severe the overlapping is, the more likely two groves are inseparable. As shown in Figures 7-6, 7-7, and 7-8, none of the selected groves are free from data overlaps in any of the three SPOT wavebands. In order to achieve a canopy-size differentiation of citrus groves, the



Note: DC--digital count.

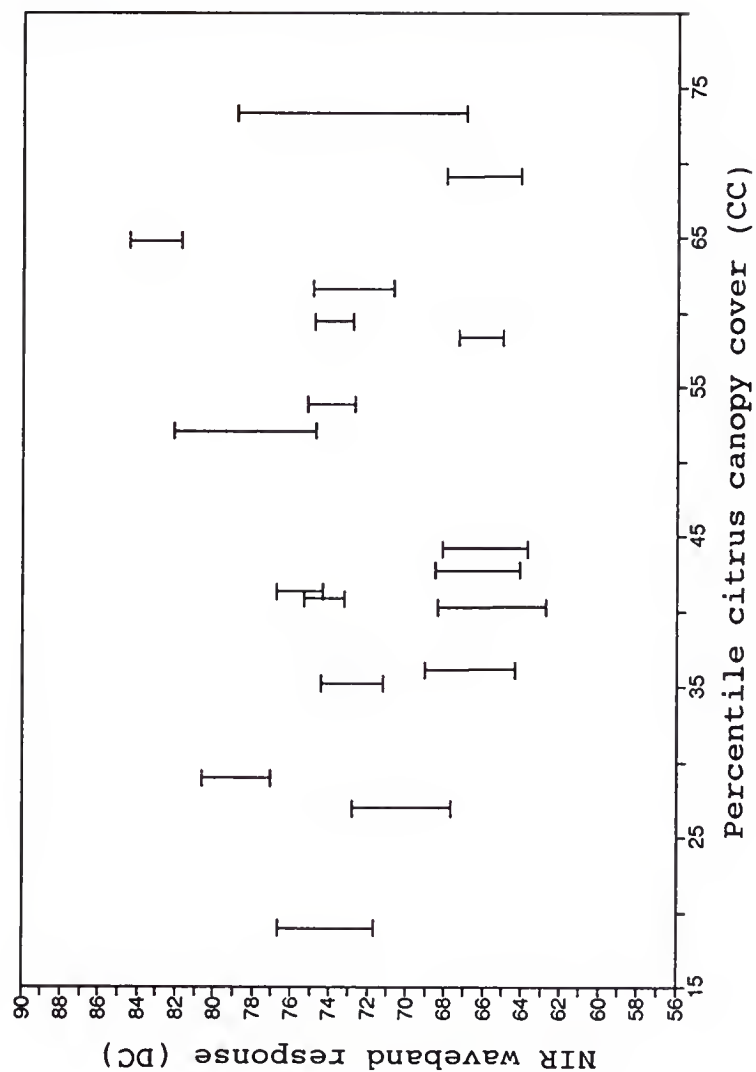
Figure 7-6. Coincident plot of SPOT green waveband response for selected citrus groves.



Note: DC--digital count.

Figure 7-7. Coincident plot of SPOT red waveband response for selected citrus groves.



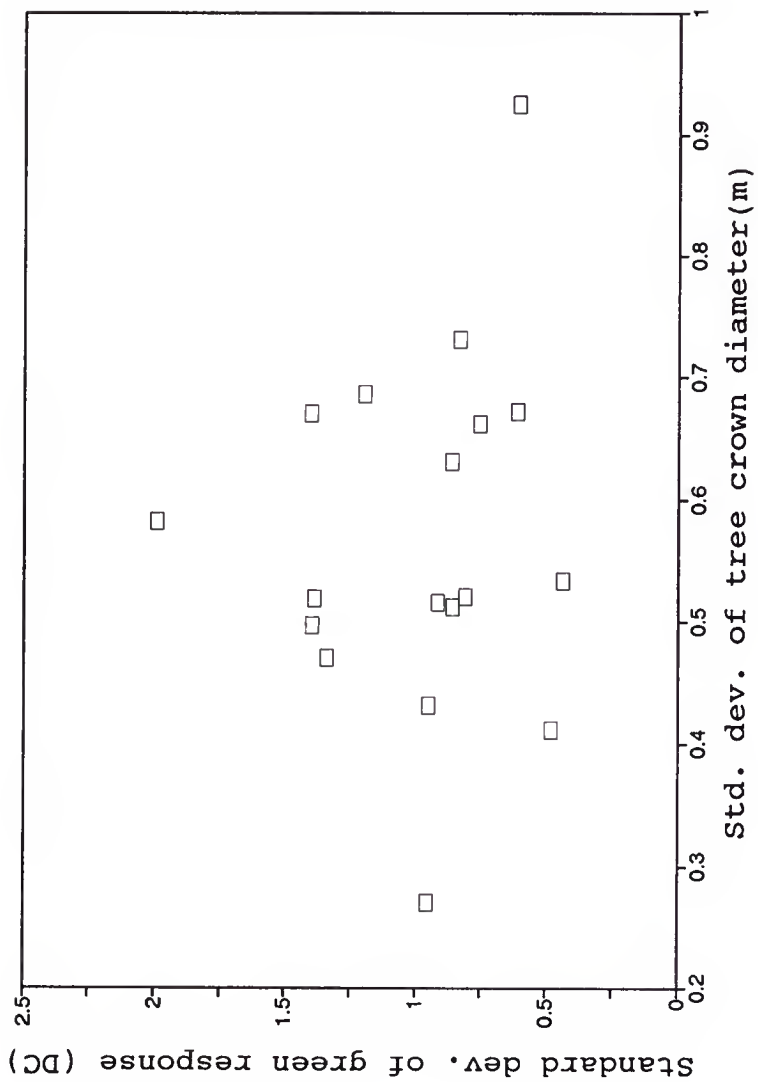


Note: DC--digital count.

Figure 7-8. Coincident plot of SPOT NIR waveband response for selected citrus groves.

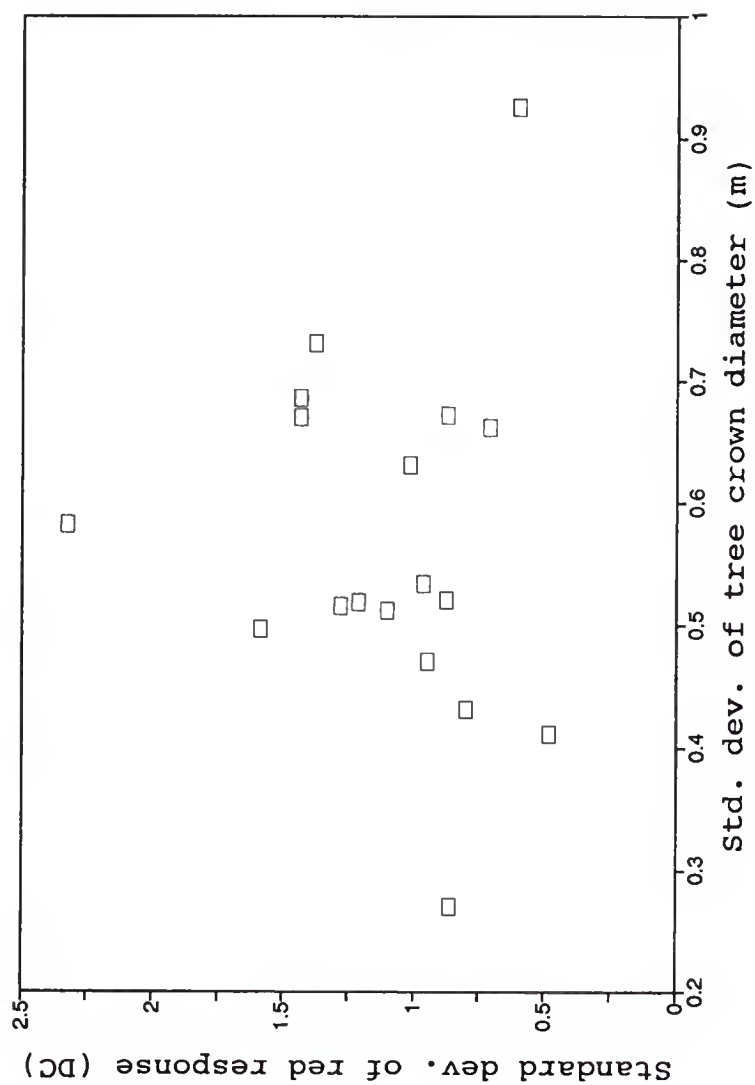
image response in some ranges of canopy cover must be unique as well as free from data overlaps in at least one waveband. In a citrus field with partial canopy cover, the response value (digital count) of a pixel is determined by the collective effect from the areas of canopy cover and exposed soils. The variability in both tree crown diameter and underlying soil substrates is a very important factor responsible for the variations of image response of a partial canopy cover grove.

The uniformity of image response of a grove is affected by the overall field conditions including the variations of tree crown diameter and soil "brightness". In general, a larger variation in tree crown diameter would result in more variable image response. However, such a relation was not observed for the green, red, and NIR wavebands (Figures 7-9, 7-10, and 7-11), suggesting that there existed significant variations of soil condition among the groves. According to Huete and Jackson (1988), the soil "brightness" had a strong influence on the spectra of partial canopy cotton fields. Also, it was noted from an early discussion that citrus canopy cover was inversely related to image spectral response. Apparently, the effect of soil brightness was so strong that canopy cover was acting only like a dampening factor to the overall spectral response of a partial canopy pixel. Hence, limiting the variability of soil conditions is very critical to the feasibility in remote sensing applications for canopy cover studies.



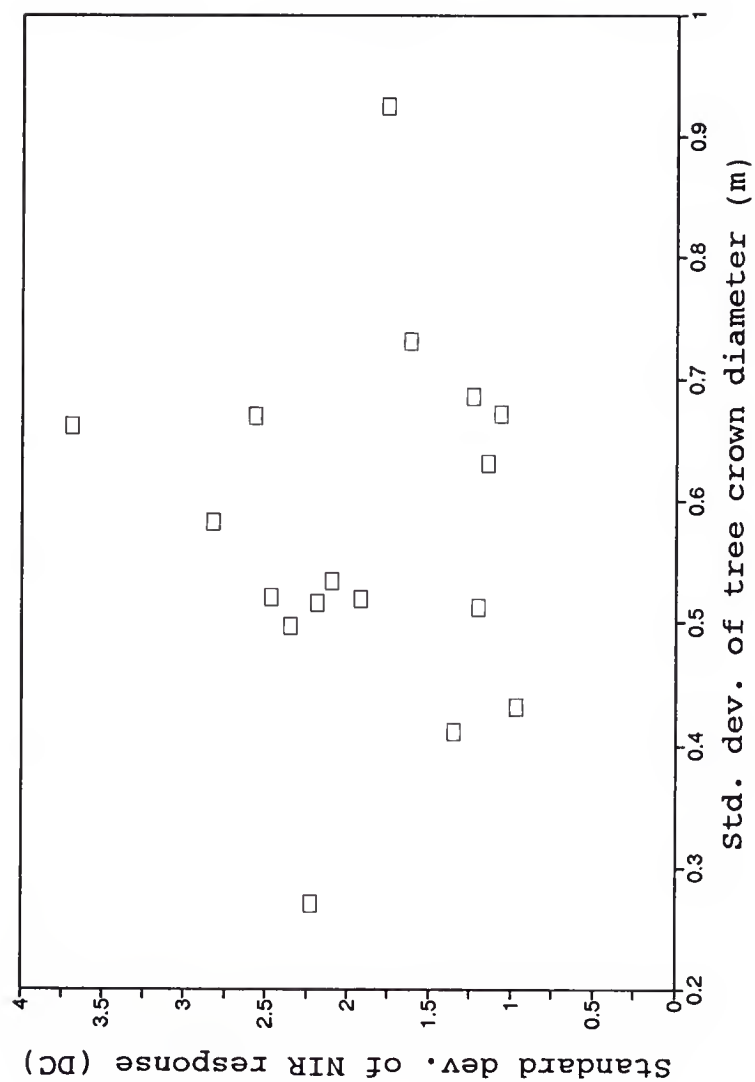
Note: DC--digital count.

Figure 7-9. Effect of tree crown variations on SPOT green waveband response variability for partial canopy groves.



Note: DC--digital count.

Figure 7-10. Effect of tree crown variations on SPOT red waveband response variability for partial canopy groves.



Note: DC--digital count.

Figure 7-11. Effect of tree crown variations on SPOT NIR waveband response variability for partial canopy groves.



Citrus trees tended to be more uniform in groves with large canopy covers (Figure 7-12). This is probably due to some increased cultural attention such as hedging and topping practices. Also, the variation of grove-wide image response was not the same across the entire 20-75% canopy cover range (Figures 7-6, 7-7, and 7-8). The image response was slightly less variable for groves with canopy sizes greater than 40%, especially for the green and red wavebands (Figures 7-6 and 7-7). When canopy cover increased, the area of exposed soils decreased. This reduced the strong effect of soil substrates. In addition, an increase in canopy cover will have less variable tree crown diameter as indicated in Figure 7-12. Consequently, groves of young citrus trees are spectrally more variable due to the greater variability in both tree crown diameter and exposed area.

Recall again that the SPOT satellite scene was acquired in late summer (October 3, 1987) when the season is generally wet and ponderous weeds/grasses are still actively growing. However, field conditions in south Florida are generally less variable in winter months than in the summer because of the dry season as well as relatively inactive growing of weeds/grasses in the field environment. Therefore, satellite scenes acquired in dry winter months (e.g. January and February) would render a greater possibility for citrus canopy cover to stand out spectrally in the area to be imaged when the influence of soil conditions is minimized.

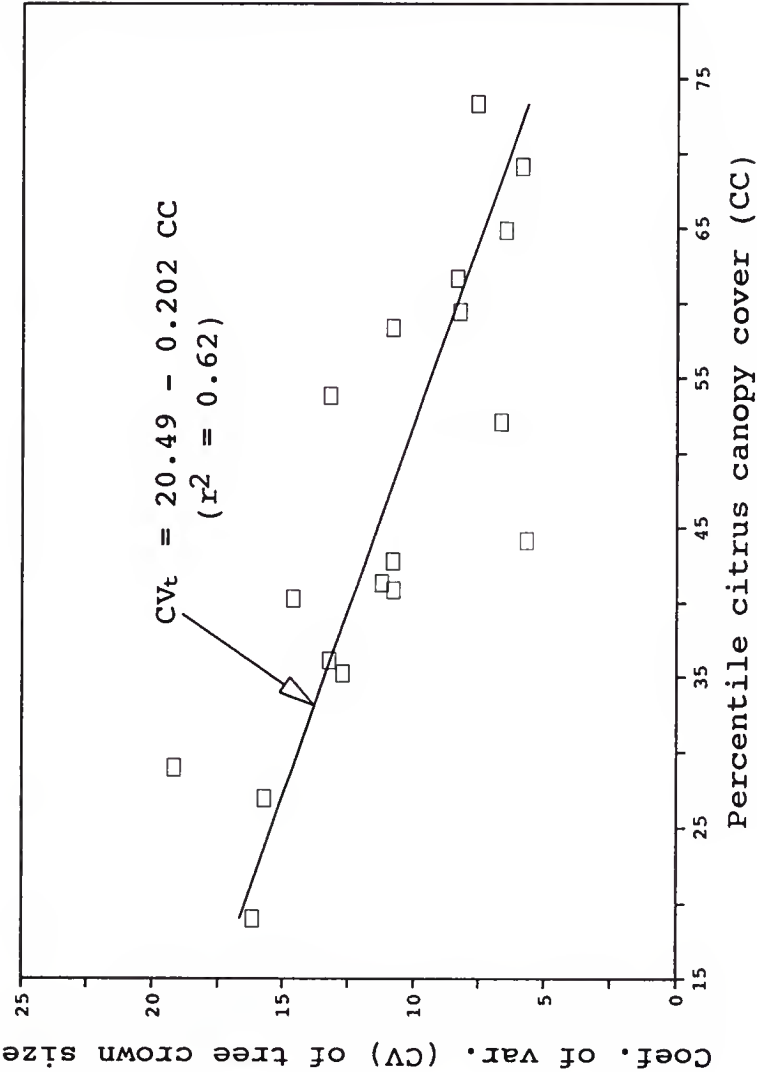


Figure 7-12. Relation of tree crown variation to canopy cover difference.

### Effect of Multiresolution Merging

For the SPOT multiresolution merged data, the correlation coefficients ( $r^2$ ) for the relations between citrus canopy cover and image response are summarized in Table 7-4. These relations did not reveal improvements after the panchromatic image was merged, and this lack of improvement is attributed to the variability of field environments. Note that, in each multispectral waveband (green, red and NIR) of the original multiresolution dataset, there existed significant variations of correlation between the panchromatic and multispectral images among the 18 selected groves (Table 7-5), even though these groves were considered relatively uniform. Because of these variations of correlation, the changes of image data among the 18 groves were not consistent within each waveband (Table 7-6) when the panchromatic waveband is merged. While the standard deviation of image data increased for some groves, it decreased for others in a merged image (Table 7-6). Consequently, the grove-wide image responses of some groves became more uniform, while those of others were more variable. Unfortunately, additional ground-truth information was not available to allow a further assessment of these image data transformations. In land-use classification analyses, the groves with more uniform image data can be easily separated as unified individual fields. However, those with more dispersed response each would split into small areas, making an entire field mingling between different classes in the classification results.

Table 7-4. Summary of correlations between citrus canopy cover and image response for multiresolution merged images.

Waveband#	Explanation	Corr. coef. ( $r^2$ )
Pan.	Original	(-) <sup>1</sup> 0.61
Green	Original	(-) 0.58
	Merged	(-) 0.60
Red	Original	(-) 0.57
	Merged	(-) 0.59
NIR	Original	(+) 0.00 <sup>2</sup>
	Merged	(-) 0.05
NDVI	NIR and red waveband	(+) 0.37
NDVI <sub>p</sub>	NIR and pan. waveband	(+) 0.40

Note: <sup>1</sup> The (-) and (+) signs are to indicate positive and negative correlations, respectively.

<sup>2</sup> Actual value is 0.003.

Table 7-5. Variations of image data correlation (r) between panchromatic and original multispectral wavebands among select groves.

Field#	Correlation coefficient (r) to pan. image		
	Green	Red	NIR
1	0.476	0.552	-0.387
2	0.675	0.757	-0.118
3	0.376	0.476	-0.082
4	0.543	0.712	-0.598
5	0.525	0.606	0.080
6	0.690	0.733	0.356
7	0.325	0.662	-0.089
8	0.666	0.696	0.413
9	0.754	0.692	-0.444
10	0.507	0.691	0.071
11	0.371	0.323	-0.032
12	0.690	0.766	-0.331
13	0.412	0.503	-0.326
14	0.677	0.698	0.207
15	0.266	0.353	0.226
16	0.313	0.200	-0.117
17	0.151	0.195	-0.189
18	0.822	0.720	0.744



Table 7-6. Standard deviations ( $\sigma$ ) of merged image data for selected citrus groves.

Field#	Original data			Merged image data standard dev. ( $\sigma$ ) (green waveband)
	(r)	( $\sigma_{\text{green}}$ )	( $\sigma_{\text{pan}}$ )	
1	0.476	0.808	1.080	1.167
2	0.675	1.399	2.183	2.312
3	0.376	0.607	1.052	1.002
4	0.543	0.832	1.407	1.401
5	0.525	1.394	2.280	2.239
6	0.690	1.990	2.843	3.205
7	0.325	0.609	1.139	1.022
8	0.666	0.956	1.347	1.542
9	0.754	0.859	1.492	1.428
10	0.507	0.913	1.380	1.462
11	0.371	0.758	0.913	1.065
12	0.690	1.197	1.877	1.963
13	0.412	0.862	1.351	1.312
14	0.677	0.949	1.537	1.596
15	0.266	0.438	0.824	0.713
16	0.313	0.484	0.751	0.783
17	0.151	1.387	1.173	1.638
18	0.822	1.337	1.650	2.087

Table 7-6 -- continued.

Field#	Original data			Merged image data standard dev. ( $\sigma$ ) (red waveband)
	(r)	( $\sigma_{\text{red}}$ )	( $\sigma_{\text{pan}}$ )	
1	0.552	0.875	1.080	1.299
2	0.757	1.436	2.183	2.402
3	0.476	0.600	1.052	1.037
4	0.712	1.379	1.407	1.997
5	0.606	1.585	2.280	2.469
6	0.733	2.327	2.843	3.569
7	0.662	0.869	1.139	1.351
8	0.696	0.861	1.347	1.473
9	0.692	1.101	1.492	1.631
10	0.691	1.283	1.380	1.902
11	0.323	0.710	0.913	1.017
12	0.766	1.436	1.877	2.215
13	0.503	1.015	1.351	1.489
14	0.698	0.802	1.537	1.488
15	0.353	0.964	0.824	1.184
16	0.200	0.484	0.751	0.750
17	0.195	1.209	1.173	1.506
18	0.720	0.944	1.650	1.663

Table 7-6 -- continued.

Field#	Original data			Merged image data standard dev. ( $\sigma$ ) (NIR waveband)
	(r)	( $\sigma_{\text{NIR}}$ )	( $\sigma_{\text{pan}}$ )	
1	-0.387	2.470	1.080	2.260
2	-0.118	2.573	2.183	2.708
3	-0.082	1.760	1.052	1.832
4	-0.598	1.619	1.407	1.332
5	0.080	2.355	2.280	2.736
6	0.356	2.827	2.843	3.638
7	-0.089	1.070	1.139	1.216
8	0.413	2.227	1.347	2.599
9	-0.444	1.200	1.492	1.133
10	0.071	2.189	1.380	2.400
11	-0.032	3.694	0.913	3.722
12	-0.331	1.239	1.877	1.287
13	-0.326	1.143	1.351	1.145
14	0.207	0.970	1.537	1.389
15	0.226	2.097	0.824	2.179
16	-0.117	1.352	0.751	1.377
17	-0.189	1.922	1.173	1.943
18	0.744	5.941	1.650	6.595

Note: r -- correlation coefficient.  
 $\sigma$  -- standard deviation with subscripts for waveband index.

In summary for the differentiation of citrus canopy cover on SPOT multiresolution images, four conclusions are reached. First, the photogrammetric estimation of citrus canopy cover is feasible and accurate using 1:24,000 ACIR photography. The measurable canopy cover is considered to be within the 20-75% range, provided that the photo scale is properly chosen (from 1:24,000 to 1:2,400). Second, the image response of the SPOT green, red, and panchromatic wavebands indicated an inverse relation to the difference of citrus canopy size. However, a definable relation to citrus canopy size was not observed for the SPOT NIR response. Third, the grove-wide spectral response of 20-75% partial canopy fields varied significantly, and the variation is attributed mainly to the soil substrate variability in the summer field environment. For this reason, it is anticipated that alternative satellite scenes acquired in dry winter months (January and February) would allow an improved differentiation of citrus canopy cover when the influence of soil conditions is minimized. Fourth, due to the influence of variable summer field environment, the variability of image response for each individual grove can be significantly affected by merging the panchromatic waveband because of the large variations of correlation between the panchromatic and multispectral images among the groves.

#### Land-use Classification

This section is focused on the effects of multiresolution processing and the use of GIS techniques for improving land-

use classification. The analyses involved all three datasets (OMD, MMD, and MMND) as shown in Table 6-2 and some special attention was given to the classification of citrus land use.

To acquire land-use information from satellite datasets, three factors must be considered. First, the image dataset to be used must have the spatial, radiometric, and spectral qualities to resolve and record the land-use elements in the scene. Second, the conceivable spectral signatures inherent in the scene environment can be extracted from the dataset through image processing procedures. This is a very important consideration in remote sensing land-use classification. Third, adequate ground-truth information is available for determining the ground actuality of generated spectral classes.

#### Potential for Signature Extraction

For the three datasets (OMD, MMD, and MMND) in Table 6-2, a summary of the statistically separable spectral signatures unveiled by the ERDAS STATCL module is presented in Table 7-7. These result conveys a useful assessment of the effectiveness with which each dataset can differentiate the scene. When used in a land-use classification process, each of these signatures will result in one spectral class that can be related to a land-use type/condition through a ground-truthing process.

From the results in Table 7-7, two comments are in order. First, a SPOT satellite scene can be differentiated to a



Table 7-7. Summary of spectral signatures unveiled by ERDAS STATCL module.

Scaled-distance	Dataset		
	OMD	MMD	MMND
1.0	37	63	63
2.0	26	51	17
3.0	10	21	10

Note: 1. OMD = original multispectral dataset which includes the original three 20-m multispectral images.  
 2. MMD = multiresolution merged dataset generated by the preserving approach with  $\beta=0.5$  for each image.  
 3. MMND = multiresolution merged and NDVI<sub>p</sub> dataset which is similar to MMD except that the merged NIR image is replaced by the NDVI<sub>p</sub> data.

significantly greater extent when a multiresolution merged dataset is used. At the scaled distance of 3.0, for example, the original dataset (OMD) could only differentiate the SPOT scene into 10 spectral classes, while merged dataset MMD was able to separate it into 21 classes. This effectiveness of dataset MMD was consistent for all three cases (Table 7-7). The increased differentiation by dataset MMD is an irrefutable advantage of using multiresolution merged data for land-use classification efforts. As a result, the acquisition of improved land-use information becomes increasingly feasible through a multiresolution processing approach.

Second, there is a limitation in using the  $NDVI_p$  image (dataset MMND) for land-use classification applications (Table 7-7). In order to understand this limitation, three factors must be considered. First, the  $NDVI_p$  method is primarily for vegetation enhancement and its effectiveness is limited to vegetative areas (Chavez and MacKinnon, 1994). This will make non-vegetative lands such as barren soils, urban lands, and water bodies inseparable in the  $NDVI_p$  image. Second, the use of a scaling factor in the  $NDVI_p$  equation to stretch the fractional results to the possibly largest range (0-255) could have exaggerated the radiometric information of the merged  $NDVI_p$  image. Therefore, the  $NDVI_p$  standard deviation is not a factual indication for the radiometric information present in the original scene. Third, the study area is covered primarily with vegetation (e.g. citrus groves, pasture lands) while non-vegetation areas were very limited.

According to ERDAS (1991), using the STATCL module with a small scaled distance will allow a tight separation to discriminate closely related classes. For the study area dominated by vegetative lands, this tight clustering will make all closely related vegetation signatures distinguishable, resulting in a large number of spectral signatures (Table 7-7). However, when the scaled distance was set at a larger value, the differentiation by dataset MMND became a problem because many originally separable signatures in a tight classification became assimilated. In addition, the spectral signatures for non-vegetative land-use elements are very limited in the NDVI<sub>p</sub> image. Consequently, only a small number of signatures were unveiled for a scale distance of 3.0 (Table 7-7). This points out that the NDVI<sub>p</sub> image is feasible only in a tight classification of vegetative land use types.

The results from the ELAS TMTR clustering module are consistent with those from the ERDAS STATCL module (Table 7-8), though these two image processing systems have a different implementation of the clustering technique. For example, merged dataset MMD had either the largest number of spectral classes for a given scaled distance or for a given number of classes it would have the largest scaled distance between the derived classes. These are important factors for improving land-use classifications from satellite datasets.

Table 7-8. Summary of spectral signatures unveiled by ELAS TMTR module.

Scaled-distance	Dataset		
	OMD	MMD	MMND
3.00	39	58	49
3.25	36	55	37
3.50	28	48	32
3.75	27	40	27
4.00	22	35	23
4.25	21	32	19
4.50	20	30	18
4.75	18	27	17
5.00	17	24	-
5.25	15	23	16
5.50	13	21	15

Note: 1. OMD = original multispectral dataset which includes the original three 20-m multispectral images.  
 2. MMD = multiresolution merged dataset generated by the preserving approach with  $\beta=0.5$  for each image.  
 3. MMND = multiresolution merged and NDVI<sub>p</sub> dataset which is similar to MMD except that the merged NIR image is replaced by the NDVI<sub>p</sub> data.

### GIS Discrete Classification

The spectral classes generated by the GIS-based discrete classification approach were each ground-truthed using the estimates of canopy cover, the ACIR photography, and field visits. For each of the three datasets of OMD, MMD, and MMND (Table 6-2), a summary of the ground-truth for the seven spectral classes is provided in Table 7-9.

As indicated in Table 7-9, a spectral class of the original dataset OMD can encompass citrus groves for a large range of canopy size. For example, class four virtually included every measured grove within the 20-75% canopy cover range. This points out that a canopy-size classification of citrus groves is very difficult using the original 20-m multispectral dataset. When multiresolution merged datasets MMD and MMND were used, an improvement was noted. The citrus groves at the upper range of canopy size tended to be less mixed with those at the lower range as indicated by the results of merged datasets MMD and MMND (Table 7-9). When a correlation was performed between the canopy covers and the spectral classes in Table 7-9, the coefficient of correlation ( $r^2$ ) was 0.01, 0.40, and 0.29 for datasets OMD, MMD, and MMND, respectively. Though this improvement was not enough to substantiate the practicality of classifying citrus groves based on some discrete ranges of canopy size, the advantage of using multiresolution processing is clear. The primary difficulty is the summer field environment, which resulted in a large variability of image data for each grove. However,



Table 7-9. Canopy cover for spectral classes by GIS-based discrete classification technique.

Dataset OMD <sup>a</sup>									
No.	Field-ID	Canopy (%)	Spectral class						
			1	2	3	4	5	6	7
1	6	19.52			x			x	
2	16	26.97			x	x			
3	10	28.01					x	x	
4	14-1	35.25				x	x		
5	15-2	36.15		x	x	x			
6	15-1	40.26			x	x			
7	14-2	40.88				x		x	
10	8	41.27		x	x	x			
8	A4	42.73				x	x	x	
9	A1	44.14		x		x			
11	7	52.07				x	x		
12	2	52.79				x	x		
13	1	56.41		x	x	x			
14	A5	59.46				x	x		
15	12	61.69				x	x		
16	#3	64.87					x		
17	9	69.15		x		x	x		
18	A2	73.31		x		x	x		

Table 7-9 -- continued.

Dataset MMD <sup>a</sup>			Spectral class						
No.	Field-ID	Canopy%	a	b	c	d	e	f	g
1	6	19.52					x	x	
2	16	26.97				x	x	x	
3	10	28.01			x		x		
4	14-1	35.25			x	x	x		
5	15-2	36.15				x		x	
6	15-1	40.26				x		x	
7	14-2	40.88					x		
10	8	41.27					x		
8	A4	42.73			x	x	x		
9	A1	44.14		x		x			
11	7	52.07			x	x	x		
12	2	52.79			x				
13	1	56.41		x		x			
14	A5	59.46			x		x		
15	12	61.69		x	x				
16	#3	64.87			x				
17	9	69.15		x	x				
18	A2	73.31		x	x				

Table 7-9 -- continued.

Dataset MMND <sup>a</sup>									
No.	Field-ID	Canopy%	Spectral class						
			A	B	C	D	E	F	G
1	6	19.52		x	x				
2	16	26.97		x	x				
3	10	28.01					x	x	
4	14-1	35.25			x	x		x	
5	15-2	36.15			x	x			
6	15-1	40.26			x	x			
7	14-2	40.88				x		x	
10	8	41.27			x	x			
8	A4	42.73				x	x	x	
9	A1	44.14					x	x	
11	7	52.07					x	x	
12	2	52.79					x	x	
13	1	56.41				x		x	
14	A5	59.46					x	x	
15	12	61.69					x		
16	#3	64.87					x	x	
17	9	69.15				x		x	
18	A2	73.31					x		

<sup>a</sup> -- Refer to Table 6-2 for dataset definition.

further improvements are expected through the use of satellite scenes acquired in dry winter months (January and February) to minimize field variability.

Also indicated in Table 7-9 is that the canopy-size differentiation by merged dataset MMND was not as effective as one would expect. In a late summer month (October) in south Florida orchards, miscellaneous vegetation (e.g. weeds and grasses between rows as well as between trees) still remains active growing in the field environment, creating the primary source for these between-class confusions among the groves of different canopy covers. In a canopy-size differentiation, the miscellaneous vegetation acted as a mask for the entire citrus land-use areas, making it difficult for the citrus groves with different canopy covers to stand out spectrally in the image dataset.

In summary, two comments are in order. First, there is a clear advantage of using multiresolution processing for land-use classification applications. For a given satellite scene, a multiresolution merged SPOT dataset will allow the land-use elements to be discriminated to a significantly greater extent. This enhanced differentiation provides a greater amount of land-use information for improving land-use classifications. Second, though multiresolution merging has indicated some improvement on a canopy-size classification of citrus groves, such an effort is still difficult in practical applications. The lack of such a differentiation for citrus

groves suggests that there exist other factors such as the differences in soil substrate, tree health/growth conditions, tree varieties, and cultural practices, which could have played a vital role individually and/or collaborately in affecting the canopy-size differentiation of citrus groves. In addition, the seasonal differences in the field environment also play a role in affecting the classification results. Without sufficient information of ground-truth, it is impossible to assess the impacts of these factors. Therefore, research efforts are needed in this regard in order to gain more understanding and to evaluate the impacts of these factors on using satellite imagery data for regional citrus land-use classification and monitoring.



## CHAPTER 8

### CONCLUSIONS AND RECOMMENDATIONS

Through the efforts undertaken in this research, several conclusions have been reached regarding merging satellite imagery data for image enhancement and multispectral analyses. Some recommendations are also discussed for future research efforts to extend the results of this research to broader applications of satellite remote sensing.

#### Research Conclusions

In the context of digitally merging satellite images, the principle of statistical variation analyses can be used as the fundamental basis to evaluate an image merging method and to assess the radiometric quality (variance and brightness) of pre-merged images including those from multiresolution datasets. The introduction of this merging principle for combining satellite images will lead to more effective use of remote sensing data.

Merging satellite images is not simply a mathematical procedure. It is a transformation of radiometric information from the combining images to the merged image data. This radiometric transformation, which has long been overlooked, can be utilized to benefit image processing efforts as well as to develop new merging methods for improving remote sensing

applications. Because a satellite image is unique in that it contains many subvariables representing the various land-use elements throughout the entire scene and because these subvariables will undergo a radiometric transformation in a merging process, an increasing amount of knowledge about the image data characteristics of various land-use types in different spectral wavelength ranges will extend this radiometric transformation to a broader scope of applications. The radiometric quality of a resultant merged image depends on (1) the data characteristics ( $r$ ,  $\sigma^2$ , and  $\mu$ ) of the images to be combined and (2) the method used to digitally merge the image data. These same criteria can also be applied to assessing the radiometric qualities of the land-use types of interest in a merged image.

Of the three merging approaches (confining, preserving, and differencing), the preserving method is the most effective approach for digitally combining image data including those with different spatial resolutions. The selection of a merging method to achieve an image enhancement objective must be made with consideration of the correlation and the radiometric variance difference between the images to be combined. To enhance the radiometric quality of merged data, the preserving method should be used for non-negatively correlated ( $r \geq 0$ ) images while the differencing method can only be applied in the case where the images to be merged have a strong negative correlation and the primary image is brighter

and has a greater radiometric variance. In every aspect, the confining method is ineffective and inferior to the preserving method. Hence, the customary use of the confining approach for multiresolution merging should not be continued. The preserving method with a merging coefficient ( $\beta$ ) of 0.5 was found to be a very effective approach for merging SPOT multiresolution datasets for both radiometric and spatial enhancements.

The photogrammetric approach for citrus canopy cover estimation is feasible and accurate using ACIR photography with a scale no smaller than 1:24,000. The spectral response in SPOT images was found to be inversely related to differences in citrus canopy cover, except for the NIR waveband. These inverse relations suggest a strong influence of soil substrates on the spectra of partial canopy groves. For this SPOT scene taken in the late summer (early October), large variations of image response were observed for each grove, suggesting that satellite scenes acquired in dry winter months of January and February will be more feasible for citrus canopy studies in south Florida. In general, the SPOT image response is less variable for canopy cover greater than 40%, while citrus trees are more uniform in groves with higher percentage of canopy cover.

Multiresolution processing of SPOT satellite images will generate both radiometrically and spatially enhanced merged datasets which increase the differentiation of a satellite

scene to a significantly greater extent. This indicates the advantage of using multiresolution processing for improving land-use classification. The enhanced differentiation provides a greater amount of land-use information for remote sensing applications. For the canopy-size classification of citrus groves, an improvement was indicated through the combined use of multiresolution merged SPOT dataset and GIS-based discrete classification techniques. However, the improvement was not enough to substantiate the practical application of a canopy-size classification of citrus groves without additional refinement. Nonetheless, further improvements are anticipated from using satellite scenes acquired in dry winter months (e.g. January and February) in south Florida when the variability of summer field environment is minimized. The GIS-based discrete classification technique was very useful for eliminating the inter-class confusions between citrus and non-citrus land-use types.

In ratioing satellite images, there are two important considerations. First, the effectiveness of a ratioing method relies on the selection of the numerator image. If a land-use type is to be enhanced, the image with larger values for the land-use type in question should be used as the numerator image. Otherwise, it should be used as the denominator data. Second, the feasibility of waveband ratioing depends on the state and strength of correlation of the ratioing image data. If a land-use element has a high positive correlation between



the two ratioing images, it will be extremely difficult to enhance its radiometric quality through a ratioing approach. In other words, successful applications of waveband ratioing can be achieved only for those land-use types which have weak or negative correlations between the images to be ratioed.

### Recommendations

The understanding of the principle and the radiometric transformations of merging images including waveband ratioing provides new opportunities for using satellite image data to improve remote sensing applications. Nonetheless, continuing research is needed to further the efforts undertaken in this study.

The customary approach of using the confining method for digitally merging satellite images including those of multiresolution datasets should be avoided because of its ineffectiveness for radiometric and spatial enhancement. The confining approach is currently the most commonly used merging method for multiresolution processing and unfortunately can only generate radiometrically inferior merged image data while creating a great possibility of corrupting the spectral information in a multispectral dataset.

The merging methods (preserving, differencing, and ratioing) demonstrated in this study should be extended to other datasets to increase the utility of current and future remote sensing data. Through an effective data merging and



radiometric transformations, the collaborate utilizations of satellite datasets including those of Landsat MSS, Landsat TM, SPOT HRV, SPOT panchromatic, and other satellite sensors will provide new approaches and opportunities in remote sensing monitoring and land-use assessment applications.

Research efforts aimed at gaining an increasing amount of knowledge about the spectral data characteristics of different land-use types/conditions in various wavelength ranges are crucial to the effective use of satellite image data for broader remote sensing applications including land-use data acquisition. These image data characteristics provides the basis for developing more productive merging approaches while avoiding ineffective efforts in using the remote sensing data of current as well as future sensors.

The image data characteristics in the form of variation and correlation for different wavebands might be of great significance in providing additional information of the land surface such as the soil/tree/crop/water conditions/relations needed for many agricultural, environmental, and water resource management applications. Therefore, research efforts in that regard will increase both the scope and effectiveness of collaborating remote sensing data for broader applications while enriching our understanding of land-sensor relations, which are vital to the continuing success of remote sensing efforts now and in the future.

Because canopy cover is an important factor used in many environmental and vegetation-related investigations, the photogrammetric approach for canopy cover estimation needs to be extended to other agricultural crops and forest plantations through further research efforts. In addition, satellite scenes acquired in the dry winter months of January and February in south Florida should be used for citrus canopy cover studies because the influence of soil conditions will be minimized.

## APPENDIX A

### RGB COLOR DISPLAY

The RGB color system is based on the color additive theory for the three primary colors (red, green, and blue) to create color display. Because the color associated with a particular object depends on the amounts of red, green, and blue lights reflected by the object, by mixing different proportions of the three color primaries, therefore, all the colors can be created (Lillesand and Kiefer, 1979).

To create a color display for remote sensing data, three images are needed and each of them represents one of the three primary colors. When the three images are mixed together by the display device, the result is colorful renditions for the image data. Because human eyes can discriminate many more colors than gray shades (Lillesand and Kiefer, 1979; Gonzalez and Wintz, 1987), it is an advantage for photo interpreters to use color products.

## APPENDIX B

### IHS TRANSFORM FOR IMAGE DISPLAY

The intensity-hue-saturation (IHS) color transform is a simulation of the process of human color perception. Unlike the well-known RGB (red, green, and blue) color display method, the IHS transform uses the attributes called brightness or intensity (I), hue (H), and saturation (S) to distinguish one color from another. Brightness refers to intensity of light (Haydn et al., 1982) or illumination (Boynton, 1980) and is associated with spatial information (Carper et al., 1990). A low intensity will have a relatively dark display. Hue is an attribute associated with the dominant wavelength in a mixture of light waves. Thus, hue represents the dominant color as perceived by an observer. When an object is called red, orange, or yellow, its hue is being specified (Gonzalez and Wintz, 1987). Saturation refers to the relative purity of hue mixed with white light. The degree of saturation is inversely proportional to the amount of added white light (Gonzalez and Wintz, 1987).

The IHS transform takes a two-step transformation which includes a forward transformation from raw RGB image data to the I, H, and S components and a reverse transformation from the IHS components to RGB color values. In practical implementation of the IHS transform for remote sensing data,

the forward transformation is accomplished by the following equations (Haydn et al., 1982):

$$I = R + G + B \quad [B-1]$$

$$H = (G - B)/(I - 3B) \quad [B-1]$$

$$S = (I - 3B)/I \quad [B-3]$$

where R, G, B represent the image data of three spectral bands (red, green, and blue). Then, another set of equations is used for the reverse transformation from the I, H, and S components to the three color values for an electronic color display device (Haydn et al., 1982):

$$r = 1/3 I (1 + 2S - 3SH) \quad [B-4]$$

$$g = 1/3 I (1 - S + 3SH) \quad [B-5]$$

$$b = 1/3 I (1 - S) \quad [B-6]$$

where r, g, and b respectively represent the primary colors for red, green, and blue for a electronic color display device. The three primary colors are used to define the visible colors when mixed together with varying magnitude (Haydn et al., 1982).

Several points need to be noted when using this color model for remote sensing data display purposes. First, a maximum of only three images can be displayed in one time. This is a drawback for multispectral datasets with more than three spectral wavebands. Second, the resultant (r, g, and b) values do not have any relations to the physical importance of



spectral information. Therefore, the merged data can only be used for display purpose and any multispectral analyses related to the transformed image data will be irrelevant. Third, the image display does not render any quantitative information for different land-use types in the image. Such information is totally left up to the user or photo-interpreter to determine. Finally, the IHS transform is only an attempt to make display colors pleasant to the human eyes rather than an image processing procedure which sharpens image data (Pellemans et al., 1993).

The IHS transform method has been successfully used in many studies (e.g. Haydn et al., 1982; Carper et al., 1990; Grasso, 1993) that aimed at improving image interpretation through color enhancement. However, the physiopsychological process of human color perception is not yet fully understood (Gonzalez and Wintz, 1987).

# APPENDIX C PROGRAM CODES TO UNPACK AVHRR LAC DATA

A Turbo-C compiler is needed to compile the following program codes. For detailed information regarding how the LAC data is packed, consult the TIROS manual (Kidwell, 1991). The the 32-bit arrangement for three 10-bit pixels is as:

```
|<----- 32 bits ----->|
00111111 11112222 22222233 33333333 00111111 11112222 22222233 33333333 00111111 11112222 22222233 33333333 ...
|---p1---|---p2---|---p3---| |---p1---|---p2---|---p3---| |---p1---|---p2---|---p3---|...
   b1      b2      b3      b4      b5      b1      b2      b3      b4 ...
```

Note: b1...b5 = bands 1 through 5.  
p1...p3 = pixels 1 through 3.

```
/***** Cut here, actual program codes begin next line *****/
#include <stdio.h>
#include <conio.h>
#include <stdlib.h>
main() {
    long Skip;
    unsigned int i,Read,Line,Pixel,Count,P1,P2,P3,I1,I2;
    unsigned int OUT[5][2050];
    unsigned char IN[4],Name[25],dummy;
    FILE *fin, *fout;

    Name[0]=20;
    printf("\n Enter input (LAC) file name : ");
    fin=fopen(cgets(Name),"rb");
    if(fin==NULL) return;

    printf("\n Skip (7400-byte) records of input file : ");
    scanf("%ld", &Skip);
    Skip=Skip*7400;
    if(Skip<0) return;

    Name[0]=20;
    printf("\n Enter output file name : ");
    fout=fopen(cgets(Name),"wb");
    if(fout==NULL) return;
```

```

printf("\n Begin unpacking input file .... ");

Line=Read=Pixel=Count=0;
rewind(f1);
if(Skip>0) fseek(f1,Skip,SEEK_SET);
fseek(fin,448,SEEK_CUR); /* Skip first 448 bytes */

while(!feof(fin)) {
    fread(IN,1,4,fin); /* read 4-byte = 3 pixels */
    Read=Read+1;
    Count=Count+1;
    dummy=IN[0];

    I1=dummy;
    I1=I1 << 4;
    dummy=IN[1];
    dummy=dummy >> 4;
    I2=dummy;
    P1=(I1+I2)/4;

    dummy=IN[1];
    dummy=dummy << 4;
    I1=dummy;
    I1=I1 << 2;
    dummy=IN[2];
    dummy=dummy >> 2;
    I2=dummy;
    P2=(I1+I2)/4;

    dummy=IN[2];
    dummy=dummy << 6;
    I1=dummy;
    I1=I1 << 2;
    I2=IN[3];
    P3=(I1+I2)/4;

    switch(Read) {
        case 1 : /* if first 4-byte */
            OUT[0][Pixel]=P1;
            OUT[1][Pixel]=P2;
            OUT[2][Pixel]=P3;
            break;

        case 2 : /* if second 4-byte */
            OUT[3][Pixel]=P1;
            OUT[4][Pixel]=P2;
            Pixel=Pixel+1;
            OUT[0][Pixel]=P3;
            break;
    }
}

```

```

        case 3 : /* if third 4-byte */
            OUT[1][Pixel]=P1;
            OUT[2][Pixel]=P2;
            OUT[3][Pixel]=P3;
            break;
        case 4 : /* if fourth 4-byte */
            OUT[4][Pixel]=P1;
            Pixel=Pixel+1;
            OUT[0][Pixel]=P2;
            OUT[1][Pixel]=P3;
            break;
        case 5 : /* if fifth 4-byte */
            OUT[2][Pixel]=P1;
            OUT[3][Pixel]=P2;
            OUT[4][Pixel]=P3;
            Pixel=Pixel+1;
            Read=0;
            break;  }

    if(Count==3415) { /* if 3415 4-byte reads or one scan */
        for(i=0;i<=4;i++)  fwrite(OUT[i],2,2048,fout);
        fseek(fin,692+488,SEEK_CUR);
        Pixel=Read=Count=0;  /* begin a new line */
        Line=Line+1;
        if(Line%100==0) printf("\n Finish line %d",Line); }
}
clrscr();
printf("\n\n Output file is written in a band interleave by");
printf("\n  line or BIL 8-bit data format. The entire scene");
printf("\n  has %d scan lines and 5 bands.",Line);
printf("\n  There are 2048 pixels per scan.\n");
fcloseall();
exit(0); }

```

## APPENDIX D

### CLASSIFICATION DECISION RULES

The classification decision rules implemented in land-use classification procedures for satellite remote sensing datasets have been well established and documented. These decision rules namely include the parallelepiped classifier, the minimum distance classifier, the mahalanobis distance classifier, and the maximum likelihood classifier (Lillesand and Kiefer, 1979; Thomas et al., 1987; ERDAS, 1991). A brief discussion for each of these four classifiers is presented.

#### The Parallelepiped Classifier

The simplest classification decision rule is the parallelepiped classifier. The criterion used to assign a candidate pixel to a spectral class are based on both the upper and lower limits of the image data values in each waveband for the spectral class in question. If the image data values of a candidate pixel fall between the upper and lower limits of a spectral class in every waveband in a multispectral dataset, the pixel is assigned to that spectral class.

The parallelepiped classifier is the simplest as well as the fastest among the four classifiers. But, if the image data of a spectral class indicates some correlations between



the spectral wavebands in a dataset, the parallelepiped boundaries defined by the upper and lower data limits (e.g. a rectangular in a two-waveband space) is unable to adequately describe the slanted or elongated clustering tendency of image data of that spectral class (Lillesand and Kiefer, 1979). In this regard, the parallelepiped classifier is not sensitive to the correlations of image data between spectral wavebands within a spectral class. Because of its fast implementation, the parallelepiped classifier is often used as a first-pass process in a more involved classification procedure (ERDAS, 1991) such as the maximum likelihood classifier to be discussed later.

#### The Minimum Distance Classifier

The minimum distance decision rule calculates, in a multi-dimensional space bound by the spectral wavebands in a dataset, the Euclidean distance between the vector of a candidate pixel and the mean vector of each spectral class. The candidate pixel is then assigned to the class to which its Euclidean distance is the smallest. The minimum distance decision rule takes no account for the data distributions of different spectral classes (Lillesand and Kiefer, 1979). Therefore, it is insensitive to the image data variations among different spectral classes. As a result, a pixel is more likely to be assigned to the classes which have smaller data variations or are more closely clustered.

### The Mahalanobis Distance Classifier

The mahalanobis distance classifier is similar to the minimum distance classifier except that an attempt is made to account for the image data variability by modifying the Euclidean distances. The approach is that the calculated Euclidean distances of a pixel in question to all spectral classes are each divided by the image data variance of the corresponding spectral class being evaluated. Then, the candidate pixel is assigned to the spectral class to which it has the smallest (modified) Euclidean distance. By this modification, a pixel is as likely to be assigned to the classes with a large data variability as to those with small image data variances.

### The Maximum Likelihood Classifier

The maximum likelihood classifier operates under the assumption that the image data of each spectral waveband are normally distributed (Gaussian distribution), which is generally acceptable for most remote sensing datasets (Lillesand and Kiefer, 1979). Using the image data of training samples, a parametric statistical approach is undertaken to prepare a multivariate probability density function for each spectral class in a multispectral dataset (Thamos et al., 1987). Then, the likelihood values or probabilities for a candidate pixel to each of the spectral classes are calculated and the candidate pixel is assigned to

the class to which it has the highest probability. The determination of a candidate pixel to a spectral class is based on the likelihood probability of that pixel rather than on the Euclidean distance (minimum distance or Mahalanobis distance) or the lower and upper data limits (Parallelepiped classifier). The maximum likelihood classifier is the slowest, but the most accurate decision rule among the classifiers.

## REFERENCES

- Albertz, J.A. and K. Zelianeos. 1990. Enhancement of satellite image data by data cumulation. *ISPRS Journal of Photogrammetry and Remote Sensing*, 45:161-174.
- American Society of Photogrammetry and Remote Sensing. 1990. ASPRS accuracy standards for large-scale maps. *Photogrammetric Engineering and Remote Sensing*, 56:1068-1070.
- Badhwar, G.D., J.G. Carnes, and W.W. Austin. 1982. Use of Landsat-derived tempol profiles for corn-soybean feature extraction and classification. *Remote Sensing of Environment*, 12:57-79.
- Bolstad, P.V., P. Gessler, and T.M. Lillesand. 1990. Positional uncertainty in manually digitized map data. *Intl. J. of Geographic Information Systems*, 4(4):399-412.
- Boynton, R.M. 1979. Human color vision. Holt, Rinehart and Winston, New York, NY.
- Carper, W.J., T.M. Lillesand, and R.W. Kiefer. 1990. The use of intensity-hue-saturation transformation for merging SPOT panchromatic and multispectral image data. *Photogrammetric Engineering and Remote Sensing*, 56(4):459-467.
- Chavez, P.S., G.L. Berlin, and M.A. Tarabzouni. 1983. Discriminating lithologies and surficial deposits in the Al Hisma plateau of Saudi Arabia with digitally combined Landsat MSS and SIR-A images. *Proc. of National Conference on Resource Management Applications, Vol. IV-Remotely Sensed/Geographic Information Systems in Geologic Applications*. San Francisco, CA. August 22-26.
- Chavez, P.S. Jr., S.C. Sides, and J.A. Anderson. 1991. Comparison of three different methods to merge multiresolution and multispectral data: Landsat TM and SPOT panchromatic. *Photogrammetric Engineering and Remote Sensing*, 57(3):295-303.
- Chavez, P.S. Jr. and D.J. MacKinnon. 1994. Automatic detection of vegetation changes in the southwestern United States using remotely sensed images. *Photogrammetric Engineering and Remote Sensing*, 60(5):571-583.



- Cliche, G., E. Bonn, and P. Tellet. 1985. Intergration of the SPOT panchromatic channel into its multispectral mode for image sharpness enhancement. *Photogrammetric Engineering and Remote Sensing*, 51(3):311-316.
- Coleman, T.L., L. Gudapati, and J. Derrington. 1990. Monitoring forest plantations using Landsat thematic mapper data. *Remote Sensing of Environment*, 33:211-221.
- Colwell, R.N. and C.E. Poulton. 1985. SPOT simulation imagery for urban monitoring: A comparison with Landsat TM and MSS imagery and with high altitude color infrared photography. *Photogrammetric Engineering and Remote Sensing*, 51(8):1093-1101.
- Curran, P.J. 1985. *Principles of remote sensing*. Longman Inc., New York, NY.
- Daily, M. 1983. Hue-saturation-intensity split-spectrum processing of Seasat radar imagery. *Photogrammetric Engineering and Remote Sensing*, 49(3):349-355.
- Daily, M.I., T. Farr, C. Elachi, and G. Schaber. 1979. Geologic interpretation from composited radar and Landsat imagery. *Photogrammetric Engineering and Remote Sensing*, 45(8):1109-1116.
- Degloria, S.D., R. Bernstein, and S. DiZenno. 1986. Discrimination of natural and cultivated vegetation using Thematic Mapper spectral data, in P.N. Slater, editor, *Earth Remote Sensing Using the Landsat Thematic Mapper and SPOT Sensor Systems*, Proc. SPIE 660, pp 144-150.
- Dye, R. and L. Wood. 1989. Resolution improvement by multi-temporal data merging. *ISPRS Journal of Photogrammetry and Remote Sensing*, 44:14-20.
- Ehlers, M. 1989. The potential of multisensor satellite remote sensing for geographic information systems. *Technical Papers of ASPRS/ACSM Annual Convention*, 4:40-45.
- Engel, J. 1986. Land satellite (Landsat) systems: Earth observation satellite company (EOSAT's) plans for Landsat-6 and beyond. *Earth Remote Sensing Using the Landsat Thematic Mapper and SPOT Sensor Systems*, in P.N. Slater, editor, *Earth Remote Sensing Using the Landsat Thematic Mapper and SPOT Sensor Systems*, Proc. SPIE 660, pp 169-174.
- Earth Observational Satellite (EOSAT). 1992a. Special Landsat-6 issue, Landsat data users notes. 4300 Forbes Blvd., Lanham, MD. 7(2):3-5.



----- . 1992b. Landsat technical notes, September, 1992.  
4300 Forbes Blvd., Lanham, MD.

Earth Resource Data Analysis System (ERDAS). 1991. Field guide (manual for pc version 7.5). ERDAS Inc., 2801 Buford Highway, Suite 300, Atlanta, GA 30329.

Environmental System Research Institute (ESRI). 1993. Arc/Info manuals. Environmental and Scientific Research Institute. Redlands, CA.

Fukushima, T. and K. Muraoka. 1988. Simple model to predict water quality in 90 Japanese lakes. Proc. of the Intl. Assoc. for Theoretical and Applied Limnology, 23(8):812-827.

Gillespie, A.R., A.B. Kahle, and R.E. Walker. 1986. Color enhancement of highly correlated images. I. Decorrelation and HSI contrast stretches. Remote Sensing of Environment, 20:209-235.

Gonzalez, R.C. and P. Wintz. 1987. Digital image processing, 2nd ed. Addison-Wesley Pub. Company, Reading, MA.

Graham, M.H., B.G. Junkin, M.T. Kalcic, R.W. Pearson, and B.R. Seyfarth. 1986. Earth resources laboratory applications software user reference, vol. I & II., Report No. 183. Earth Resources Laboratory, National Space Technology Laboratories, National Aeronautics and Space Administration.

Grasso, D.N. 1993. Applications of the IHS color transformation for 1:24,000-scale geologic mapping: A low cost SPOT alternative. Photogrammetric Engineering and Remote Sensing, 59(1):73-80.

Harris, J.R., R. Murray, and T. Hirose. 1990. IHS transform for the integration of radar imagery with other remotely sensed data. Photogrammetric Engineering and Remote Sensing, 56(12):1631-1641.

Haydn, R., G.W. Dakle, J. Henkel, and J.E. Bare. 1982. Application of the IHS color transform to the processing of multisensor data and image enhancement. Proceedings of the Intl. Symp. on Remote Sensing of Arid and Semi-Arid Lands, Cairo, Egypt. January 19-25.

Huete, A.R. and Jackson. 1988. Soil and atmosphere influences on the spectra of partial canopies. Remote Sensing of Environment, 25:89-105

- Idso, S.B., R.J. Reginato, and R.D. Jackson. 1977. Albedo measurement for remote sensing of crop yields. *Nature*, 266(4):625-628.
- Jackson, L.K. and J. Sauls. 1983. Fruit crops fact sheet: The sweet orange. FC-25, Inst. of Food and Agric. Sci., Univ. of Florida, Gainesville, FL.
- . 1984. Fruit crops fact sheet: Grapefruit. FC-35, Inst. of Food and Agric. Sci., Univ. of Florida, Gainesville, FL.
- Judd, D.B. and G. Wyszeci. 1975. Color in business, science and industry, 3rd edition. John Wiley & Sons, Inc., New York, NY.
- Kidwell, K.B. 1991. NOAA polar obitor data (TIROS-n, NOAA-6, NOAA-7, NOAA-8, NOAA-9, NOAA-10, NOAA-11 & NOAA-12) users guide. National Oceanic and Atmospheric Adaministration, National Environmental Satellite, Data, and Information Service, National Climatic Data Center, Satellite Data Devision, Princeton Executive Square, Rm 100, Washington D.C., 20233.
- Lillesand, T.M. and R.W. Kiefer. 1979. Remote sensing and image interpretation. John Wiley & Sons, Inc., New York, NY.
- Lo, T.H.C., F.L. Scarpance, and T.M. Lillesand. 1986. Use of multitemporal spectral profiles in agricultural land-cover classification. *Photogrammetric Engineering and Remote Sensing*, 52(4):535-544.
- Mendenhall, W., R.L. Scheaffer., and D.D. Wackerly. 1986. Mathematical statistics with applications, 3rd edition. Prindle, Weber & Schmit, Duxbury Press, PWS Engineering, Breton Publishers, Salter Office Bldg., 20 Park Plaza, Boston, MA.
- Mood, A.M., F.A. Graybill, and D.C. Boes. 1974. Introduction to the theory of statistics. McGray-Hill, Inc., New York, NY.
- Moore, H. 1989. SPOT vs. Landsat TM for the maintenance of topographical databases. *ISPRS J. of Photogrammetry and Remote Sensing*, 44:72-84.
- Munehika, C.K., J.S. Warnick, C. Salvaggio, and J.R. Schott. 1993. Resolution enhancement of multispectral image data to improve classification accuracy. *Photogrammetric Engineering and Remote Sensing*, 59(1):67-72.

- Novotny, V. and G. Chesters. 1981. Handbook of nonpoint pollution sources and management. Van Nostrand Reinhold Company, New York, NY.
- Pellemans, A.H.J.M., R.W.L. Jordans, and R. Allewijn. 1993. Merging multispectral and panchromatic SPOT images with respect to the radiometric properties of the sensor. Photogrammetric Engineering and Remote Sensing, 59(1):81-87.
- Pionke, H.B. and J.B. Urban. 1985. Effect of agricultural land use on ground-water quality in a small Pennsylvania watershed. Ground Water, 23(1):68-80.
- Piwowar, J.M., E.F. LeDrew, and D.J. Dudycha. 1990. Integration of spatial data in vector and raster formats in a geographic information system environment. Intl. J. Geographical Information Systems, 4(4):429-444.
- Price, J.C. 1984. Comparison of information content of data from the Landsat-4 thematic Mapper and the Multispectral Scanner. IEEE Trans. Geosci. Remote Sensing, GE-22:272-281.
- . 1987. Combining panchromatic and multispectral imagery from dual resolution satellite instruments. Remote Sensing of Environment, 21:119-128.
- Rees, W.G. 1990. Topics in remote sensing 1: Physical principles of remote sensing. Cambridge University Press, New York, NY.
- Schowengerdt, R.A. 1980. Reconstruction of multispatial multispectral image data using frequency content. Photogrammetric Engineering and Remote Sensing, 46(10):1325-1334.
- Shih, S.F. 1984. Landsat data availability. Proc. Fla. Soil and Crop Science Society, 43:21-25.
- . 1988. Satellite data and geographic information system for land use classification. J. of Irrig. and Drainage Engineering, 114(3):505-519.
- Shih, S.F., D.L. Myhre, G.J. Edwards, C.H. Blazquez, and J.M. Gardner. 1985. Wavelength intensity indices in relation to tree condition and leaf-nutrient content. 11th Intl. Symp. on Machine Processing of Remotely Sensed Data, June 25-27, 1985. Purdue Univ., West Lafayette, IN. pp.350-356.



Spotlight. 1991. SPOT Image Corporation Newsletter. SPOT Image Corporation, Reston, VA. March, 1991.

Swain, P.H. 1978. Fundamentals of pattern recognition in remote sensing, in P.H. Swain and S.M. Davis, editors, Remote sensing: The quantitative approach. McGraw-Hill, Inc., New York, NY.

*Système Probatoire de l'Observation de la Terre (SPOT)*. 1989. SPOT user's handbook, Vols. I and II, 1st ed. SPOT Image Corporation, Reston, VA.

Tan, Y.R. and S.F. Shih. 1991a. GIS in monitoring agricultural land use changes and well assessment. Trans. ASAE, 33(4):1147-1152.

----- . 1991b. Geographic errors involved in data entry of geographic information systems. Proc. Intl. Conference on Computer Applications in Water Resources, Taipei, Taiwan, R.O.C., July 3-6. pp 627-634.

Thomas, I.L., V.M. Benning, and N.P. Ching. 1987. Classification of remotely sensed images. IOP Publishing Limited Techno House, Redcliffe Way, Bristol BS1 6NX, England.

Thorpe, J. 1990. The need for photogrammetry in building an urban GIS. Photogrammetric Engineering and Remote Sensing Florida Section, Civil Engineering Department, University of Florida, 14(4):1-5.

Tou, J.T. and R.C. Gonzalez. 1974. Pattern recognition principles. Addison-Wesley Pub. Company, Reading, MA.

United States Environmental Protection Agency (USEPA). 1973. Methods for identifying and evaluating the nature and extent of nonpoint sources on pollutants. Office of Air and Water Programs, Washington D.C.

----- . 1984. Report to Congress: Nonpoint sources pollution in the U.S. Water Planning Division, Washington D.C.

Walsh, S.J., J.W. Cooper, I.E.V. Essen, and K.R. Gallager. 1990. Image enhancement of Landsat thematic mapper data and GIS data integration for evaluation of resources characteristics. Photogrammetric Engineering and Remote Sensing, 56(8):1135-1141.

Welch, R. and M. Ehlers. 1987. Merging multiresolution SPOT HRV and Landsat TM data. Photogrammetric Engineering and Remote Sensing, 53(3):301-303.

- Wong, F.H. and R. Orth. 1980. Registration of Seasat/Landsat composite images to UTM coordinates. Proc. of the 6th Canadian Symp. on Remote Sensing, Halifax, Nova Scotia, May 21-23.
- Zobrist, A.L., R.J. Blackwell, and W.D. Stromberg. 1979. Integration of Landsat, Seasat, and other geo-data sources. Proceedings of the 13th Annual Symp. on Remote Sensing of Environment, Environmental Research Institute of Michigan, Ann Arbor. pp 271-279.



## GLOSSARY

$\alpha$	merging coefficient for primary image.
$\beta$	merging coefficient for secondary image.
$\beta_c$	merging coefficient for minimum variance in merged image by confining method.
$\beta_d$	merging coefficient for equal variance in merged image by differencing method.
$\mu_1$	mean for image one or variable one.
$\mu_2$	mean for image two or variable two.
$\mu_c$	mean for merged image by confining method.
$\mu_d$	mean for merged image by differencing method.
$\mu_p$	mean for merged image by preserving method.
$\mu_r$	mean for merged image by ratioing method.
$\mu_y$	mean for merged image or merged variable (Y).
$\sigma_1^2$	variance for image one or variable one.
$\sigma_2^2$	variance for image two or variable two.
$\sigma_m^2$	minimum variance at $\beta_c$ by confining method.
$\sigma_r^2$	variance of merged image ( $Y_r$ ) by ratioing method.
$\underline{\sigma}_1^2$	normalized variance for image one or variable one.
$\underline{\sigma}_2^2$	normalized variance for image two or variable two.
$\underline{\sigma}_y^2$	normalized variance for merged image or merged variable (Y).
$\underline{\sigma}_c^2$	normalized variance for merged image ( $Y_c$ ) by confining method.
$\underline{\sigma}_d^2$	normalized variance for merged image ( $Y_d$ ) by differencing method.

$\sigma_p^2$	normalized variance for merged image ( $Y_p$ ) by preserving method.
$\sigma_y^2$	normalized variance for merged image or variable ( $Y$ ).
$\theta$	canopy cover (%).
$A_o$	canopy overlapping area.
$a$	tree spacing.
$b$	row spacing.
<u>CV</u>	coefficient of variation.
$d$	tree crown diameter.
$D$	distance on photo.
$f$	focal length.
$F_v$	variability factor.
$h$	flying height.
$H$	hue (component).
$I$	intensity (component).
$L$	ground distance (measured from photo).
$r$	correlation coefficient.
$R_b$	brightness ratio.
$S$	saturation (component).
$X_1$	variable one or image one.
$X_2$	variable two or image two.
$x_1$	photo coordinate x for point one.
$x_2$	photo coordinate x for point two.
$y_1$	photo coordinate y for point one.
$y_2$	photo coordinate y for point two.
$Y$	merged image or merged variable.
$Y_c$	merged image by confining method.

$Y_d$	merged image by differencing method.
$Y_p$	merged image by preserving method.
$Y_r$	merged image by ratioing method.
ACIR	aerial color infrared (photography).
AVHRR	advanced very high resolution radiometer.
DC	digital count (image gray shade).
DEM	digital elevation model.
ELAS	earth resource laboratory application software.
ERDAS	earth resource data analysis system.
GIS	geographic information systems.
GPS	global positioning system.
HPF	high pass filter.
HRV	high resolution visible (sensor).
IHS	intensity-hue-saturation (transform).
LAC	local area coverage.
MI	merged image.
MMD	multiresolution merged dataset by the preserving method with $\beta=0.5$ .
MMND	multiresolution merged and $NDVI_p$ dataset (similar to MMD with merged NIR waveband replaced by $NDVI_p$ ).
MSS	multispectral scanner.
NDVI	normalized difference vegetation index.
$NDVI_p$	normalized difference vegetation index by panchromatic waveband.
NIR	near-infrared.
NOAA	National Oceanographic and Atmospheric Administration.
OMD	original multispectral dataset.

OMD	original multispectral dataset.
PAN	panchromatic (image or aveband).
RBV	return beam vidicon.
RGB	red, green, and blue.
RMS	root-mean-square (error).
RSAL	Remote Sensing Applications Laboratory.
SAR	synthetic aperture radar.
SPC	state plane coordinate (system).
SPOT	(French) <i>Système Probatoire de l'Observation de la Terre</i> .
TIR	thermal infrared.
TM	thematic mapper.
UTM	universal transverse mercator (coordinate system).
USGS	United States Geological Survey.

## BIOGRAPHICAL SKETCH

The author was born and raised in a countryside in Guangdong Province, The People's Republic of China. He received his Bachelor of Science in Agriculture degree from South China Agricultural University in 1982. Then he was assigned to work as a lecturer in Nanjing Agricultural University until 1985 when he was awarded a one-year scholarship from the Ministry of Education of China for studying abroad. In 1986, he was admitted to a graduate program in the Department of Agricultural Engineering at the University of Florida, and in 1988 he received his Master of Engineering degree.

He continued his graduate study at the University of Florida in 1988 and is completing all the requirements for a Ph.D. degree in agricultural engineering.



I certify that I have read this study and that in my opinion it conforms to acceptable standards of scholarly presentation and is fully adequate, in scope and quality, as a dissertation for the degree of Doctor of Philosophy.



Sun Fu Shih, Chairman  
Professor of Agricultural  
Engineering

I certify that I have read this study and that in my opinion it conforms to acceptable standards of scholarly presentation and is fully adequate, in scope and quality, as a dissertation for the degree of Doctor of Philosophy.



Brian J. Boman  
Associate Professor of  
Agricultural Engineering

I certify that I have read this study and that in my opinion it conforms to acceptable standards of scholarly presentation and is fully adequate, in scope and quality, as a dissertation for the degree of Doctor of Philosophy.



Edward P. Lincoln  
Associate Professor of  
Agricultural Engineering

I certify that I have read this study and that in my opinion it conforms to acceptable standards of scholarly presentation and is fully adequate, in scope and quality, as a dissertation for the degree of Doctor of Philosophy.



Allen R. Overman  
Professor of Agricultural  
Engineering


I certify that I have read this study and that in my opinion it conforms to acceptable standards of scholarly presentation and is fully adequate, in scope and quality, as a dissertation for the degree of Doctor of Philosophy.



Byron E. Ruth  
Professor of Civil Engineering

This dissertation was submitted to the Graduate Faculty of the College of Engineering and to the Graduate School and was accepted as partial fulfillment of the requirements for the degree of Doctor of Philosophy.

December, 1994

\_\_\_\_\_  
Winfred M. Phillips  
Dean, College of Engineering

\_\_\_\_\_  
Karen A. Holbrook  
Dean, Graduate School

LD  
1780  
1994

.T 1611

